Tampere University

Jaakko Haapamäki

ACCELERATED ELECTRO-THERMAL ENDURANCE TESTING AND LIFETIME MODELLING OF BIAXIALLY ORIENTED POLYPROPYLENE INSULATION FILMS

Master of Science Thesis
Faculty of Information Technology
and Communication Sciences
July 2020

ABSTRACT

Jaakko Haapamäki: Accelerated electro-thermal endurance testing and lifetime modelling of biaxially oriented polypropylene insulation films
Master's Degree Programme in Electrical Engineering
Tampere University
Examiners: Adjunct Professor Kari Lahti and M.Sc. Minna Niittymäki
July 2020

This thesis was carried out as part of the EU-funded GRIDABLE project whose one objective is to develop and produce novel silica-BOPP (biaxially oriented polypropylene) electrical insulation films. The contribution of this thesis is to study how well the lifetime of these new, experimental materials will compare with established materials under long-term DC electro-thermal (E-T) endurance tests. Experiments were carried out for self-constructed metallized film capacitors insulated with the BOPP film under test, incorporating two separate sheets of metallized films as electrodes. The real operating conditions for commercial-grade metallized film capacitors were simulated by conducting endurance testing at elevated temperatures in an inert, oxygen-free ambient environment utilizing the self-healing capability of the metallized films.

The experiments had two objectives. The first was to conduct and compare endurance tests for different materials, and based on the results, perform lifetime modelling in order to evaluate their lifetime at lower E-T stress levels. The lifetime of a film was modelled separately as a function of an electric field (inverse power law) and temperature (Arrhenius model), and by their concurrent effects (multi-stress model). The second objective was to evaluate whether changes in preconditioning, i.e. the preliminary electro-thermal conditioning used to bring the sample to test conditions, could significantly influence the sample's lifetime in the ensuing endurance tests. This influence was studied by varying the preconditioning variables and evaluating their effect on the sample's lifetime in the endurance tests.

The preconditioning tests demonstrated that the life expectancy of the samples tends to increase in the endurance tests. However, this effect depended upon the electrical stress level employed in the endurance test combined with the temperature and duration of the preconditioning period. The effect was noticeable for all the films, including those without nano structuration, at 480 V/μm & 60 °C. However, in the lower stress endurance tests, the preconditioning effect was first observed to decrease (at 380 V/μm & 60 °C), and subsequently, to disappear (at 280 V/μm & 60 °C). It is suggested that the longer lifetimes observed in the high-stress endurance tests may be partly related to the annealing of the polymer film, which may have resulted in, e.g. its increased crystallinity. This could improve the polymer's resilience to local plastic deformation, and thus explain the longer lifetimes. Since the preconditioning did not influence the sample's lifetime at an electric field of 280 V/μm, it is plausible that the changes in preconditioning are related to a similar type of annealing effect which occurs during the actual, longer-term endurance testing. Further research is still needed to confirm this hypothesis.

The overall findings of the lifetime modelling imply, firstly, that the inverse power law may also be used to model the lifetime of experimental films and, secondly, that comparable lifetimes were predicted for both nanocomposite and commercial films under real service conditions (~200 V/μm). However, at the elevated stress levels used in the endurance tests, the commercial pure BOPP reference film had somewhat better performance than the nanocomposite film. The lifetimes for the commercial films predicted by the models were shorter than had been expected, and indeed shorter than what is known. The reasons for this were not thought to be connected to the range of electro-thermal stresses used in the accelerated life experiments, but rather to the structure of the utilized test capacitors, which do not represent all the real properties of commercially-wound capacitor elements, such as winding pressure. Despite these inconsistencies, these kinds of tests can be useful when comparing different insulation films with each other. However, it is recommended that future studies should evaluate how much the endurance performance of polymer film can be improved if the characteristics of the test samples correspond more closely to those of commercial capacitors.

Keywords: Polypropylene, ageing, degradation, BOPP, electro-thermal stress, inverse power law, Arrhenius model

The originality of this thesis has been checked using the Turnitin Originality Check service.

TIIVISTELMÄ

Jaakko Haapamäki: Orientoitujen polypropyleenieristekalvojen kiihdytetty elinikätestaus ja eliniän mallintaminen
Diplomityö
Tampereen yliopisto
Sähkötekniikka
Tarkastajat: Dosentti Kari Lahti ja Diplomi-insinööri Minna Niittymäki
Heinäkuu 2020

Tämä diplomityö tehtiin osana GRIDABLE-projektia, jossa kehitetään ja tuotetaan uudenlaisia piidioksidi-BOPP-ohutkalvoeristemateriaaleja (biaxially oriented polypropylene, kahteen suuntaan orientoitu polypropeeni). Työn tarkoituksena oli verrata kokeellisten ja vakiintuneiden eristemateriaalien käyttäytymistä kiihdytetyissä elinikätesteissä käyttäen yhdistettyä DC sähkökenttä- ja lämpörasitusta. Elinikätestit suoritettiin itsetehdyille, metalloiduille kalvokondensaattoreille, joissa käytettiin eristemateriaalina testattavia BOPP-kalvoja ja elektrodeina kahta metalloitua kalvoa. Todellisten metalloitujen kalvokondensaattoreiden käyttöolosuhteiden simuloimiseksi testit suoritettiin korotetuissa lämpötiloissa ja reagoimattomassa, happivapaassa ympäristössä hyödyntäen metalloitujen kalvojen itseparanemismekanismia.

Testeillä oli kaksi tavoitetta. Ensimmäisenä tavoitteena oli tehdä kiihdytettyjä elinikätestejä eri materiaaleille, verrata niiden käytöstä ja mallintaa materiaalien elinikää matalammilla rasituksilla. Elinikää mallinnettiin erikseen sähkökentän (inverse power law, käänteinen potenssilaki) ja lämpötilan (Arrheniuksen malli) funktiona, sekä näiden yhteisvaikutusten pohjalta (useamman rasituksen malli). Työn toinen tavoite oli arvioida, onko testauksen esivalmisteluvaiheen muutoksilla merkittävä vaikutus itse elinikätestiin. Tätä vaikutusta tutkittiin vaihtelemalla esivalmisteluvaiheen parametreja ja arvioimalla niiden vaikutusta elinikätestin tulokseen.

BOPP-kalvon elinajan odotuksen huomattiin kasvavan elinikätesteissä, kun esivalmisteluvaiheen rasitusta kasvatettiin. Vaikutuksen suuruus riippui kuitenkin sekä elinikätestissä käytetystä sähköisestä rasitustasosta että esivalmisteluvaiheen lämpötilasta ja kestosta. Vaikutus havaittiin kaikilla kalvotyypeillä, myös nanotäytteistämättömillä kalvoilla, kun elinikätestauksen rasitustaso oli 480 V/µm & 60 °C. Matalammalla rasituksella esivalmisteluvaiheen vaikutuksen havaittiin ensiksi laskevan (380 V/µm & 60 °C) ja myöhemmin katoavan (280 V/µm & 60 °C). Elinajan kasvu voi osittain liittyä polymeerikalvon annealing-ilmiöön, mikä on esimerkiksi voinut johtaa polymeerikalvon kiteisyyden kasvuun. Tämä voisi parantaa polymeerikalvon sietokykyä plastiseen muodonmuutokseen ja täten selittää korkeamman eliniän. Koska esivalmistelu ei vaikuttanut näytteen elinikään 280 V/µm rasituksella, on mahdollista, että muutokset esirasituksessa ovat yhteydessä samanlaiseen annealing-ilmiöön, joka tapahtuu pidemmällä aikavälillä ja myös varsinaisen elinikätestin aikana. Hypoteesin vahvistaminen vaatii kuitenkin vielä lisätutkimusta.

Kokonaisuudessaan eliniän mallintamisen tulokset viittaavat siihen, että käänteistä potenssilakia voidaan käyttää myös nanokomposiittikalvojen eliniän mallintamiseen ja että mallinnus ennustaa varsin samalaista elinikää tutkituille nanokomposiittikalvolle ja kaupalliselle BOPP-kalvolle niiden suunnitellulla käyttökentänvoimakkuudella. Tätä tasoa korkeammilla rasituksilla yksittäisissä elinikätesteissä puhtaalla BOPP-verrokkikalvolla mitattiin kuitenkin hieman parempi suorituskyky. Mallien ennustamat eliniät olivat odotettua lyhyempiä. Työssä tehdyn analyysin mukaan tämä voi kuitenkin vain osittain liittyä elinikätesteissä käytettyihin korkeisiin rasitustasoihin. Sen sijaan perustelu tälle voi olla ennemminkin siinä, ettei testikondensaattorin rakenne vastaa täysin kaikilta ominaisuuksiltaan kaupallista kondensaattorielementtiä (esim. elementin kääminnän aiheuttamaa paine). Tästä huolimatta työssä käytettyjä testejä voi pitää hyödyllisenä, kun erilaisia eristekalvoja verrataan toisiinsa. Jatkotutkimukseksi voidaan kuitenkin suositella tutkimusta, jossa selvitetään tarkemmin testikondensaattorirakenteiden vaikutuksia elinikätestien tuloksiin.

Avainsanat: Polypropeeni, ikääntyminen, BOPP, sähköterminen rasitus, käänteinen potenssilaki, Arrheniuksen malli

PREFACE

This Master of Science thesis was done for the unit of Electrical Engineering at Tampere University as a part of the EU-funded GRIDABLE project. The thesis examined the ageing behaviour of thin polymer films under long-term electro-thermal (DC) endurance tests.

I would like to express my deepest appreciation to Adjunct Professor Kari Lahti for this extremely interesting M.Sc. thesis topic and for his valuable and constructive suggestions during this thesis work. I very much appreciate the support of M.Sc. Minna Niittymäki who extended a great amount of assistance during the empirical work and thesis writing process. I am also grateful to D.Sc. (Tech.) Ilkka Rytöluoto for the invaluable insight into the practical measurements and the unparalleled support he was always willing to provide. My thanks also go to D.Sc. (Tech.) Mikael Ritamäki for suggestions regarding the empirical work.

Tampere, 2 July 2020

Jaakko Haapamäki

This project has received funding from the European Union's Horizon 2020 research and innovation programme under grant agreement No 720858.

CONTENTS

LIST OF SYMBOLS AND ABBREVIATIONS

AC	Alternating current
ALT	Accelerated life testing
BOPP	Biaxially oriented polypropylene
DC	Direct current
DMM	Dissado-Mazzanti-Montanari
DP	Degree of polymerization
ESL	Equivalent series inductance
ESR	Equivalent series resistance
FM	Fisher Matrix
HIC	Halving Interval in Celsius
HV	High voltage
HVDC	High Voltage Direct Current
HVP	High voltage probe
HOMO	Highest occupied molecular orbital
IPL	Inverse power law
LCC	Line Commutated Converter
LUMO	Lowest unoccupied orbital
MD	Machine direction
MED	Median ranks
PD	Partial discharge
PET	Polyethylene terephthalate
PP	Polypropylene
RRX	Rank regression
SRM	Standard ranking method
TD	Transverse direction
USB	Universal Serial Bus
VSC	Voltage Source Converter

A	Area
a	Experimental constant
B	Experimental constant
B_1	Experimental constant
B_2	Experimental constant
b	Experimental constant
C	Capacitance
C_s	Capacitance of sample
c	Experimentally defined constant
Co	Vacuum capacitance
$\boldsymbol{D}$	Dielectric flux density
$\boldsymbol{D(t)}$	Dielectric flux density as a function of time
d	Distance
E_0	Threshold stress for electrical ageing
$\boldsymbol{E}$	Electric field
EC	Commercial reference film
$\boldsymbol{E(t)}$	Electric field as a function of time
$E_{discharge}$	Discharged energy in one self-healing event
E_σ	Activation energy
$F(x)$	Probability of the failure as a function of variable x
f	Frequency
h	Experimental constant
J	Current density
K	Experimental constant

K_E	Experimental constant
K_T	Experimental constant
K_1	Experimental constant
K_2	Experimental constant
k	Boltzmann's constant
k_n	Endurance coefficient (exponential law)
L	Lifetime
L_o	Lifetime at the threshold stress E_0
$L(E)$	Lifetime as function of electric stress
$L(T)$	Lifetime as function of temperature
$L(E,T)$	Lifetime as function of electric stress and temperature
$Mavg$	Average molecular weight
m	Molecular weight of the repeat unit
n	Endurance coefficient (inverse power law)
n_1	Experimental constant
n_2	Experimental constant
$\boldsymbol{P}$	Polarization
$P1$	Prototype 1 reference film
$P1N$	Prototype 1 nanofilm
$\boldsymbol{P(t)}$	Polarization as a function of time
P_L	Power losses
Q	Charge
Q_R	Reactive power of capacitor
R_a	Current viewing resistor
R_c	Leakage resistance
R_d	Polarization resistance
R_{ESR}	Series resistance
R_{series}	Series resistance
R_s	Contact losses
R_{sr}	Sheet resistance of the electrode
R_∞	Steady state (DC) resistance
s	Experimental constant
T	Temperature
T_g	Glass temperature
T_m	Melting temperature
U	Voltage
U_b	Breakdown voltage
w	Energy density
W	Total energy
X	Electric stress
x	Electric stress
X_c	Capacitive reactance
α	Weibull parameter (time to reach 63.2% probability of failure)
$\alpha(P)$	A function which relates the interlayer pressure of a capacitor to the cleaning energy
β	Weibull parameter (measures spread of the data)
ε	Permittivity
ε_0	Permittivity of vacuum
ε_r	Relative permittivity
ε_s	Steady state permittivity
ε_{sr}	Relative steady state permittivity
$\underline{\varepsilon}$	Complex permittivity
ε'_r	Real permittivity
ε''_r	Imaginary permittivity
σ	Electrical conductivity

σ_e	Electrical conductivity of electrons
σ_{ion}	Electrical conductivity on ions
σ_o	Pre-exponential factor
ρ	Resistivity of the material
τ_d	Dielectric relaxation time
$tan(\delta)$	Loss factor
ω	Angular frequency
χ	Electric susceptibility

1. INTRODUCTION

While the majority of electrical power nowadays is generated in centralized power stations and transported via AC transmission lines, this type of power infrastructure may undergo considerable changes in the future as the demand for renewable energy sources increases. It is already generally acknowledged that AC transmission does not always provide the optimum method for integrating distributed energy production into power transmission networks. One of the main reasons for this is that the distances over which AC power can be transmitted through underground or undersea cables are limited. Much better suited to this task are High Voltage Direct Current (HVDC) systems, which in addition to longer transmission distances, have greater capacity/size and can also be used to connect unsynchronized AC systems. As the overall cost of HVDC transmission has steadily declined, it is not surprising that their role in electrical power transmission has grown. [21] Nevertheless, there are still technical, economic, and safety concerns that are hindering the large-scale adoption of HVDC technology. The materials that are used to insulate energized components at different potentials are associated with each of these factors.

Increasingly often, modern electrical insulating materials are produced from polymers. However, primarily due to differences in space charge behaviour, many of the current insulating materials that have been manufactured for AC technology may not be suitable for DC use [14]. Therefore, the materials used for HVDC applications, such as power cables and capacitors, are usually specially designed for the purpose. For power capacitors, the expected lifetimes are long and the reliability requirements extremely high. Despite the prerequisite of a very low failure probability over the operational life, even higher operating electric fields are sought to increase the energy densities of power capacitors. In order to meet the desired requirements, new polymeric materials are continuously being studied. One recent development is in materials that incorporate nanometric fillers. However, before such materials can be adopted for a mains power grid, they must be thoroughly tested to ensure that they conform to their application-specific requirements (e.g. a 30-year lifetime with a failure probability of less than 1%). It is the testing of such newly developed materials that forms the basis for this thesis

This thesis was carried out under the aegis of the EU-funded Horizon 2020 project, a.k.a. the GRIDABLE project, wherein polypropylene-silica nanocomposites are studied. The

project aims to research and develop cost-efficient, reliable, and safe electrical insulating materials that can be used in the smart grids and industrial applications of the future. The principal idea of the thesis is to investigate the long-term DC dielectric strength of these new materials, and compare them with the established ones. More specifically, the particular focus of this study is to evaluate the lifetime of biaxially oriented polypropylene (BOPP) dielectric films used in metallized HVDC power film capacitors. Therefore, the dielectric films were tested in an inert, oxygen-free ambient environment under long-term DC electro-thermal stress utilizing the self-healing capability of the metallized films. In the literature, these experiments are generally referred to as endurance tests. The purpose of these endurance tests, however, is not merely give a stamp of approval to materials that pass the short-term, high-stress testing. Instead, the objective is to establish any link between high- and low-range electric stresses, so that the lifetime of a material at lower operating stresses can be predicted using a mathematical lifetime model. Assuming that both the mathematical model and the measured data are adequate, the results can be used to determine whether an insulating material may withstand a particular level of in-service stress for a specified lifetime (e.g. 10-30 years).

Before any actual measurements could be carried out, a review of the literature on the accelerated testing of electrical insulating materials was conducted. These findings are presented in the first part of this thesis. In Chapter 2, the theories behind dielectric materials (i.e. substances used in electrical insulating applications) under electric fields are introduced. These include phenomena such as polarization and electrical conductivity. Chapter 3 introduces the fundamental properties of polymers which are now commonly used as dielectric materials. The chapter also includes a short overview of the structure of metallized film capacitors. Chapter 4 presents a discussion of our current knowledge of dielectric strength, mainly with reference to solid polymeric materials. Additionally, the principles of accelerated testing and the fundamentals of lifetime modelling are reviewed. In the second part of the thesis, the experimental research plan is described in detail in Chapter 5, and the results of the measurements are presented in Chapter 6. A summary of the findings, and the main conclusions, are presented in Chapter 7.

2. DIELECTRICS UNDER AN ELECTRIC FIELD

2.1 Polarization

An electric field ***E*** (V/m) applied across a material produces a force on the charged particles. The charges that are not bound to the material may become electrically conductive. In good electrical conductors, such as metals, the charge carriers are weakly bound. Conversely, in poor electrical conductors (especially in electrical insulating materials), the electric charge carriers are tightly bound in the molecular structure and can only shift a small distance from their equilibrium positions. This displacement of positive and negative charges under an electric field creates an electric dipole whose magnitude is measured by the electric dipole moment. In dielectrics, however, this excitation of the electric field may result in the formation of a high number of dipoles. Therefore, a material's response to an external electric field is characterized by a macroscopic quantity known as *polarization,* which expresses the average electric dipole moment density within a unit volume. In order to compare this behaviour in different materials, two variables called *electric susceptibility* and *electric permittivity* are used. [22]

Electric permittivity is a parameter that connects the electric field, ***E,*** to the *dielectric flux density,* ***D*** (C/m^2). In contrast, electric susceptibility connects ***E*** to the polarization, ***P.*** The difference between an electric field and the dielectric flux density is that the electric field is influenced by polarization, whereas the dielectric flux density is caused by free charges and is unaffected by the polarization. There is a further link between the dielectric flux density and the electric field, which is that an electric field in the material may be determined from free charges alone using a static (2-1) or a time-varying voltage (2-2):

$$\boldsymbol{D} = \varepsilon_0 \varepsilon_\mathrm{r} \boldsymbol{E}, \tag{2-1}$$

$$\boldsymbol{D}(t) = \varepsilon_0 \varepsilon_\mathrm{r} \boldsymbol{E}(t), \tag{2-2}$$

where ε_0 is the permittivity of a vacuum (approx. $8.854 \cdot 10^{12}$ F/m) and ε_r is the relative permittivity (dimensionless). These equations only hold true if the material is isotropic and linear. The dielectric flux density can also be expressed as

$$\boldsymbol{D}(t) = \boldsymbol{P}(t) + \varepsilon_0 \boldsymbol{E}(\boldsymbol{t}), \tag{2-3}$$

a substitution of which leads to the polarization equation

$$\boldsymbol{P}(t) = \boldsymbol{D}(t) - \varepsilon_0 \boldsymbol{E}(t) \tag{2-4}$$

$$= \varepsilon_0 (\varepsilon_\mathrm{r} - 1) \boldsymbol{E}(t) \tag{2-5}$$

$$\boldsymbol{P}(t) = \varepsilon_0 \chi \boldsymbol{E}(t), \tag{2-6}$$

where χ is ($\chi = \boldsymbol{\varepsilon}_r - 1$). This is called the electric susceptibility and it depends on time. According to Equation (2-6), polarization can only occur when an electric field is applied. Even though the polarization and the electric field both depend on time (Equation 2-6), their time-dependency is not the same, since different polarization processes have different time-delays. The following section uses a parallel plate capacitor to demonstrate how polarization changes as a function of time. [25][23]

2.1.1 Dielectric permittivity and the discharging of electrodes

A capacitor is a device that contains two parallel electrodes separated by a distance, *d*. If edge effects are ignored, the electric field between the electrodes is uniform and its magnitude is given by

$$E = \frac{U}{d}. \tag{2-7}$$

Once a voltage is applied (assuming a fixed DC step voltage is applied across the electrodes) the electrons move from one electrode to another until the total charges have equal magnitude and opposite signs. This process is known as capacitor charging. Capacitance (*C)* is the accumulated charge (*Q)* divided by the applied voltage (*U):*

$$C = \frac{Q}{U}. \tag{2-8}$$

If the capacitance is first measured without a dielectric material (C_o) and then with a dielectric layer inserted between the electrodes (C), the relative permittivity (ε_r) is given as the ratio of the capacitances:

$$\varepsilon_r = \frac{C}{C_0} = \frac{Q+P}{Q}, \tag{2-9}$$

where *P* is the polarization. An increased charge with the dielectric slab placed between electrodes is depicted in Figure 2.1.1 (b). In the literature, relative permittivity is often called the dielectric constant. [2]

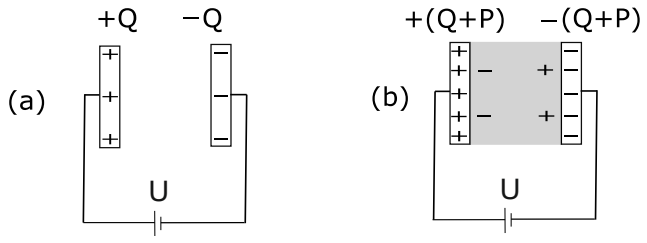

Figure 2.1.1*. Polarization in a parallel plate capacitor: (a) in a vacuum and (b) with a dielectric between the electrodes [2].*

The above example assumes that all the polarization processes have had enough time to take place when a dielectric material is placed between the electrodes and a voltage is applied. It is only then that the measured permittivity represents its maximum, steady-state value, ($\varepsilon_s = \varepsilon_{sr} \cdot \varepsilon_0$). Even though this process takes time and varies for different materials, the permittivity always increases gradually from a vacuum to a steady state. In practice, this is often modelled as a two-step process in which the fast and slow mechanisms make separate contributions to the polarization. For the fast polarization mechanisms, the delay between the initiating electric field and polarization (i.e. transition time) is negligible. However, for slow polarization mechanisms, this delay can be quite long. Thus, fast polarization mechanisms will at first increase the permittivity from the relaxed state (~0) to the vacuum permittivity (ε_∞) almost instantly (t=0 s). Thereafter, the slower polarization processes gradually increase the permittivity to the steady state with time (t_s). Both transitions occur in a lossy medium and therefore result in dielectric losses. Changes in permittivity, polarization, and dielectric losses as a function of time are shown in Figures 2.1.2 (a) and (b).

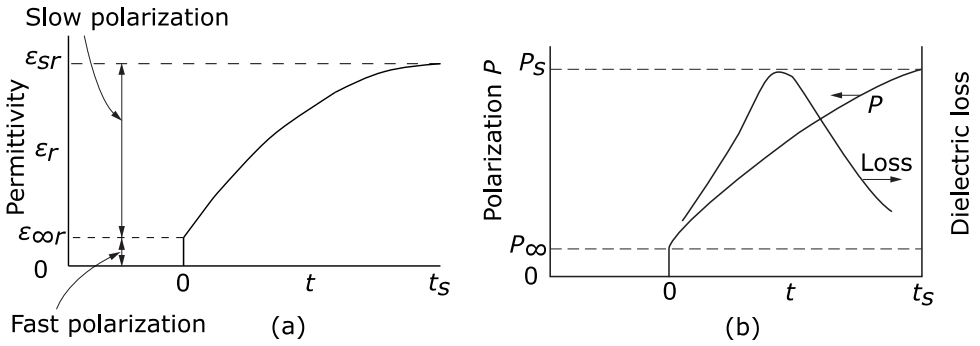

Figure 2.1.2. *(a) Permittivity versus time and (b) polarization versus dieletric loss. Adapted from [22].*

Once the polarization build-up is complete, no further changes occur as long as the electric field is maintained. However, once the electric field is switched off, the polarization starts to decay. This process is termed *depolarization*. As in the polarization process, depolarization occurs in two stages. At first, the fast depolarization mechanisms decrease the polarization immediately, although not completely. Thereafter, the slow depolarization mechanisms gradually reduce the polarization back to zero. These two stages further resemble the two stages in *polarization* because the mechanisms that are responsible for fast polarization are the same ones that are responsible for fast depolarization and, likewise, the slow polarization mechanisms are the same as the ones that are responsible for the slow depolarization. For this reason, depolarization is also called relaxation, referring to the restoration of the polarization as the electric field is switched

off. Figure 2.1.3 shows both processes in this reverse behaviour of the depolarization process. [22]

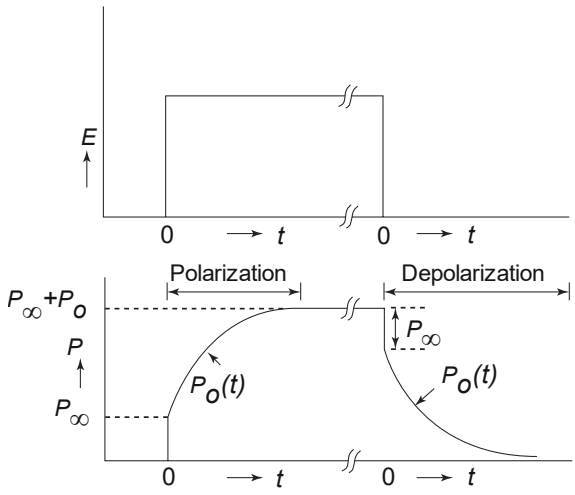

Figure 2.1.3. *Polarization and depolarization under a step-function electric field. Adapted from [22].*

The depolarization behaviour of a material determines how rapidly the material will restore itself to its relaxed state, and thus, how rapidly any charges are discharged from the material. It is because of the slow depolarization that not all of the charges are neutralized, even if a capacitor is briefly short-circuited. In theory, only the free charges on a plate are discharged, but in practice, the fast depolarization mechanisms, and some of the slow ones, relax very rapidly. Consequently, some of the charges which the polarization processes have bound are neutralized instantly. The leftover charges, however, can recharge the electrodes and cause recovery voltage. Nevertheless, even these charges will diminish with time, since all electrical insulating materials have finite conductivity. [22]

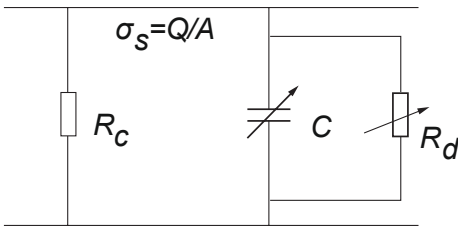

Figure 2.1.4. *The equivalent circuit of a dieletric material. Adapted from [22].*

In order to model the charge depletion from a dielectric (i.e. its self-discharging rate) an equivalent circuit, as shown in Figure 2.1.4, may be used. This model has constant leakage resistance (R_c), time-varying capacitance (C), and time-varying polarization resistance (R_d). As mentioned above, the capacitance varies as a function of time because the fast and slow (de)polarization processes contribute to the permittivity over different

time scales. Since polarization causes time-dependent power losses, polarization resistance is not constant either. Nonetheless, once the polarization reaches a steady state, the capacitance and polarization losses remain the same. Thus, no polarization losses are generated, and the capacitance is at its maximum static value (corresponding to ε_s). It can be shown that the charge decay as a function of time, *t,* is given by the equation 2-10:

$$\sigma_s(t) = \sigma_s(0)e^{-t/\tau_d}, \tag{2-10}$$

$$\tau_d = p * \varepsilon_s, \tag{2-11}$$

where τ_d is the dielectric relaxation time (a time constant that is required for the originally induced charge to decay to 36.7% of its original value) and ρ is the resistivity of the material. For some materials, it may take days for all the charges to drain away. [22]

2.1.2 Polarization and depolarization current

When electrodes are (dis)charged, an external circuit carries a measurable current. This corresponds to current density *J(t)* (A/m^2) in dielectrics and it has three contributory factors:

$$J(t) = \sigma E(t) + \varepsilon_0 \frac{dE(t)}{dt} + \frac{dP(t)}{dt}. \tag{2-12}$$

The first part on the right-hand side of the equation represents the (volume) *conduction* current, the middle part is the *vacuum displacement* current, and the third part is the (de)*polarization* current. [50] Any external current depends on how polarized (or relaxed) the material is initially and how the material will (de)polarize under the applied electric field. In the following example, it is assumed that: (1) the dielectric material is not polarized before the step-up voltage is applied, (2) the voltage is applied for long enough for all the polarization phenomena to be completed, and (3) the test object is short-circuited once the polarization is complete. Figure 2.1.5 illustrates the charging and discharging currents as a function of time according to these assumptions. Their behaviour is discussed further below. [22]

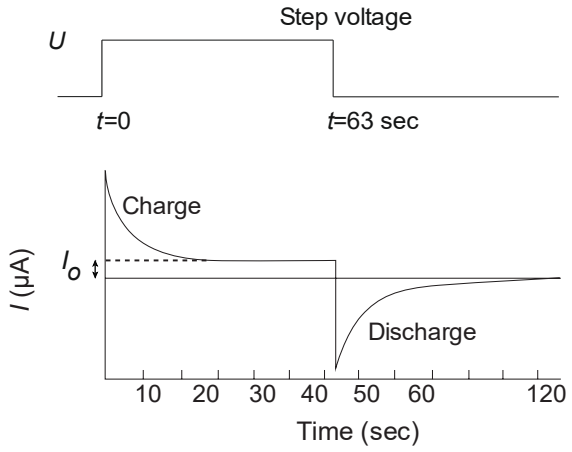

Figure 2.1.5. *Insulator current versus time [22].*

The charging current attenuates because of the movement of the charges related to the vacuum displacement and the completion of the polarization processes. Since the vacuum displacement declines fastest, the charging current is mainly composed of the polarization current, which diminishes at a slower rate. In ideal dielectrics, there would be no measurable current once polarization is complete. Nevertheless, in reality, a small residual current remains due to the continuous leakage of charges. Hence, a constant voltage is needed to preserve any charges on the electrodes. If the test object is short-circuited, then the reverse discharge current, which is related to charge decay (depolarization) from the electrodes, will flow. In this case, the current vanishes entirely once the depolarization processes are complete. In essence, the profile of the inverted discharge current is the same as the charging current except for the fact that it lacks any residual conduction current. [22]

The (dis)charging current of a dielectric may be modelled using equivalent electrical circuits. As mentioned earlier, due to various (de)polarization processes, the corresponding charge accumulation and depletion occurs at different rates. The fastest rate is the formation of the vacuum capacitance, which can be modelled by a vacuum capacitance (C_0 in the equivalent circuit, Figure 2.1.6). Any subsequent fast and slow (de)polarization processes are accounted for by the separate parallel-connected RC-elements. The final steady-state DC conduction is represented by a resistance (R_∞). [24] Unlike in Figure 2.1.5, the conduction current in real polymers is not necessarily constant. It has been shown that even after long measurement times (hundreds of hours), the current may still fluctuate [17].

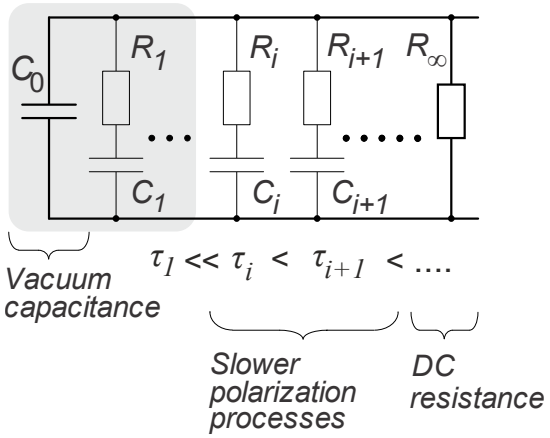

Figure 2.1.6. *Equivalent circuit representation of polarization in time domain [24].*

2.1.3 Polarization mechanisms

The previous sections have shown that the relative permittivity of a dielectric material increases at varying rates due to differences in the completion times of the polarization mechanisms. This section reviews the fundamentals of these mechanisms for solid materials. A material's real polarization behaviour can be rather complex because its atoms and molecules may affect its polarization behaviour. However, there are essentially five different types of polarization: (1) *electronic*, (2) *atomic*, (3) *oriental*, (4) *hopping* and (5) *space charge* polarization. Figure 2.1.7 shows the approximate completion times of these processes for a step-function electric field. As mentioned above, these values are approximate because an accurate description of the polarization behaviour is contingent upon the particular material's properties and its state of matter. [22]

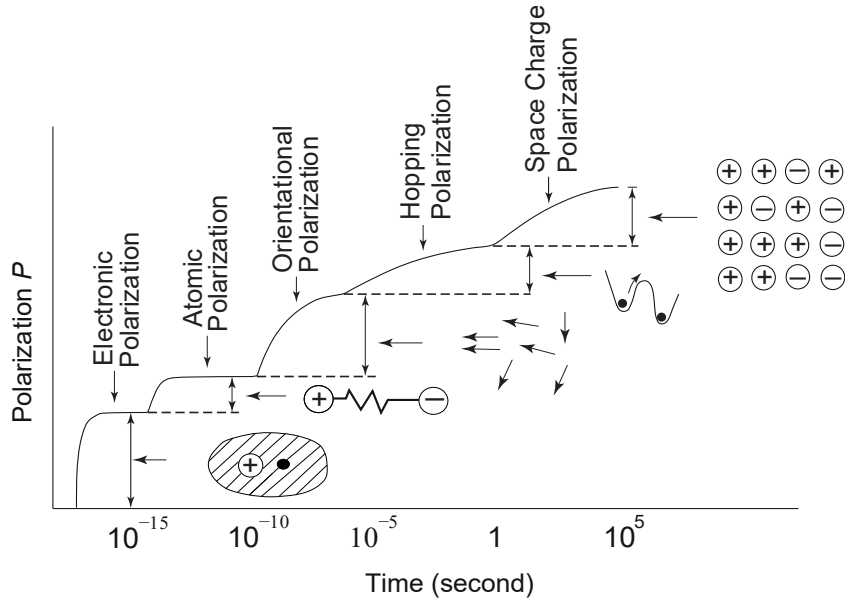

Figure 2.1.7. *Polarization versus time as a step-function voltage has been applied at t=0 s [22].*

A classical view of the material is that a solid substance has an atomic nucleus where the center of the atom consists of positively charged protons and neutral neutrons. In a neutral atom, the number of electrons orbiting the nucleus is equal to the number of protons in the nucleus. Without an electric field, the net charge of a neutral atom is zero, and the positive and negative charges are located so that there is no net average dipole moment. When an electric field is applied, the electrons are displaced by short distances relative to each other and a net average dipole moment is formed. Polarization, however, is not only restricted to the shift of the electrons within an atom. The valence electrons in the covalent bonds and the ions in the ionic bonds may be rearranged as well. [22][23] Therefore, three different polarization types may arise from the displacement of the charges.

(1) The fastest polarization mechanism is *electronic polarization*. It arises as the negative electron clouds are shifted from the positively-charged center. (2) The formation of *atomic polarization* is analogous to electronic polarization. The only difference is that in atomic polarization, the ions of the polyatomic molecules (not the electron clouds) are displaced relative to each other. Both electronic and atomic polarization are independent of temperature and are considered *fast (instant)* polarization mechanisms. (3) *Oriental polarization* represents the first slow polarization process. It may occur only in molecules that have *permanent dipole moments*. Without an electric field, these dipoles are randomly oriented because of thermal agitation. Once an electric field is applied, the dipoles are aligned in the direction of that electric field, and there is a net average dipole moment. [22][23]

While the first three polarization mechanisms are caused by the finite displacement of the charges, the remaining two polarization mechanisms have a different origin. Fundamentally, these mechanisms arise from the migration of positively and negatively charged particles (ions and vacancies, or electrons and holes). In *hopping polarization*, the charged particles may move from one site to the next, but they will eventually end up trapped in some localized state. Once they are trapped, these charges act similarly to electrical dipoles and induce polarization. In *space charge,* or *interfacial polarization*, the accumulation of the charge carriers may occur either (1) at an interface between two materials (e.g. dielectric-metal interfaces) or (2) within two regions in the bulk of the material (e.g. crystalline areas separated by amorphous areas in polymers). Interfacial polarization is an important phenomenon because charge separation will modify the distribution of the electric field. Interfacial polarization at dielectric-metal interfaces is depicted in Figure 2.1.8 and is discussed further below. [22][23]

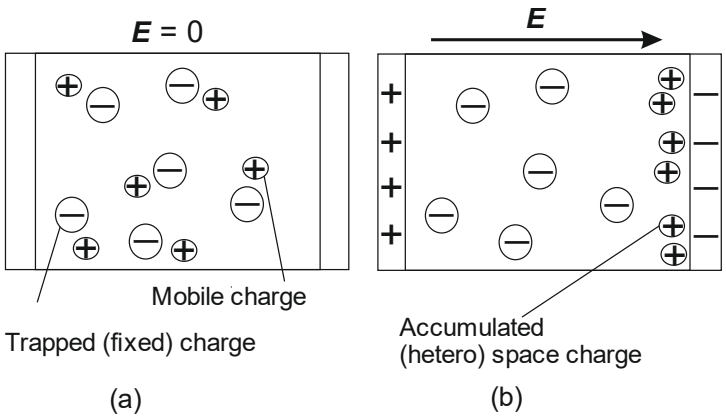

***Figure 2.1.8**. Interfacial polarization. Adapted from [23].*

Without an electric field, there is no gap between the charges (Figure 2.1.8 a). Once an electric field is applied, the trapped charges can't move so they remain where they are. In contrast, the mobile charges can migrate but they will end up trapped between the dielectric-metal interfaces (Figure 2.1.8 b). This separation of the charges at the dielectric-metal interfaces produces more dipole moments and thus increases the polarization. Consequently, more charges (bound by the polarization process) will appear in the electrodes. As a result, the capacitance of the material increases. [23] Any distortion of the local electric field, however, may have drastic consequences, since an insulating material can only stand a certain degree of electric stress before it will fail. Whether the electric field is enhanced or diminished depends on the polarity of the charge compared to the adjacent electrode. The charges in Figure 2.1.8 (b) are termed hetero-charges because they have opposite polarity to the electrode. These hetero-charges may significantly enhance an electric field at the dielectric-metal interface; although the electric field in the bulk of the material is diminished. If the charges have the same polarity as the electrode, they are called homo-charges. Homo-charges will diminish the electrode's field, but enhance the bulk one [5][14][24]. Finally, it is important to note that the build-up of a local space charge cannot be accurately assessed merely by measuring permittivity, because the polarization includes all the dipoles within the material per unit volume. Consequently, if only a small amount of local space builds up, additional dipoles may indeed form, but this effect is averaged out within the unit volume.

2.1.4 Frequency domain approach and dielectric losses

Thus far we have discussed how a step electric field influences polarization build-up (and decay), and consequent changes in permittivity, specifically in a time domain. Another approach is through the frequency domain, in which dielectric permittivity is measured for alternating electric fields of different frequencies. Although the actual measurement is different, these approaches are not mutually exclusive, and they should produce the

same results once the appropriate mathematical relationships are applied. The fundamental link is provided by the Fourier transformation, which expresses a continuous, arbitrary time-varying electric field in terms of the frequencies of different sinusoidal AC fields. These conversions are not covered here (introduced in [32]), since from the measurement viewpoint, it is enough to know how energy losses and permittivity behave under alternating fields electric fields. [22] In the literature, this is called the dielectric system response [24].

When an alternating electric field is applied across a dielectric material, there is a phase shift between polarization and the initiating electric field. The degree to which the electric displacement lags the electric field is given by the following equation:

$$D(t) = \underline{\varepsilon} E(t), \tag{2-13}$$

where $\underline{\varepsilon}$ is complex permittivity

$$\underline{\varepsilon} = \varepsilon' - j\varepsilon'' = (\varepsilon_r' - j\varepsilon_r'')\varepsilon_0. \tag{2-14}$$

In Equation (2-14), ε_r' is the relative permittivity, which is used to calculate the capacitance of a capacitor (the real part) and ε''_r (the imaginary part) is associated with the polarization losses. As all electrical insulating materials conduct electricity to a certain degree, there will be some Ohmic losses. For AC fields, the polarization of the material induces another source of loss, e.g. due to molecular friction. [24]

In order to represent the efficiency of dielectrics, a *loss factor* or *dissipation factor* (*tan δ)* is defined and is given by the following equation

$$\tan\delta = \frac{\sigma + \omega\varepsilon_0\varepsilon_r''}{\omega\varepsilon_0\varepsilon_r'}, \tag{2-15}$$

where σ is conductivity and ω angular frequency ($2\pi f$). In this context, complex permittivity represents the dielectric material's active (lossy) part and reactive power the (lossless) part. In the numerator, the first part represents conduction losses and the latter part polarization losses. If conduction losses are neglected, the loss factor is

$$\tan\delta = \frac{\varepsilon_r''}{\varepsilon_r'}. \text{ [24]} \tag{2-16}$$

Both permittivity and polarization losses depend on the frequency of the field (referred to as *dispersion*). If the field is alternating too rapidly, polarization processes cannot keep pace with the changes. As a result, the permittivity equals that of a vacuum field, and the loss factor tends to diminish. At lower frequencies, a variety of polarization mechanisms are possible, and thereby both permittivity and dielectric losses increase. The dispersion

is illustrated in Figure 2.1.9. In real life, however, the peaks in ε'' and the transition zones in ε'_r are broader than the ones depicted below. [23]

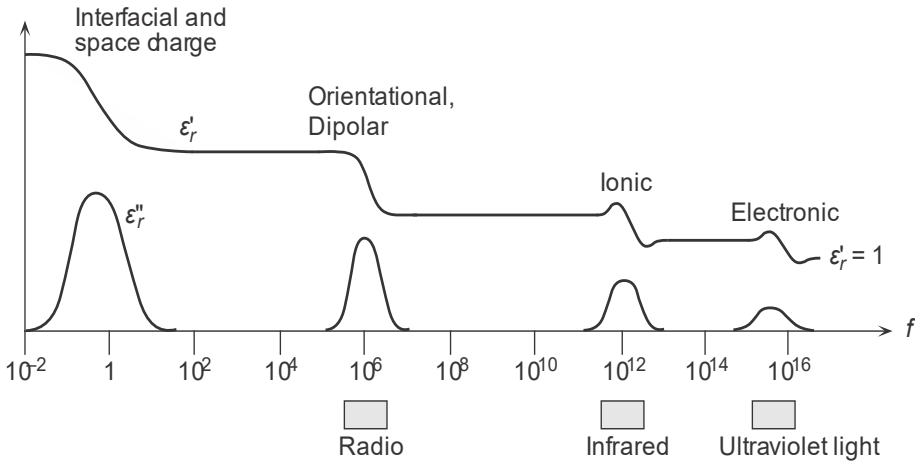

Figure 2.1.9. *Real and imaginary parts of the dielectric constant as a function of frequency [23].*

2.2 Conductivity

2.2.1 Conduction mechanisms

As discussed earlier in Section 2.1.2, electrical insulating materials do have a small conduction current under a DC field. Based on their electrical conductivity, materials can be classified into conductors, semiconductors, or insulators. The electrical conductivity (σ) for a material may be given as

$$\sigma = q\left(\mu_n n_n + \mu_p n_p\right) + q(\mu_- n_- + \mu_+ n_+) \tag{2-17}$$

$$= \sigma_e + \sigma_{ion} \tag{2-18}$$

where q is the electric charge, n is the concentration (m^{-3}) and μ the mobility ($m^2V^{-1}s^{-1}$) of the charge carrier. The subscripts are for electrons (n), holes (p), negative ion species (–) and positive ion species (+). Fundamentally, Equation 2-17 states that conductivity is not only affected by the amount of charge carriers, but also by their rate of movement. [22]

The type of charge carrier affects how a charge moves in a material, i.e. its conductivity. Basically, these processes can be divided into three different mechanisms: *intrinsic conductivity*, *extrinsic conductivity*, and *injection-controlled conductivity*. Whereas the intrinsic conductivity depends on the chemical properties of the dielectric material, the extrinsic conductivity depends on any impurities in the material. Injection-controlled conductivity refers to conduction in which charge carriers are injected from outside of the dielectric material, usually from metallic electrodes, through a metal-dielectric interface. [22]

The determining mechanisms are governed by the insulating material, the electrode material, the temperature and the electric field [24].

2.2.2 Low and high field conduction in polymers

In a good polymer insulator, there is hardly any electrical conduction. However, the conduction mechanisms in solid polymers are still not thoroughly known. For metals and semiconductors, electrical conductivity can be explained by the energy band theory. The same cannot be said for polymers because of their structure. In polymers, an electronic transfer may occur *intramolecularly* or *intermolecularly*. It is assumed that although energy band theory may apply to intramolecular structure, it does not apply to intermolecular structure. [22]

The intermolecular structure of polymers is rather random. Hence, extended states are far apart, and the energy required to cross a band gap is high. As no material is perfect in reality, structural and chemical imperfections create localized states that are accessible for charge carriers in the forbidden gap. Localized states are commonly referred to as trap states since charge carriers may end up trapped there. These arise due to potential wells in the interfaces of different permittivities and conductivities [22]. Depending on the trapping energy, there are two types of traps. Shallow traps are those associated with lower energy levels, whereas deep traps have higher energy levels. The density level of deep traps is, however, lower than it is in shallow traps, as is shown in Figure 2.2.1. [56]

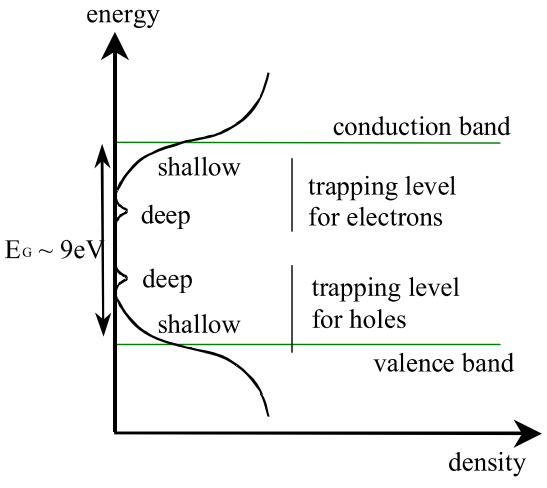

***Figure 2.2.1**. Trap densities and energies in a dielectric material [56].*

The effects of shallow and deep traps are different. Since the energy levels of the traps determine the charges' residence times in the traps, shallow traps may capture charges for less than a second due to their lower energy levels. In contrast, deep traps may keep

them almost indefinitely. Thus, it is generally accepted that shallow traps assist conduction by enabling “hopping" for charges that are injected or are already present in the insulation. [56] These traps may be in the polymer because of ionic impurities arising from the fabrication processes, or they may be generated by different charging processes [14]. Deep traps contribute notably less towards conductivity, and in fact, may decrease conductivity either by holding the charge carriers in the traps or by acting as recombination centers [22][57].

In addition to the composition of the material, the dominant conduction mechanism depends on the applied physical parameters, such as stress duration, electric field strength, and temperature. Both temperature and electric field strength increase conductivity. In low electric fields (**<10 V/µm**), electrical conduction in *polypropylene* is thought to be caused by impurities in the material caused by the fabrication processes (e.g. residual catalysts). These may provide a small number of charge carriers in the form of ions (ionic hopping). Furthermore, conductivity is generally more temperature-dependent in low fields and follows the Arrhenius function:

$$\sigma = \sigma_0 e^{\frac{-E_\sigma}{kT}}, \tag{2-19}$$

where σ_0 is a pre-exponential factor, E_σ is the activation energy (eV), k is Boltzmann’s constant, and T is the temperature (in kelvin). At higher field strengths (**>10-15 V/µm**), conductivity is due to electron hopping from one trap to the next and is field-dependent. Conductivity for three different temperatures as a function of electric field for biaxially oriented polypropylene film is shown in Figure 2.2.2. [19]

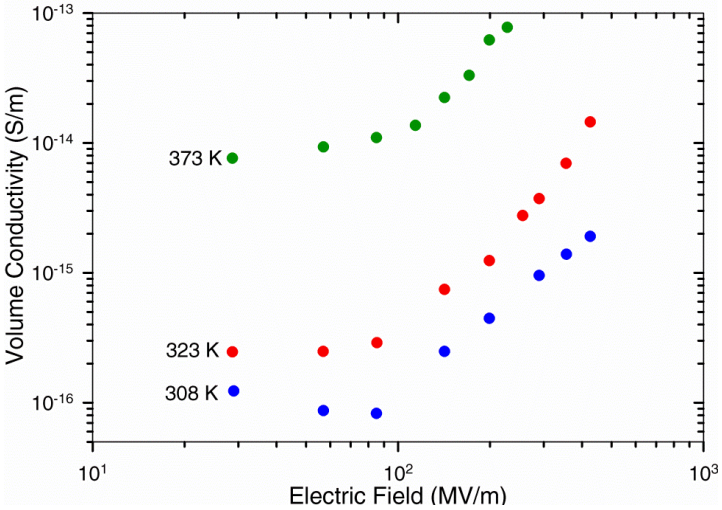

***Figure 2.2.2**. Electrical conductivity versus electric field at three temperatures in 7 µm thick biaxially oriented polypropylene film [19].*

3. POLYMERS

Polymeric materials are often used in electrical insulators. One of the most common applications is a power capacitor in which the polymer forms a dielectric film between the electrodes. Fundamentally, polymers are large macromolecules composed of several small repeating molecules, commonly termed repeating units. They form the backbone of the polymer molecule by establishing covalent (carbon) bonds with the adjacent repeating unit. As the number of repeating units increases, they form chain-like lamellas which are bound by inter-molecular Van Der Waals forces, and in specific polymers, by covalent cross-links. These lamellas will stack up and form ordered structures, referred to as crystallites. One such structure is called spherulite. Spherulites are common in semi-crystalline polymeric materials such as polypropylene, which is composed of non-ordered amorphous parts between ordered crystallites. This structure is depicted in Figure 3.1. [44]

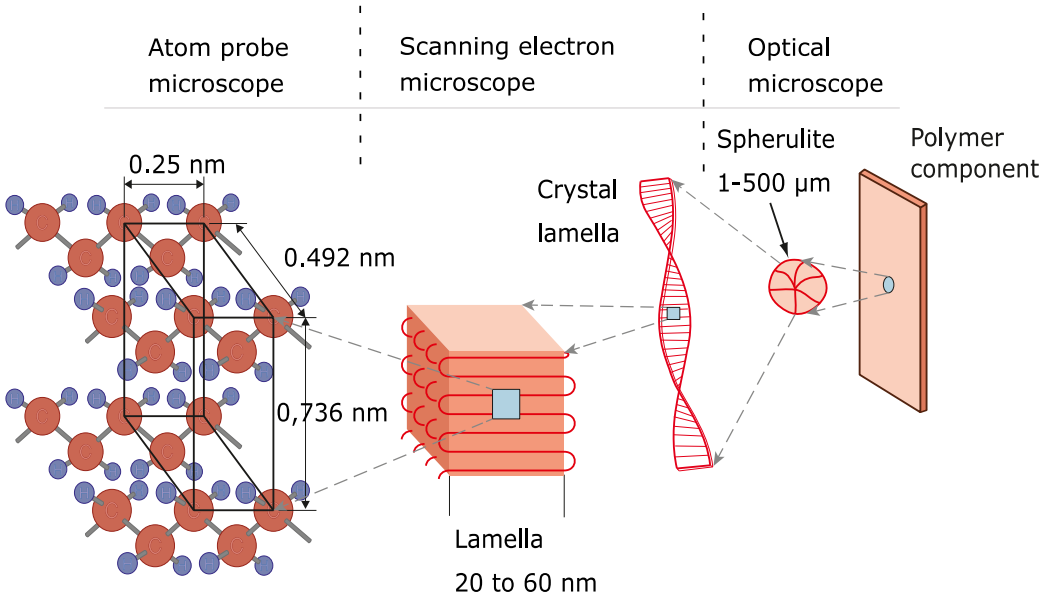

Figure 3.1. *Schematic representation of the general molecular structure in a semi-crystalline polymer. Adapted from [44].*

The following sections will describe the fundamental aspects of the polymer structure in more detail, firstly by reviewing repeat units and the orientation of polymer chains, then by looking at phase transitions and polymer crystallization, and finally, by focusing on polymer additives and the specific properties of biaxially oriented polypropylene.

3.1 The molecular characteristics and structure of polymers

3.1.1 The repeat unit

As polymer molecules consist of long repeating chains, their chemical structure is presented using a *repeat unit.* In Figure 3.1.1, the repeat unit for polypropylene is the molecular block inside the parentheses, and the subscript, *n,* represents how many times it appears in the chain. The total number of repeat units in the polymer chain is also termed the *degree of polymerization* (DP). Due to randomness in the polymerization reaction, not all polymer chains are the same length. As the chain length affects the polymer's properties (e.g. mechanical strength), it is necessary to express the average chain size of the polymer. [3][44]

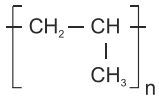

Figure 3.1.1. *Repeat unit of the polypropylene [51].*

The size of the polymer chain can be calculated statistically or by using an average molecular weight. The averaging approach, however, is not unambiguous, since there are multiple definitions for how to calculate average molecular weight and they all give a slightly different result. One of these formulas is expressed as

$$DP = \frac{M_{avg}}{m} \tag{2.1}$$

where M_{avg} is the average molecular weight and m is the molecular weight of the repeat unit. [3][44]

3.1.2 Chain structure

Atoms in a polymer chain are capable of rotating and bending in three dimensions. In a straight-chain segment, there is a 109° angle between carbons (Figure 3.1.2), which results in a zigzag arrangement between the backbone atoms (Figure 3.1.2 b). Since the atoms in the backbone may rotate, polymer chains are not straight but will twist into different positions (Figure 3.1.2 c). As a result, the polymer backbone may become rather complicated. [3]

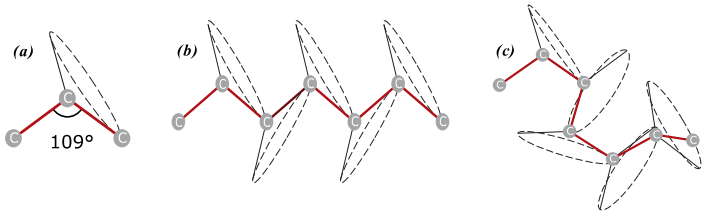

Figure 3.1.2. Shape of a polymer [3].

Even though the backbone of a polymer may twist and bend, polymers do have consistency in their chain structures. Figure 3.1.3 illustrates four types of chain structures: (1) Linear, (2) Branched, (3) Cross-linked, and (4) Entangled. The *Linear* structure is a cascade structure, in which the molecular chains are bent but not connected. In the *branched* structure, the branches appear in the main chains. The *cross-linked* polymer has chains that are connected to each other by covalent bonds. In the entangled chain structure, linear molecules are twined together by van der Waals forces, which creates multiple twist and kinks between the polymer chains. [12]

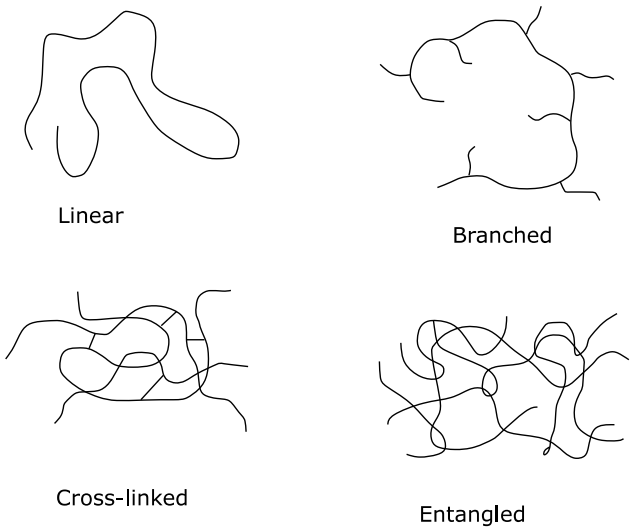

Figure 3.1.3. *Chain structures in polymers [12].*

3.2 Polymer crystallinity and phase transitions

For certain crystalline solids, such as metals or ionic crystals, the atoms are generally repeated in the same, ordered manner. Polymers are peculiar materials in that they do not have a regular crystallized structure. Instead, their structure consists of ordered crystallized regions separated by amorphous regions wherein the polymer chains are arranged randomly. Polymers that have sufficient volumes of both regions are referred to as *semi-crystalline*. Highly crystallized polymers are referred to as *crystalline* polymers, while sparsely crystallized polymers are *amorphous*. These three polymer types are illustrated in Figure 3.2.1. Since polymer crystallization occurs during solidification, in addition to its chain configuration and chemistry, the *degree of crystallinity* depends on the rate of cooling.

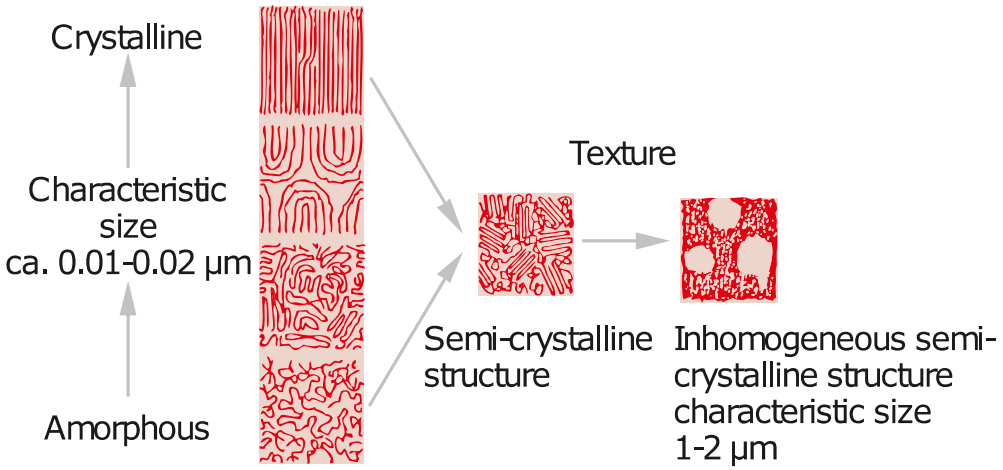

Figure 3.2.1. *Crystalline, amorphous and semi-crystalline polymers [44].*

The degree of crystallinity influences a polymer's properties. One characteristic is how crystalline, semi-crystalline or amorphous polymers react to heating and cooling. When polymers undergo a change in temperature, a transformation from one state (solid, elastic, and liquid) to another may occur. These transition points are termed *glass* (T_g) and *melting* (T_m) temperatures and are shown in Figure 3.2.2. A **melting** transition is a property exhibited by a crystallized polymer. When the temperature of the polymer rises above *Tm*, polymers turn from a solid into a viscous liquid. At the melt state, the polymer structure is disordered, and there is a sudden increase in volume at the melting point. **Glass** transition is possible only for amorphous and semi-crystalline (its amorphous part) polymers. If polymers are cooled from their liquid state, the motion of the molecular chains is reduced, and the polymers become rubbery. If the cooling is continued below the glass temperature, the polymers turn into a solid (brittle glass). Crystallized polymers do not have a rubbery state as when they are cooled below their melting temperature they become solid. [3]

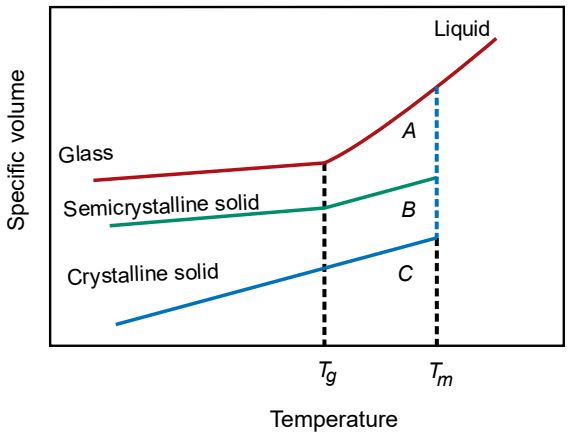

Figure 3.2.2*. Thermal transition in polymers [3].*

In real polymers, however, the thermal transitions are not as distinct as they are in theory. For example, melting does not occur at only one temperature but takes place over a

range of temperatures. There can be many reasons for this. First, polymers have a range of molecular weights which melt at different temperatures. Second, the heating and cooling rate will modify the melting behaviour of the polymer. Finally, the thermal history of the specimen affects its melting behaviour. For instance, the melting temperature is higher if the lamellae are thicker. Lamellar thickness can be increased by *annealing,* i.e. heat-treating the polymer to near its melting temperature and then slowly cooling it. Annealing can influence a polymer's structure by decreasing the number of vacancies and imperfections.[3]

3.3 Additives

Some polymer properties are related to their molecular structure, and therefore such properties are intrinsic to specific polymers. A polymer's properties can be modified (improved) by introducing foreign substances i.e. additives. There are a variety of additives for different purposes, such as fillers, plasticizers, stabilizers, colourants, and flame retardants. Traditionally, a polymer's mechanical and thermal properties can be improved with the use of micrometric fillers. [3] Polymers containing fillers are also called composite materials. An issue with micro-fillers has always been that, even though the material's other properties (e.g. mechanical) may be successfully enhanced, they tend to lower the dielectric strength of the polymer. [51]

It has been suggested that fillers with nanometric dimensions could mitigate this problem, paving the way for a variety of multifunctional materials. It is thought that the differences between the properties of micro- and nano-metric sized particles will be caused by the increased surface area wherein the nanoparticles can interact with the base polymer matrix. Any chemical reaction is fundamentally linked to the surface-area-to-volume ratio of a polymer. It this ratio increases, then the material's reactivity will increase. Thus, a polymer's properties could be modified by changing the properties of the interaction zone - particularly the size of the surface area. The particles of the filler must be uniformly spread throughout the material in order to ensure its homogeneity. In practice, fillers are spread through the polymer matrix in the compounding process. [51]

3.4 Biaxially oriented polypropylene film

The experimental work for this thesis is focused on the long-term dielectric strength of biaxially oriented polypropylene (BOPP) films. Biaxial orientation refers to a manufacturing process wherein Polypropylene (PP) film is mechanically stretched in a semi-molten state in two directions, the machine direction (MD) and the transverse direction (TD).

This orientation is performed in order to increase the mechanical and electrical strength of the polymer [10]. Polypropylene is, fundamentally, a thermoplastic polymer which softens when it is heated and hardens when it is cooled. Thus, it can be re-formed into different shapes and is thus ideal for recycling. The main polarization mechanisms in polypropylene are electronic and atomic polarization [30]. However, due to its semi-crystalline structure, interfacial polarization may also occur [30]. The conduction mechanism is through the hopping of charge carriers [19]. The other main properties are summarized in Table 3.1. Before proceeding to its applications in capacitors, there must first be a brief description of the manufacturing process for a BOPP film.

Table 3.1. Properties of BOPP film. Adapted from [11].

Properties	**Unit**	**BOPP film**
Thickness	μm	3.5 ~ 15
Density	g/cm^3	0.91 ± 0.01
Glass transition temperature [49]	˚C	-10
Melting point [49]	˚C	165-170
Breakdown strength (Weibull α)	V/μm, DC	≥700 (23°C)
Loss factor (20°C, 1 kHz)	x10^{-4}	≤ 3
Dielectric constant	-	2.25 ± 0.1

The first step in polymer manufacturing is to produce monomers from raw materials. Once the monomers have been made, the polymers can be formed by linking the monomers to each other using either addition or condensation reactions. These reactions produce polymer resins, which can then be processed further using additives. Finished polymer resins usually come in the forms of pellets, and BOPP films are formed from these pellets in a specific process. The thin films themselves can be produced by an extrusion process without the need for biaxial drawing. During extrusion, the plastic pellets are fed into a hopper and heated. Then, the molten polymer mass is forced through a shaping die and extruded as a film. This process is illustrated in Figure 3.4.1. [3][49]

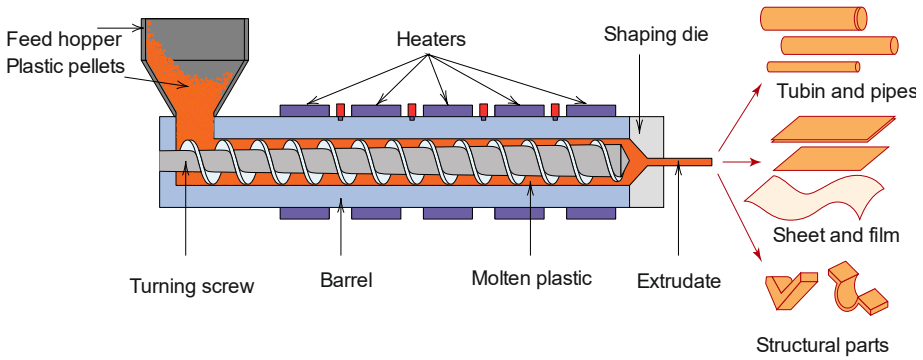

Figure 3.4.1. *Extrusion process [3].*

In order to produce BOPP films, these die-cast thin films are further processed in order to give them their biaxial orientation. This is done using either a blowing (bubble) or planar drawing (tenter) process. The characteristics of the stretched film, e.g. the degree of crystallinity, crystal morphology and the degree of orientation depend on the processing conditions, so the properties required for the material's final application may influence the selection of certain processing conditions. In the blowing process (Figure 3.4.2 a), gas is blown through a circular tubing die, while the film is stretched axially in two directions concurrently. As a result, both orientations (the transverse and machine directions) are produced simultaneously [3][10]. Owing to its higher production rates and lower costs, the majority of BOPP film production is done using the tenter process. In the tenter process, the orientations can be done either separately or simultaneously [10][52]. If done separately, the material can first be stretched in one direction (machine or transverse) and then it is stretched in the other direction. In practice, the film is usually first stretched in the machine direction (MD) and then in the transverse direction (TD). Stretching in the transverse direction is done in an oven and usually has three sections (Figure 3.4.2 b) [10]. In the simultaneous tenter-frame process, the material is stretched along both axes in one step. This is done using the more recent, LISIM technology (linear motor simultaneous stretching) [52]. LISIM can not only improve the mechanical properties of a polymer film, such as its tensile strength and tensile modulus, but can also improve its optical properties (increased transparency) [10]. Because of its cost, however, LISIM has not been widely adopted as a sequential tenter technology [10].

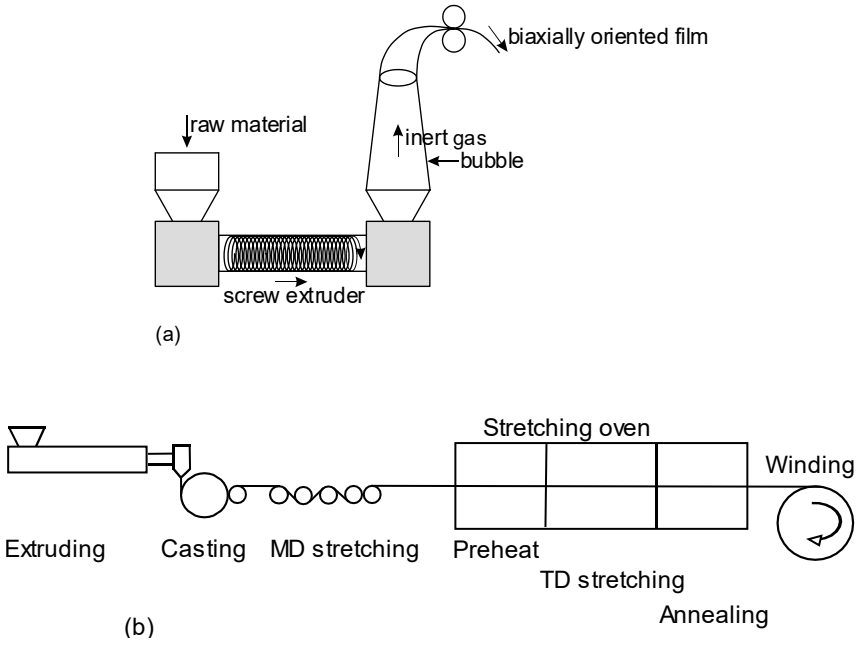

Figure 3.4.2. *Biaxial film production process by (a) blowing [49] and (b) sequential tenter process [10].*

3.5 Metallized polypropylene film capacitors

3.5.1 Fundamentals

The operating principle of the capacitor and the way the dielectric functions in an electric field has already been introduced in Section 2.11. This section will illustrate and discuss the basic properties of capacitors, such as their capacitance, energy density, and equivalent electric circuits.

Capacitance defines how much charge a capacitor can store at a given voltage, i.e. capacitance (C) is the ratio of charge (Q) to an applied voltage (U). It is easy to show that capacitance depends only on the distance, d, between the electrodes, the area (A) of the conducting plates and the permittivity (ε) of the dielectric material. This is given by

$$C = \frac{Q}{U} = \frac{\varepsilon A}{d} = \frac{\varepsilon_r \varepsilon_0 A}{d}. \tag{3-11}$$

One objective for capacitors is to store energy. If the aim is to store the same amount of energy in a smaller capacitor, the relevant quality to improve is its energy density (w) which is expressed as

$$w = \frac{1}{2}\varepsilon E^2 = \frac{1}{2}\varepsilon_0 \varepsilon_r E^2. \tag{3-12}$$

If the total amount of energy (W) that a capacitor can store is more important than the physical dimensions of the capacitor, it may be expressed by the following equation (in a linear capacitor)

$$W = \frac{1}{2}CU^2. \tag{3-13}$$

A capacitor's properties depend on the magnitude and frequency of the electric field, and the temperature. In order to model a capacitor's performance under different operating conditions, equivalent electric circuits are used. One such circuit is depicted in Figure 3.5.1 (a), wherein the idealities of the capacitor are represented by its capacitance and its non-idealities by a single inductance and two resistances. The resistances model the power losses due to contact (R_s) and the dielectric (R_p) losses, whereas the inductance (an equivalent series inductance, ESL) accounts for any parasitic effects of the capacitor [11]. The non-ideal qualities of the capacitor are often summarised in the form of an equivalent series circuit (Figure 3.5.1 b). In this circuit, the operating losses are represented by a single equivalent series resistance (ESR) which is frequency-dependent). [51]

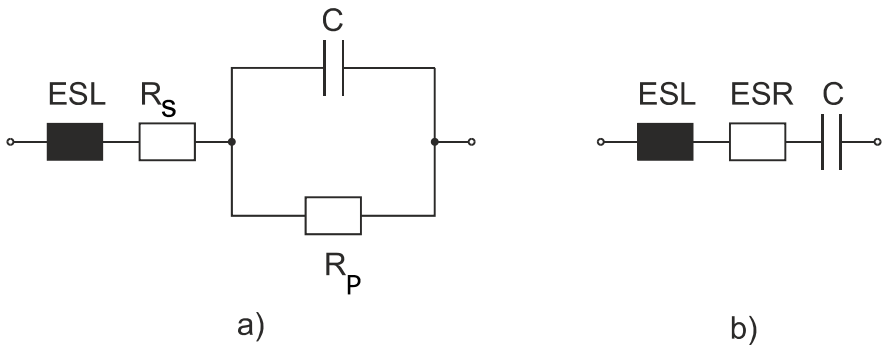

Figure 3.5.1. *Equivalent circuits of the capacitor [51].*

The ESR is particularly important because it influences the dissipation factor (tanδ). The dissipation factor of a capacitor is defined as the ratio of power losses to generated capacitive reactive power. This is given by the following equation [6][49]:

$$\tan\delta = \frac{P_L}{Q_R} = \frac{I_{RMS}^2 \cdot R_{ESR}}{I_{RMS}^2 \cdot X_C} = \frac{R_{ESR}}{X_C} = R_{ESR} \cdot \omega C = R_{ESR} \cdot 2\pi f C, \quad (3\text{-}14)$$

where R_{ESR} is series resistance, *f is* frequency and *C* is capacitance. Assuming a constant frequency and capacitance, it can be seen from Equation (3-14) that any increase in R_{ESR} leads to higher power losses and less efficiency. Higher power losses also generate more heat, thus increasing the temperature of the capacitor. This can cause problems because too high a temperature will reduce the lifetime of the capacitor and may cause it to malfunction [6].

3.5.2 Film capacitors and self-healing

A broad range of capacitors may be categorized according to their end-use, the nature of the dielectric material and the electrodes. If the dielectric is a selection criterion, there are three basic capacitor types: *electrostatic capacitors*, *electrolytic capacitors*, and *electrochemical* capacitors. Electrostatic capacitors can be further divided into two sub-categories, fixed and variable capacitors. *Film capacitors,* which are dealt with in this section*,* belong to the sub-category of fixed capacitors. There are two types of film capacitors: *film/foil, and metallized capacitors*. One of the primary differences between a film/foil and a metallized capacitor is that the film/foil capacitors have separate layers of conductive aluminium foil electrodes and thin films. In contrast, the metallized capacitors have films with a thin metallic coating on their surface, commonly aluminium, zinc or one of their alloys (Figure 3.5.2). These metallized capacitors have a distinct quality in that they are self-healing. Before going further into what this means, there will be a short overview of the manufacturing process of film capacitors. [11]

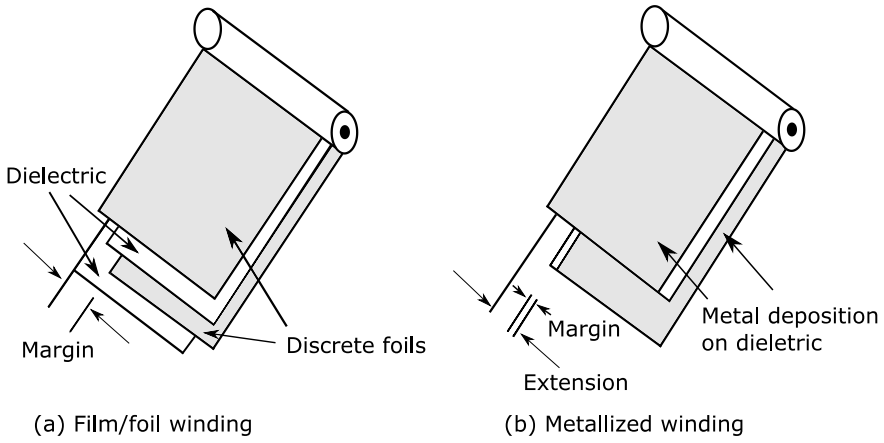

Figure 3.5.2. *(a) Film/foil and (b) metallized capacitors. Adapted from [11].*

When film/foil capacitors are manufactured, the first step is to roll up a plastic film around thin aluminium foils. Instead of just one thick dielectric layer, multiple layers (up to seven) of the film are used as a precaution against failures in the entire dielectric film. The reason for this lies in statistics; because of its multi-layer structure the material is unlikely to have multiple weak points in the insulating layer at the same location. After the windings have been done, two different processes called '*insert tab*' and '*extended foil*' can be applied.

In an 'insert-tab' winding, dielectric films and narrower layers of aluminium foil are wound over each other sequentially and twisted around of the central core. Small, tin-coated wires are embedded into the aluminium foils at a pre-determined number of turns. In the 'extended-foil' approach, the dielectric films and the aluminium foils are wound as they are for the 'insert-tab' winding. However, the aluminium foils are placed differently, at opposite ends of the dielectric films (Figure 3.5.3 b) rather than in line (Figure 3.5.3 a). The tin-plated wire is soldered onto the ends of the aluminium foils. For both capacitor types, the windings are typically placed in cans with a valve for oil. The capacitors are often given vacuum and heat treatments to remove excess air and moisture. After that, they can be impregnated with oil and sealed hermetically, or they can be sealed without oil using epoxy resin. [11]

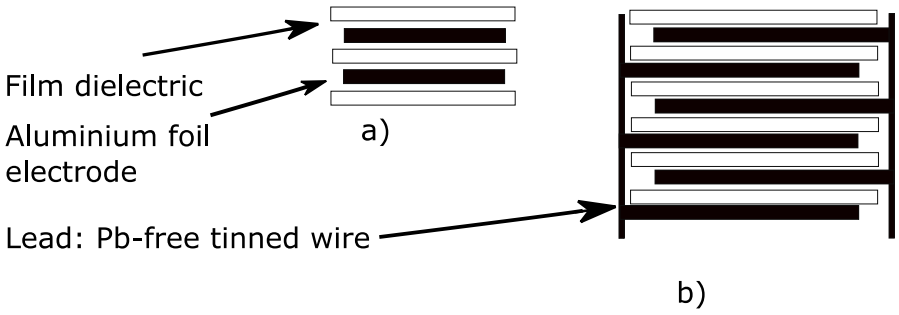

Figure 3.5.3. *Winding of the film capacitor: a) insert-tab and b) extended-foil [11].*

For the metallized capacitors, a thin metal layer is deposited in a vacuum into the dielectric film with a small unmetallized strip around the edges. The metal layer serves as an electrode at the end of the adjacent film-ends (Figure 3.5.4 left). To make the electrical connections, a tin-plated wire is connected into a metal-sprayed end connection ("schoopage") which reaches the metallized film (Figure 3.5.4 right). The winding of the *metallized films* is done around hollow plastic cores, or on a coreless mandrel. In order to solidify mass, the structure is then subjected to heat treatment under pressure. After that, it is sealed hermetically. In practice, several film/foil or metallized capacitors (referred to as "elements") are combined to function as a single capacitor unit (e.g. a power capacitor). This structure is shown in Figure 3.5.5. [11]

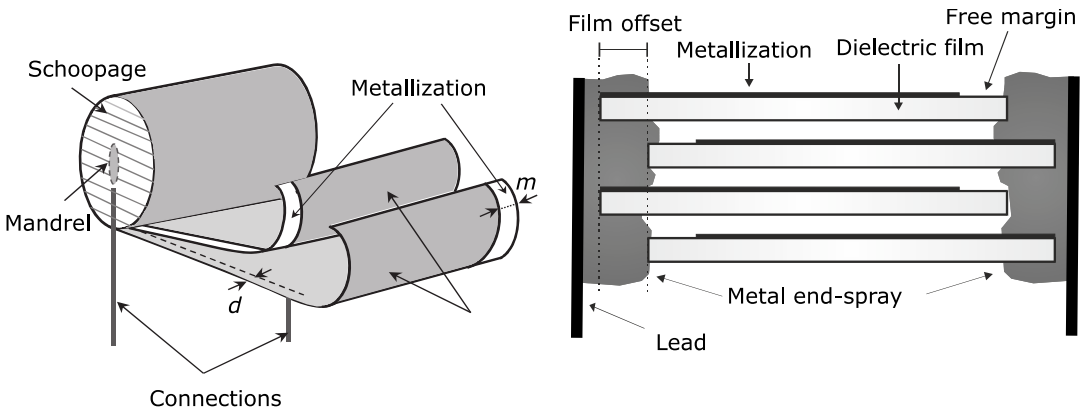

Figure 3.5.4. *Metallized film capacitor (on the left) and a blow-up of the end connections (on the right). Adapted from [33] and [51].*

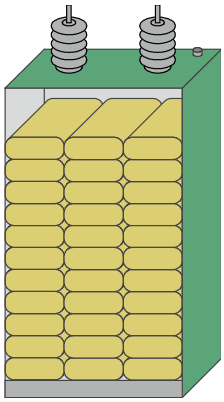

Figure 3.5.5. *Multiple capacitor elements combined to function as a single capacitor unit [49].*

So, now we return to the unique feature of metallized film capacitors, their self-healing capacity. Since any polymer film may have weak spots caused by the manufacturing process, it is these spots that can only withstand relatively low electrical stress and are thus likely to fail first. In a one-layer structure, any failure will render the insulation useless, so hefty safety margins must be observed. Metallized film capacitors, however, can recover from a failure without the capacitor having to be replaced. This is what is meant

by describing them as self-healing. The self-healing process is shown in Figure 3.5.6, where the fault is isolated and cleared. When a local breakdown occurs, it causes high current density. This rapidly increases the temperature so much that the metal around the weak spot is evaporated. As a result, each self-healing event does cause a small decrease in the capacitance. However, a single failure at a weak point does not lead to the immediate failure of the entire capacitor, so higher electric stresses can be applied for a given thickness of film. [11]

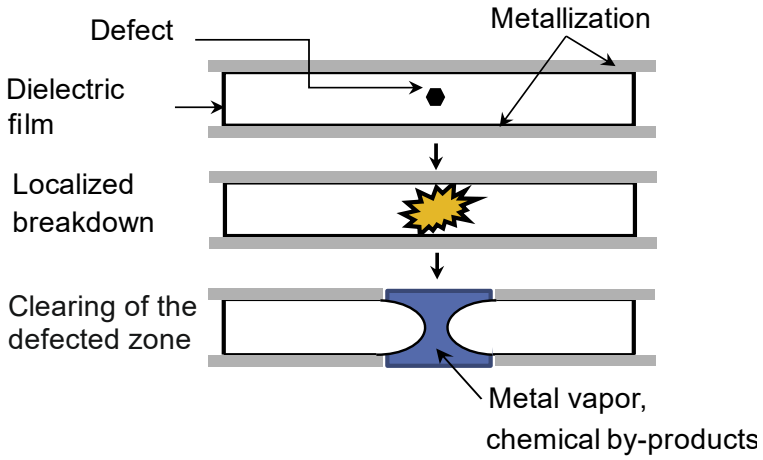

Figure 3.5.6. *The self-healing process of a metallized film capacitor [33].*

This clearing phenomenon is complicated, and depends on several variables such as pressure, the thickness of the metallization and the materials (metal layer and polymer). Thus, the self-healing does not always lead to full vaporization of the metallized area, and as a result, some areas of the insulation may carry a leakage current. In such cases, the loss factor increases and more heat is generated. If there are too many of these partial clearings, it may eventually lead to thermal runaway. Discharged energy $E_{discharge}$ during a self-healing event can be approximated by the following equation:

$$E_{discharge} = \frac{hCU^b}{R_{sr}^s \alpha(P)}, \tag{3-15}$$

Where *h* and *s* are (experimentally defined) material-specific constants, *U* is the applied voltage, *C* the capacitance, *R* the sheet resistance of the electrode (Ω/sq), and α(P) a function for inter-layer pressure [49]. If the metallization thickness and the pressure are held constant, Equation (3.15) can be simplified to

$$E_{discharge} = aU^b, \tag{3-16}$$

where a and b are constants. [11][48][49]

4. DIELECTRIC BREAKDOWN AND AGEING IN POLYMERS

4.1 Dielectric strength

All electrical insulators have an upper limit for the electric field they can withstand. When the applied electric field is higher than that, the insulator fails and rapidly discharges its stored energy through a small local area between the electrodes. After a breakdown, a solid dielectric without any self-healing capability is permanently damaged and loses its electrical insulation property. *Dielectric strength* is defined as the maximum *electric stress* that can be applied across an insulator without a failure. For a uniform electric field, the dielectric strength E_b is calculated by dividing breakdown voltage (U_b) by the thickness of the sample (d):

$$E_b = \frac{U_b}{d}. \text{ [23]} \quad (4\text{-}1)$$

In practice, there are multiple values for dielectric strength, since it does not depend solely on the material's properties. Other variables, such as temperature and the waveform and duration of the applied electric field, affect the material's dielectric strength. Furthermore, experiments have demonstrated that dielectric failure is only a statistical likelihood, and one cannot determine an exact, failing voltage level for an insulator in advance. [24] Depending on the type of insulation system, different breakdown probability distributions may be valid. For polymers, and typically for all solid insulators, the probability is frequently represented by a two-parameter *Weibull distribution* whereby the unreliability function is

$$F(x) = 1 - e^{-\left(\frac{x}{\alpha}\right)^{\beta}}, \quad (4\text{-}2)$$

where $F(x)$ is the probability of the failure, α is the scale parameter that gives a time or voltage to reach the 63.2% quantile (i.e. $F(x)$ = 0.632), β is the shape parameter that measures the spread of the data, and x is a random variable (time or voltage) [9].

The link between failures and fluctuating stresses may arise from material non-uniformities, impurities and defects. It is widely acknowledged that any or all of these might originate in the manufacturing processes. First, despite the strictest of manufacturing procedures, the properties of a dielectric material may still vary (e.g. thickness) so the strength of an electric field can vary locally within the material. Second, manufactured materials contain imperfections (weak points) which may lead to failure in service. As a result,

dielectric strength is considerably determined by the manufacturing processes, and thus much lower electric stresses than a defect-free material could endure must be used in service. [24] The failure of an insulating material, however, is not solely determined by a single, abrupt event exceeding the critical electric field (Figure 4.1.1). Instead, failures are usually the result of several mechanisms (breakdown, degradation and ageing) with different dielectric strengths and times to failure.

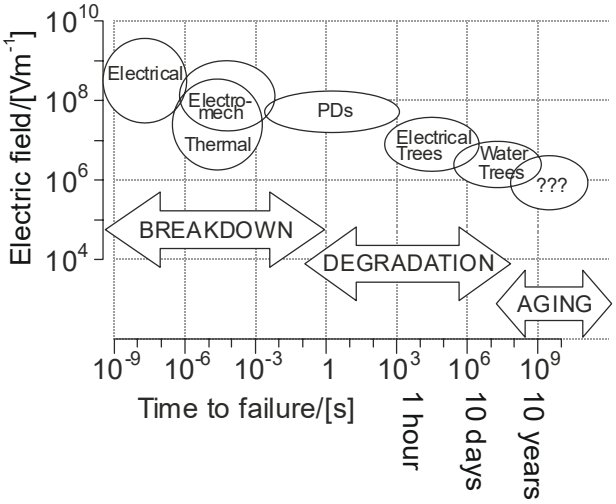

Figure 4.1.1. *Electric field versus time to failure [15].*

According to the above chart, a failure (“breakdown”) will occur almost immediately if the applied electric field is close to the theoretical dielectric strength of the material. If a lower field is applied, the failure may be attributed to degradation (partial discharges PDs, electrical trees and water trees) in which the time to failure can be anything from hours to months, or even years. Failures encountered substantially later are marked by “???” which accounts for the diverse *ageing* mechanisms that can occur in lower electric fields. Ageing is defined as an irreversible process that changes a material’s properties over time. Ageing itself may not cause a direct failure, but instead it can cause degradation that will eventually lead to breakdown. This gradual and complex process might go on for decades. [15]

Without spending too much time measuring all possible breakdown processes, we do have reasonably accurate knowledge of the short-term dielectric strength of electrical insulating materials. However, significantly lower electric fields are used in practice in order to avoid rapid breakdowns. Not enough is known about the time and origin for slowly developing failures, so failure can occur with the normal electric stresses used in service. It might take a considerable amount of time before the deterioration is noticed. [15] However, once the damage has been done, the insulating material cannot cope with

as high electrical stress as it did before, i.e. its short-term dielectric strength has diminished. Thus, measurements performed with high electric stresses could be used to estimate whether a sample has undergone ageing or not [63]. Unfortunately, as high electric stress tests lead to the destruction of the test material, such methods cannot be used in service.

4.2 Categorizing breakdown, degradation and ageing

The previous section demonstrated that when the electrical stress is moderate, failure seldom arises from a single critical event. Instead, the final breakdown is usually preceded by the gradual deterioration of the insulating material. As the phenomena of slower failures are a fundamental part of this thesis, the following sections attempt to distinguish between the most common terminology – particularly degradation and ageing – which are often used interchangeably in the literature. A framework for this terminology can be found in [15,] wherein these concepts are introduced. A summary of the differences between breakdown, degradation and ageing is presented in Table 4.1.

Table 4.1. Breakdown, degradation, and ageing [15].

	Breakdown	Degradation	Ageing
Effect	**Catastrophic:** insulation cannot be used afterwards	**Leads to breakdown:** reduces breakdown voltage	**May lead to degradation:** may not reduce breakdown voltage
Speed	**Fast:** occurs in << 1s	**Less than required service life:** ~hours - years	**Continuous process:** whole service life
Evidence	**Direct observation:** normally by eye - hole through insulation	**Observable directly:** may require microscopic or chemical techniques	**Difficult to observe:** may even be difficult to prove existence
Place	**Continuous filament:** bridges electrodes	**Occurs in weak parts:** may form fractal structures	**Assumed to occur throughout insulation**
Size	**>mm:** dependent on energy of event.	**>mm:** may form larger structures	**>mm:** molecular scale
Examples	Thermal Electromechanical Mixed mode Avalanche Intrinsic	Electrical Trees Water Trees Partial Discharges	Bond scission Nano-voids Trap formation Non-electrical changes (oxidation etc.)

Even though this thesis is primarily focused on steady-state DC applications, it must be emphasized that failure mechanisms under electric stress do not only depend on the magnitude and duration of the stress. They are also influenced by the voltage waveform characteristics (DC, AC or pulsed). Other stresses (e.g. thermal stress) may also considerably change the time to failure but are not included in this overview. Figure 4.2.1 summarizes how different voltage profiles (top and middle) and their stresses may be represented (bottom). [24]

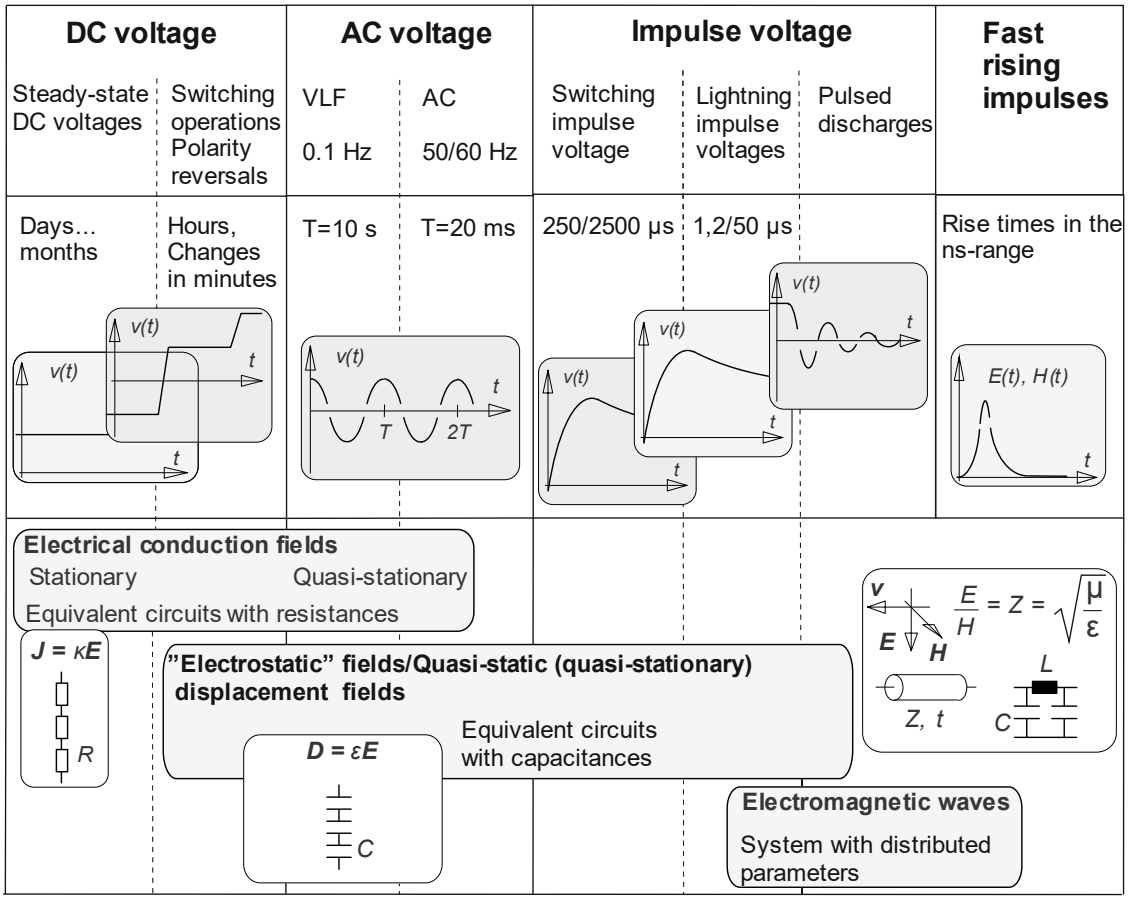

Figure 4.2.1. *Overview of voltage stresses in high voltage engineering [24].*

It can be seen from the above figure that the distribution of voltage stress in steady-state DC applications (even in composite, layered insulations) may be represented with pure resistances. Under AC voltage, and additionally under DC voltage when switching operations occur, the distribution of electrical stresses may be represented by capacitances. The most rapid voltage phenomena, i.e. voltage transients, distribute stresses in different ways. Any accurate estimation of the distribution of electric stress must be calculated using electromagnetic field theory. [24]

The operating conditions in the field of electrical power distribution vary considerably, and this is reflected in the different stresses that the electrical insulating materials must withstand. In DC applications, the steady state is not as steady as the term implies, as

changes in the DC voltage occur due to switching operations and polarity reversals. During power transmission the voltage may contain more than one waveform, and therefore the electric stress is not distributed purely by conductivities. As a result, electric stresses during transition are not the same as they are in the steady state. Nevertheless, even when the voltage is steady-state, electric stresses are not necessarily distributed uniformly. For example, in polymers the electric fields may be higher in some localized regions because the amorphous and crystalline regions in the material have different conductivities [59]. Furthermore, it is well known that *space charge* modifies the local electric field [38]. Space charge is particularly problematic for polarity reversals. In practice, polarity reversals result from the use of Line Commutated Converters (LCC), which are needed to control the power flow in HVDC systems. Since electrical insulating materials have low electrical conductivity, a space charge may persist for a long time even if the electric field is changed. If the polarity of the voltage is reversed, the homo-charges are not immediately neutralized, but instead, they turn into hetero-charges that will magnify the local electric field. For the newer Voltage Source Converter (VSC) technology, polarity reversals are no longer required. Thus, the distortion of the local electric field is greatly reduced so long as a limited amount of homo-charge accumulation occurs [14]. [24]

4.2.1 Breakdown

Fundamentally, all breakdown processes originate from unstable conditions that will lead to the final failure. There are three different types of breakdown processes (*electrical*, *thermal*, and *electromechanical*) which may occur, depending on the original cause of the instability.

Despite a considerable body of research, there is still some uncertainty as to what exactly causes an *electrical* breakdown, and thus there are a number of different theories that seek to explain it. [22]. It has been assumed earlier that all materials have a certain dielectric strength (1) which depends only on the chemical structure and the temperature of the material and (2) which is independent of the size of the specimen and the electrode material. This dielectric strength represents the maximum attainable breakdown strength for a given substance and is referred to as the *intrinsic strength*. It is presumed that the intrinsic strength of a material represents the point at which enough electrons in the insulator have managed to cross to the conduction band to make it conductive. However, no indisputable theory has been established to explain how intrinsic breakdown occurs. [25] One theory has attributed the intrinsic strength of solids to *avalanche breakdown*. It assumes that once a large enough electric field is present, any free electrons in the con-

duction band would have enough energy to ionize the lattice atoms. The liberated electrons could release further electrons from other atoms, which would generate a chain avalanche effect. This would lead to carrier multiplication and the final breakdown. [23] Avalanche breakdown, however, does not seem applicable to thin polymer films [59].

The second type of unstable condition is related to thermal instability, in which Joule heating causes a *thermal breakdown*. When a dielectric material is subjected to an electric field, heat will be generated due to electrical conduction and polarization losses. If the heat generation is higher than the heat dissipation, the temperature of the insulation will increase. As a general rule, both conductivity and polarization losses will increase as a function of temperature, so more heat is generated at higher temperatures. An unstable condition is reached once the heat generation exceeds the ability of the insulator to dissipate it. [23]

The third type of unstable condition is related to electromechanical instability which arises from the compression of the dielectric medium between the metallic electrodes. More specifically, this results from the attractive forces between the opposite electric charges, which is resisted by the elasticity of the dielectric material. However, if the electric field is high enough, the compression force will rise and the thickness of the insulating material will start to decrease. As a result, the electric field (i.e. voltage divided by the thickness of the material) increases, and this increases the compression further. So, breakdowns can be caused by this mechanical instability. However, in polymeric insulating materials, such *electromechanical breakdowns* can be prevented by encapsulation [22]. [23]

4.2.2 Degradation

When electrical insulating materials fail in service, it is not usually the result of high, short-term electric stress. More often, the failure is the result of moderate electric stress that degrades the material over time. It has long been accepted that degradation may be caused by *partial discharges (PD)*. [15] These are discharges that do not connect the electrodes, but only occur in part of the dielectric material. There are four different types of partial discharge: (1) corona, (2) surface, (3) internal discharge and (4) electrical treeing. Corona and surface discharges occur outside the insulating material, whereas internal discharges and electrical treeing occur inside the insulating material. [22] For insulating materials, a complete electrical breakdown means that the electric current has broken through the insulating material, so, only internal discharges and electrical treeing are discussed in this section.

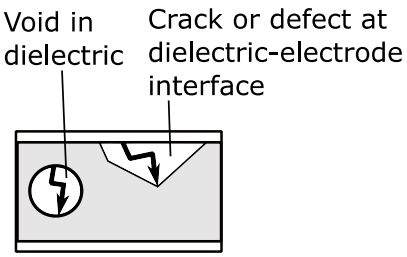

***Figure 4.2.2**. Internal discharges. Adapted from [23].*

Internal discharges are partial discharges that can occur in voids and defects in the material, as depicted in Figure 4.2.2. Internal discharges damage and gradually erode the material. *Electrical treeing* is a phenomenon in which the internal discharges continually erode the material and produce tree-like conductive channels [23]. It is well known that partial discharges (PDs) degrade the insulation in AC fields, but it is unclear how damaging they are in DC fields. If a partial discharge's intensity and repetition rate are low, their occurrence might not decrease the insulation's lifetime by much. However, in some circumstances PDs can be extremely harmful. For example, higher temperatures and electric fields occurring in defects and cavities in the material can raise the discharge frequency, in particular [22]. [40]

One factor that distinguishes *electrical ageing* from *electrical degradation* is that degradation is considered to be caused by PDs while ageing results in charge carriers that do not cause discharges but instead cause molecular changes in the material. Although the different stages in electrical ageing are still unclear, the scenario presented in Figure 4.2.3 is considered viable. It has been suggested that all polymeric materials contain nanometric defects or voids that are either already present in the material or are generated by electrical stress. These imperfections, however, are initially too small to cause discharges. This is because, in order to accumulate enough energy to ionize molecules, electrons require an adequate mean free path. [42] As discharges, and thus electrical degradation, are not initially possible, it is assumed that the ageing of an insulating material precedes degradation. In ageing, molecular changes will increase the damage arising from the voids and defects in the material. [27]

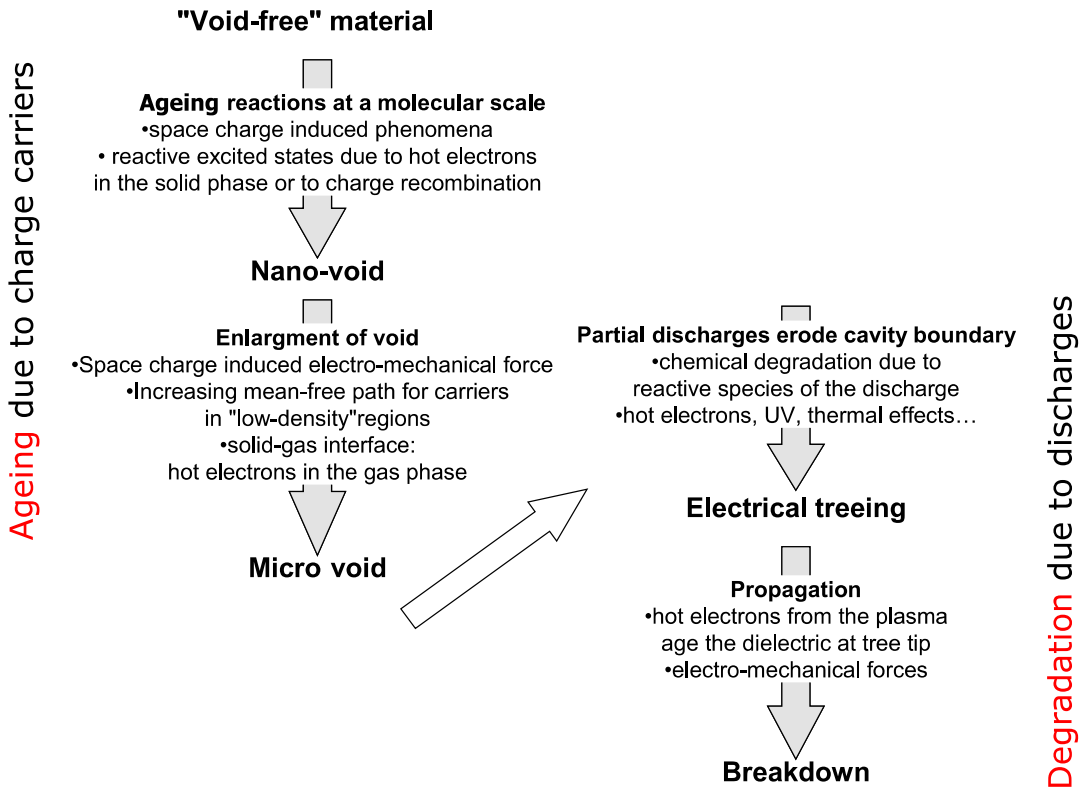

Figure 4.2.3. *Ageing leading to degradation. Adapted from [27].*

Once the size of the defects has increased enough (i.e. they become microvoids), partial discharges may occur, and degradation will ensue. However, experiments have demonstrated that although partial discharges can increase the diameter of the branches in a tree, it cannot alone explain the growth of the cavity. Hence, it has been theorized that the damage progresses from the cavity walls through pits (semiconductive paths) which increase the electric field at their ends [42]. Thereafter, electrical trees start to form, and these may propagate the voids further and lead to a final breakdown. Fundamentally, degradation results from damage in the cavity and has three different stages: (1) electron injection into a cavity, (2) hot electron production in a cavity, and (3) damage growth. Although not discussed further here, a detailed description of these processes can be found in [37] and [40].

4.2.3 Ageing

As mentioned earlier, ageing occurs even in low electric fields and can lead to the eventual degradation of an electrical insulating material. Thus, regardless of the level of electrical stress, although the stress might not cause degradation it may induce ageing. The ageing of a material is influenced by the stresses applied to it in that these will affect how the chemical ageing of the material evolves. *Chemical ageing* refers to chemical changes that can occur in polymer structures, such as a chain scission [4][35]. These changes

may be caused by a chemical reaction, but they can also be caused by thermal degradation or exposure to radiation (not discussed further in this thesis) [3][4].

One of the chemical reactions is *oxidation,* which involves the transfer of electrons between two chemical species (atoms, molecules, or ions). Oxidation requires oxygen, ozone or some other substance that can trigger the formation of free radicals, and thus significantly increase their number in polymers [3][35]. Even in the absence of air, all polymers have some free radicals since they are created in the fabrication process. Free radicals are an unstable and reactive chemical species that lead to further reactions within the base polymer material. Despite its name, thermal degradation is in fact related to chemical ageing. The reason for this is that when polymeric materials get hot, the chemical reactions that can cause chain scission are accelerated due to reaction kinetics. Reactions that lead to chain scission may be inhibited by adding protective elements called stabilizers into a polymer. These (antioxidants) can either consume the substances which cause the formation of free radicals (e.g. ozone) or eliminate the free radicals themselves before the damage progresses further. [3] Stabilizers do not halt an oxidation reaction completely, but they will decrease the rate of the reaction [44]. In other words, oxidation can still occur even if there are stabilizers in the material [4]. Another problem with these protective additives is that they are not uniformly distributed throughout the material and thus there may be localized areas in the material that they do not reach.

Since ageing occurs in an electric field, it is natural to assume that ageing is related to the chemical and physical changes induced by electricity. However, there is no clear consensus on whether it is an electrical response or a mechanical one that induces the onset of ageing. *Electrical models* assume that the dissociation of polymer macromolecules (i.e. breakage of molecular bonds) is central to the ageing process [22] [60]. One model considers that when electrons are injected into the polymer, they become trapped, and will subsequently release an energy equal to the trap depth or to a recombination event. This energy may be dissipated directly, or it may be transferred to another electron that then has enough kinetic energy to break its molecular bonds. That is, electrons with adequate kinetic energy are able to dissociate from molecules and turn into free radicals. Electrons that become trapped may also release their energy into another injected electron. This provokes a chain reaction which produces an increasing number of new free radicals and traps. Schematically, this is represented as

$$AB + e(\text{hot}) \xrightarrow{\text{dissociation}} \dot{A} + \dot{B} + e(\text{cold}) \longrightarrow A + B + e(\text{trapped}) + \text{new energy release.}$$

[22][60]

Another electrical model predicts that both ageing and breakdown are caused by the field ionization (tunneling ionization) of macromolecules. In field ionization, electrons between neighboring molecules may tunnel from the highest occupied molecular orbitals (HOMOs) to the lowest unoccupied orbitals (LUMOs) if the electric field is high enough. Field ionization of molecules leads to the formation of new macro-ions and chemically active free radicals that may react with nearby molecules. The resulting chemical defects provide electrons with another tunneling path, which may form more traps. Since electrons cannot escape from deep traps, positive molecular ions and electrons accumulate in local regions of the polymer. This concentration of charges leads to the formation of solid-state plasma wherein the Debye charge screening effect decreases the ionization energy of the neutral atoms or molecules. As a result, the molecular ionization rate increases, which sets off a distinct, self-accelerating ionization process, in which impact ionization does not occur. [59][61] This model emphasizes the importance of avoiding deep traps in polymers [57]. It has been proposed that deep traps introduced by nanofillers are beneficial for increasing the dielectric strength of an insulation material [57]. However, the whole issue of how nanoparticles affect the long-term dielectric strength of polymers has recently also been questioned by some researchers [29].

The electromechanical view of ageing is that electro-mechanically induced stress may create and propagate nano-cavities. Notable ageing models postulated in this context are the *Crine*, *Lewis* and *Dissado-Mazzanti-Montanari* (DMM) models. All three of these models are based on a thermodynamic approach. They assume that electrical ageing is initiated by a mechanical response in the polymer, which will induce structural changes over time. It is suggested that there are two states, unaged and aged, separated by the activation energy (Δ), which under normal circumstances, inhibits an ageing reaction (Figure 4.2.4). It is presumed that this energy barrier is lowered when the thermoelectrical stresses increase to a certain point. However, the models differ over what exactly are the contributory factors, as do the shapes of their energy diagrams. [26]

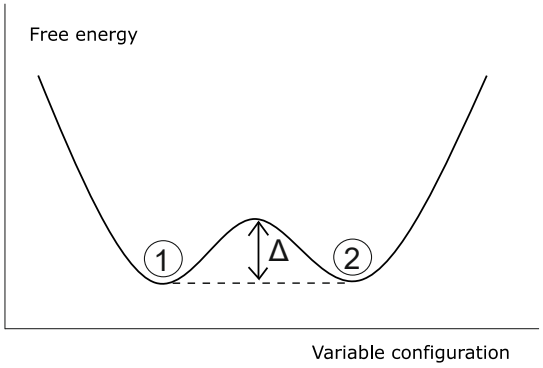

Figure 4.2.4. *Schematic representation of the energy barrier between the unaged (1) and aged (2) states [26].*

Crine's model considers that both forward and backward reactions have thermodynamic equilibrium. When an electric field supplies more energy than the molecular cohesion energy for the insulator (critical stress, 7-15 V/µm), intermolecular van der Waals bonds are deformed. When this happens, the polymer chains rearrange themselves and become closer to each other. It is theorized that the holes in the amorphous region may then coalesce and grow to a nanometric size. Thereafter, space charges injected into these voids could produce further damage. Thus, in Crine's model an increase in space charge is seen as a marker of ageing. In contrast, the **DMM** model regards ageing as a direct consequence of the space charge. It considers that defects and cavities from the manufacturing process may trap charges, which in turn may store electromechanical energy. The energy in space charge clusters could diminish the energy barrier and thus cause ageing reactions. These reactions are not induced by a single mechanism but result from the overall impact of the weakening and/or breaking of the inter-chain cohesion and the intra-chain bonds in the material. Once the damage has progressed far enough, the small local deformations will start to coalesce into larger voids. According to **Lewis**, ageing is related to an electromagnetic field which generates a local mechanical force that will influence the polymer's morphology if the electric field is high enough. His theory is that ties in the amorphous phase between the lamellar crystallites are extended and subsequently opened. The nanocavities then enlarge, and over time these can cause cracks to develop in the material. [7][15][20][26][37-38][42]

Montanari et al. state that the Crine and Lewis models are not applicable for polypropylene because some of the assumptions behind Crine's model do not hold for polypropylene, or indeed for many other polymers. For example, one premise of Crine's model is that the material has to be brittle [40]. Semi-crystalline polymers are only brittle if they are below their glass transition temperature (T_g), which is -10 °C for polypropylene. Furthermore, it has been proposed that craze formation in semi-crystalline polymers does not involve cavitation above T_g. The model presented by Lewis is not specifically an ageing model, as it requires an electric field of 500 V/µm for polyethylene (PE). This is far greater than what is used in service. Even if local field distortion by space charge is taken into account, another model is more likely. The space charge limited field (SCLF) theory postulated by Boggs, which functions for fields of only a few hundreds of V/µm seems more probable. [40]

While the DMM model is the most plausible mechanism, it is difficult to conclude that electrical ageing is solely determined by space charge clusters, which are what the model presumes the local field strength to be dependent upon. Although there have been

studies indicating that one material may accumulate more space charge than another without this signifying an earlier failure, space charge has been known to shorten the time-to-failure considerably [14]. Specifically, it is known that when an electrical threshold for space charge accumulation is exceeded, the local electric field will be distorted, which will decrease the life expectancy of the material. As explained in [14], the short-term degradation of XLPE cable insulation can be caused by the accumulation of hetero-charges. However, it is worth noting that some of the insulation materials produced nowadays do have a very low content of foreign particles (cross-linking by-products and contaminants), and hetero-charge accumulation is no longer seen in these materials at the same level of stress. This raises the question as to whether there might be another electrically-induced process, in addition to space charge, which contributes to the long-term ageing process. It would be straightforward to study the cables at different stresses and draw a conclusion based on the experiments. The greatest challenge with this approach, however, is that no single measurement has ever been established that can accurately determine the state of ageing in an insulator [39]. As a result, it cannot be concluded whether ageing occurred during the experiment.

Recently, the traditional ageing models have been enhanced by Montanari et al. who have presented a new electromechanical model [40][43]. This postulates that ageing under static mechanical stress and electrical stress (DC) could both share the same ageing phenomenon: *plastic deformation*. Plastic deformation under an electric field is based on a similar thermodynamic approach, as was discussed earlier. The model considers that electromechanical energy stored in the weakest spots of the insulation material (nanocavities) may provide enough energy to lower the potential barrier. The amount of energy that is required to initialize ageing reactions is related to the energy that is required to form elemental strain in a localized region of the polymer structure. According to this model, elemental strain can occur in an electric field at around 200 V/μm. A local field might well exceed this threshold, e.g. due to space charge or due to variations in conductivity. Plastic deformation will lead to cavities or crazes large enough to trigger highly energetic discharges, and thus bring on degradation. [40][43]

4.3 Testing short- and long-term dielectric strength in practice

Since the dielectric strengths of electric insulation materials are largely known, it could be assumed that there are defined time ranges for short- and long-term testing of dielectric strength. While a guideline for short-term testing exists, there is no agreement about how long long-term testing should be. Short-term testing can be anything from tens of seconds to tens of minutes and can be measured either by a constant DC voltage, or

more commonly, by ramp testing [63]. Unlike the short-term tests for dielectric strength, long-term tests for dielectric strength are more difficult to define because the lifetimes of electrical insulating materials may vary from several years to several decades. In order to support such long lifetimes, the electric stress must be considerably lower than the theoretical, short-term dielectric strength. In practice, the design fields and the corresponding long-term lifetimes are assessed from some thousands of hours of stress tests [11][36].

A graph of a material's dielectric strength as a function of time produces either a straight or a curvilinear plot. These plots correspond to the voltage endurance of an insulator, and one possible shape is depicted in Figure 4.3.1. In this graph, E_d denotes the theoretical dielectric strength of a material, which is approximately the same as what could be determined by ramp testing, with time t_1. For subsequent times (t_2 and later), testing is conducted under a constant DC voltage. As can be observed, the time-to-breakdown increases as the electric stress is reduced. One peculiarity in this curve is the electric threshold ($E_{threshold}$). This refers to the level of electric stress that does not induce ageing even after a long period of stress (several years or even decades). Consequently, endurance graphs tend to flatten out at lower electrical stresses, which signifies that the effects of ageing in insulation are negligible near to the threshold. It is considered that at this stress level, other stresses alone, mainly thermal stress, will cause the ageing to progress. Nevertheless, assuming a long-term breakdown can be avoided, design fields can be higher than the electrical threshold [39]. [47]

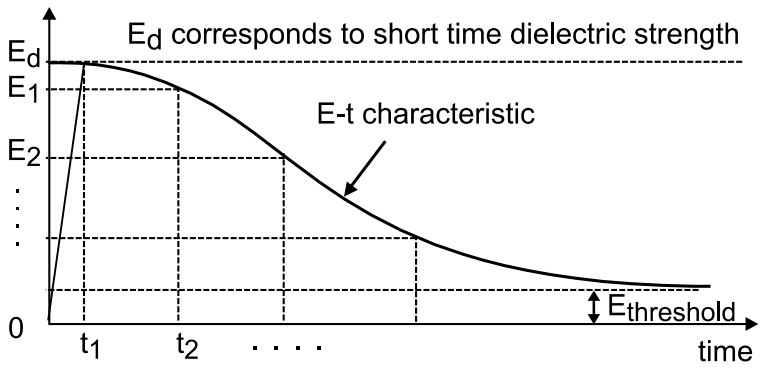

Figure 4.3.1. *Voltage endurance curve. Adapted from [47].*

The existence of an electrical threshold, however, is difficult to prove since long testing times are commonly required to determine the level of stress at which it might occur. Moreover, in practice, there is usually more than one stress factor. As the ageing process is hastened under multiple stress conditions, there are interactions between these stresses. [9][39] Even if an electrical threshold can be detected in the laboratory, it will not necessarily be present in service. Therefore, in real operating conditions failure may

be induced much faster than the theoretical models might predict. In order to gather more information on the effects of this synergy, ageing must be studied using specific stresses that prevail in operating conditions. In the literature, such experiments are based on accelerated tests [13].

4.4 Accelerated testing

Accelerated testing is a process in which a product is operated at higher stresses than it would meet in its normal service life. The purpose of accelerated testing is to cause noticeable deterioration in a product's performance so that a relationship can be modelled between time, performance, and stress. Once this model has been established, the application's performance, which can be any parameter of the application, can be predicted under different levels of stress. Probably the most commonly used performance criterion is the lifetime of the product, and so this type of testing is called *accelerated life testing* (ALT). [13]

If the performance of an electrical insulating material can be determined under different levels of stress, improving or assuring the quality of the materials used in an electrical application can take substantially less time. For example, suppose that a manufacturer wants to compare the long-term dielectric strength of different polypropylene films. Since short-term testing might not reliably predict long-term breakdown behaviour [29], the manufacturer could perform a test under normal-use conditions. As such, a test could take up to 20 years, or even longer, which is not a viable option. However, by using accelerated test conditions, a manufacturer could perform the tests in only a few months. As long as the accelerated-test model is correct, a few months of accelerated testing in a laboratory should be enough to predict the level of deterioration a product might suffer after, say, 20 years of normal in-service use. [13]

4.4.1 Accelerated life testing

In order to conduct accelerated life testing, a specific research plan must first be formulated, before any experimentation can take place. While the plan may vary for different applications, it should always define the sample size and the conditions for the accelerated testing. Hence, at least (1) the stress levels and (2) their loading pattern must be clearly determined, as well as (3) for how long and (4) what accelerating stresses are used. [13]

The *stress level* is a critical factor when planning accelerated tests because it affects both the *amount* of damage and the *mechanisms* of the damage. The higher the stress,

the faster the ageing and thus the shorter the test. However, if the induced ageing mechanism does not occur in normal operating conditions, the test will be of very limited value. There is a limit to how much the stresses can be changed. A good rule of thumb is to make sure the *stress level* ensures ageing during the test, but does not induce failure mechanisms that rarely occur in normal service. [13]

After deciding the stress level, the next step is to determine how that stress level behaves as a function of time. A specific stress level may be applied and maintained in different ways. The loading and the duration of the stress, i.e. the overall test pattern, can affect a material's ageing mechanisms. Figure 4.4.1 shows some common stress-test *patterns,* such as constant, step, ramp and cyclic. In order to induce the same ageing mechanisms that appear in normal service, stress patterns should simulate real conditions as closely as possible. However, this is not always possible, because of constraints in the research plan (e.g. equipment, duration and cost) which may oblige the researcher to modify the stress pattern. Additionally, real stress patterns might include minor yet complicated (random) stresses that cannot be reproduced under AT conditions in the laboratory. [13]

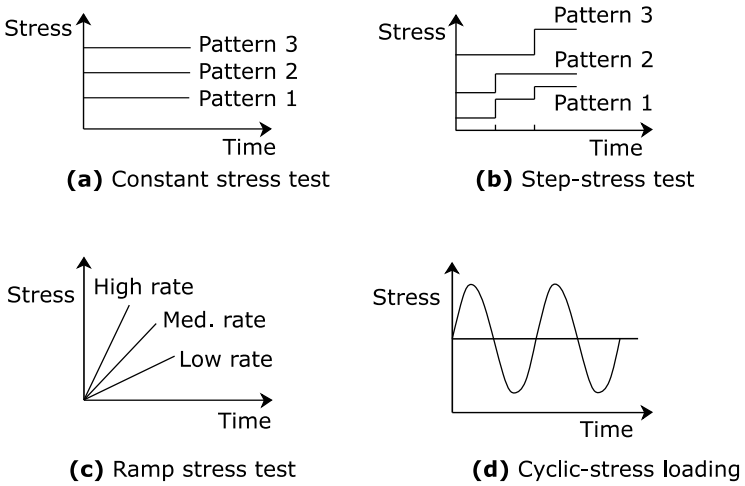

Figure 4.4.1. *Stress pattern versus time. Adapted from [13].*

In order for artificial conditions to mimic ageing under normal service conditions, in addition to selecting the appropriate stress levels and patterns, the researcher must also make sure that the accelerating *stressors* are correct. Stress factors may be classified according to the source of the stress, which could be electrical, thermal, mechanical and environmental. The stress factors themselves, however, are not isolated but influence each other (Figure 4.4.2). [9] For instance, a voltage which is a self-evident stressor for electrical insulating materials, may induce thermal stress via power losses. Fluctuation in temperature may, in turn, cause mechanical forces due to thermal expansion. This may lead to crack development, and eventually cause chemical reactions as a result of

moisture trapped in the material. Hence, the most relevant stress factors are ultimately determined by the application.

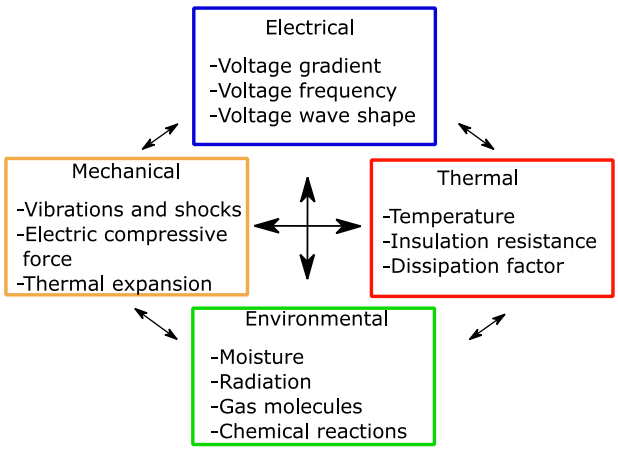

Figure 4.4.2. *Accelerating stresses. Adapted from [9].*

Since BOPP films are typically impregnated in oil or sealed with epoxy in airtight housings, they are isolated from oxygen and moisture. Thus, it is the temperature and the voltage that are the most relevant stressors for hermetically-sealed thin film capacitors. [5] The literature provides some valuable insights into what are the most suitable stress levels for power capacitor applications. According to [5], the electrical stress of the power capacitors in an HVDC converter station is regularly over 100 V/µm, and the ambient temperature often exceeds 80°C. It should also be noted that the electric field is not a pure DC field but is comprised of complex harmonics. Other sources state that capacitors may operate in electric fields as high as 225 V/µm – 240 V/µm [16][50]. The accelerating stresses in these studies are considered mainly from a dielectric film point of view, rather than that of a capacitor. More accurately, it is assumed in these studies that no dielectric film will fail due to moisture as long as the structure of the capacitor is intact. In practice, moisture can corrode the metallization in a capacitor and lead to changes in the metal layer [6][48][51]. If the corrosion persists long enough, the surface area of the electrodes will decrease. This increases current densities in the unaffected paths [51] and increases the ESR of the capacitor as result [6]. A summary of the causes and mechanisms for the failure of capacitors is presented in Table 4.2.

Table 4.2. Failure causes, mechanisms and modes in capacitors. Adapted from [18].

Root cause	Failure mechanism	Failure modes
High Ambient Temperature	Deterioration of quality of electrode metallization	Change in the non-linearity of current-voltage characteristics
Over-Voltage Stress	Self-healing ("soft failure")	Capacitance loss, ESR increase
Excess Ripple Current	Electrochemical corrosion; increased core temperature	Capacitance loss, ESR increase
Continuous Charge/Discharge Cycle (Pulsed Discharge)	Self-healing; electrochemical corrosion	Capacitance loss, ESR increase; detachment of the sprayed ends (schoopage) under high electric stress
Humidity	Electrochemical corrosion; dielectric loss due to moisture absorption by film	Capacitance loss, ESR increase

4.4.2 Single and combined stress models

Modelling the lifetime of electrical insulators under electrical and thermal stress started decades ago. Two branches – physical and phenomenological – have emerged from the original models. The main difference between these approaches is that the phenomenological models attempt to determine the design parameters for electrical insulating material by fitting mathematical models to data from accelerated experiments. In contrast, physical models study actual ageing mechanisms under stress. [39] The fundamental mechanisms behind the physical models were briefly discussed in Section 4.2, but since these are still a matter of debate, their lifetime modelling is not covered any further here. Instead, only the phenomenological models are presented. As the lifetime of an insulating material in phenomenological models is influenced by stress factor(s) (see Table 4.3), only the models with a constant DC voltage and a temperature factor are discussed in this section.

Table 4.3. Capacitor lifetime modelling corresponding to stress type [18].

Stress Type	Model Used	Major Contribution
Temperature	Arrhenius model	Life model proposed for time-varying thermal stress, using Miner's cumulative damage theory
DC Voltage, Temperature	Exponential regression equation, Eyring law	Capacitance degradation with time; constant high temperature and voltage. Lifetime estimated by regression model and Eyring law
Ripple Current	Regression equation based on underlying physics-of-failure	Electrochemical corrosion introduced as a failure mechanism in presence of ripple current. Regression equation proposed for capacitance loss with time based on theory of the oxidation kinetics.
Pulsed Discharge	Birnbaum–Saunders distribution (fatigue life distribution), Poisson distribution Random variable deterioration method, Gamma process deterioration model	Standard life prediction models (regression, Weibull) are compared with the newly introduced Birnbaum–Saunders distribution (to model steady capacitance loss) and Poisson distribution (to model sudden capacitance loss) for pulsed power applications. Steady capacitance loss is modeled by random variable deterioration method and sudden loss is modeled by a gamma process deterioration method.
AC Voltage, Temperature, Humidity	Regression equation	Capacitance and ESR modelling according to the "ingress time" of moisture
Humidity, Temperature	Weibull distribution, combined model (Arrhenius model + inverse power law for humidity)	Time to failure is fitted into a Weibull distribution curve and B1 life, B10 life and MTTF are estimated under the required confidence intervals and the model parameter for the lifetime equation is estimated for all lifetime definitions.

The simplest lifetime models apply only one accelerating stress at a time and are hence referred to as *single-stress models*. Both thermal and electrical stresses have been utilized as stressors. Lifetime under thermal stress, *T*, is modelled by the *Arrhenius model* and is given by the following equation

$$L(T) = K_T e^{B/T}, \tag{4-3}$$

where *L* is the time to failure under thermal stress and *T*, K_T and *B* are constants. The Arrhenius model is based on chemical reaction rates, and its validity may be verified by plotting the lifetime on a logarithmic scale against a reciprocal of the absolute tempera-

ture (*1/T*). If a straight-line plot results, Equation (4-3) can be used for the given temperature range. Figure 4.4.3 shows the estimated plot for a transformer's lifetime at different temperatures. The Arrhenius model clearly shows how small changes in temperature can drastically modify the lifetime of the material. This effect is expressed as HIC (Halving Interval in Celsius) which defines the change in temperature needed to halve an insulating material's lifetime; in Figure 4.4.3 this is approximately 6 °C. Although the Arrhenius model applies to thermal ageing, its validity is only for a limited temperature range, because any of the straight lines could curve when a broader temperature range is investigated. Therefore, the results of tests at higher temperatures cannot automatically be extrapolated to operating conditions. [9][47]

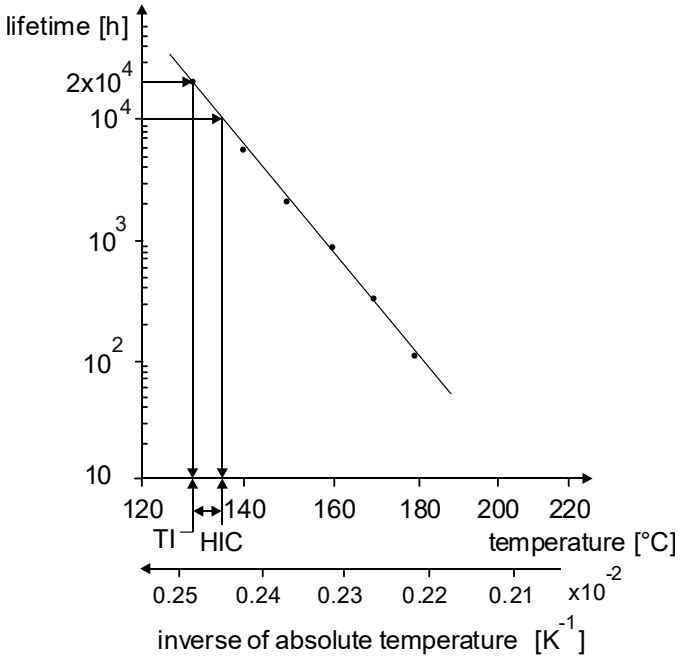

Figure 4.4.3. *Arrhenius behaviour [49].*

The single-stress model may be adapted into an electrical stress, *E,* using the *inverse power* or *exponential* law. The inverse power law (IPL) is given by

$$L(E) = K_E E^{-n}, \tag{4-4}$$

$$\ln L(E) = \ln K_E - n \ln E \tag{4-5}$$

where *L* is lifetime at the applied electric stress, *E,* and K_E and *n* (endurance coefficient) are constants determined from the experimental data. As its name implies, the endurance coefficient (*n*) is used to evaluate the electrical endurance properties of an insulating material: the larger the *n*, the better the endurance. The inverse power law was originally determined from experiments, but it can be shown that it has a theoretical background as well [1][9]. Nevertheless, due to its simplified form, IPL and thus *n* are only applicable for a small range of electric fields [1]. The validity of the model may be verified

by plotting lifetime and electric stress on a logarithmic scale. If a straight line fits the data, the model is valid. The exponential law is expressed as

$$L = ce^{-k_n E} \tag{4-6}$$

$$\ln L = \ln c - k_n E, \tag{4-7}$$

where *c* and *k* (endurance coefficient) are constants. For a valid exponential model, a straight line can be fitted to the data as well. However, in the exponential case, the lifetime is only plotted on a logarithmic scale. From a theoretical perspective, it is speculated that the exponential model represents a global degradation mechanism, while the inverse power law is related to failures arising from local defects. Generally, failures are presumed to be driven by local defects, and thus the data usually fits better to the inverse power law, which is widely employed in testing standards. [9][39][47]

When the electric stress has reduced enough, electrical ageing becomes limited and the lifetimes increase significantly. This is not predicted by previous models, and this is why real lifetimes can be longer than the modelled ones. A boundary for electrical ageing may be used for both models by incorporating the stress threshold. For the inverse power law, one possible model is given by the following equation

$$\frac{L}{L_0} = \left(\frac{E}{E_0}\right)^{-n}, \tag{4-8}$$

and for the exponential law

$$L = \frac{K_2}{E - E_0} e^{[-K_1(E-E_0)]}, \tag{4-9}$$

where L_o is lifetime at the threshold stress and E_0, K1 and K_2 are constants. [9][47]

Although single-stress testing is relatively straightforward, and therefore attractive to researchers, there is usually more than one accelerating stress in practical applications. Acceleration studies have shown that when multiple stresses are applied simultaneously, not only do the stresses themselves accelerate ageing, but they also add a synergy effect. This is why an insulator ages faster under combined stresses than if the same stresses are applied sequentially. The ageing rate is more than the sum of the effect of each stress but less than their product [39]. Thus, an upper limit for ageing in a *multi-stress* scenario can be given as a product of the equations (4-3) and (4-5):

$$L(T, E) = K_T e^{B/T} \cdot K_E E^{-n}. \tag{4-10}$$

By combining the constants K_T and K_E, this simplifies into

$$L(T, E) = K e^{B/T} \cdot E^{-n}. \text{ [47]} \tag{4-11}$$

However, equation 4-11 does not include a coupling factor between *T* and *E* which can account for the synergism of electrical and thermal stresses. Depending on the model, this coupling factor may have different forms. In order to minimize the number of the fitting parameters, it may be assumed that the endurance coefficient *n* depends on temperature, *T*, but the thermal activation energy, *B,* does not depend on the electric stress, *E*. Formally these are given as

$$n = n_1 - \frac{n_2}{T} \tag{4-12}$$

$$B = B_1 + \underbrace{B_2 E}_{=0}. \tag{4-13}$$

Hence, the equation with a coupling factor is

$$L(T,E) = Ke^{B/T} \cdot E^{-(n_1 - n_2/T)} \tag{4-14}$$

$$= Ke^{B/T} \cdot E^{-n_1} \cdot E^{n_2/T}. \text{ [47]} \tag{4-15}$$

The main drawback with the above-mentioned lifetime models is that although they can be used to indicate when a capacitor will fail, they do not provide any means to monitor the state of health of capacitors as a function of time [18]. If the remaining life could be estimated, a capacitor could be utilized optimally without the risk of failure. Capacitor condition monitoring relies on tracking different capacitor parameters, such as its capacitance and *ESR*, and ensuring that they do not exceed a predetermined threshold (Figure 4.4.4). If either limit is crossed, the capacitors may malfunction or fail in their application and should be changed. [54] It has been suggested that a decrease in the capacitance of metallized capacitors is mainly caused by self-healing, and thus ageing in elevated temperatures and voltage stresses could be tracked by measuring the relative change in capacitance [34]. In the literature, a loss of 2-10 % of capacitance is commonly considered as an end-of-life marker [18][30][54].

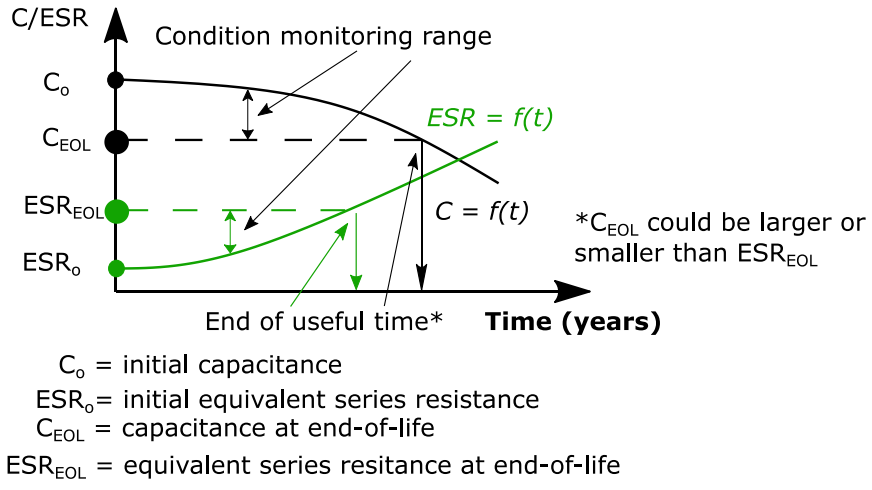

Figure 4.4.4. *Capacitor condition monitoring. Adapted from [54].*

5. THE MATERIALS AND THE TEST SET-UP

5.1 Overview of the voltage endurance tests

BOPP films are commonly used in metallized (self-healing) HVDC power capacitor applications, and their expected service lifetime can be as high as 30 years [5]. One of the research questions for this thesis was to assess at which levels of electro-thermal stress such a long lifetime could be safely achieved. It is also necessary to evaluate how the lifetimes of different insulating materials are affected by these stresses. In order to accomplish these goals, the accelerated life tests (ALT) of BOPP films were conducted under specific, simultaneous and constant thermal and electrical stresses. In the literature, acceleration studies that establishes a time-to-failure at a given electric stress are called voltage endurance tests. The shape of the endurance curve, which is seen in Figure 5.1.1, may be straight or curvilinear. From a theoretical point of view at least three stress levels are required to establish the curve's shape and one (or more) of these tests should result in a failure after 1000 hours or more [63].

In this thesis, the endurance curve was evaluated in two parts. First, *the beginning* part of the voltage endurance curve (denoted by "1" in Figure 5.1.1) was determined. Subsequently, *the middle part* of the curve ("2") was examined using a single, longer-term test. The purpose of these tests was to see whether the ageing rate starts to decline, which would indicate a change in the prevailing ageing mechanisms at lower stress levels.

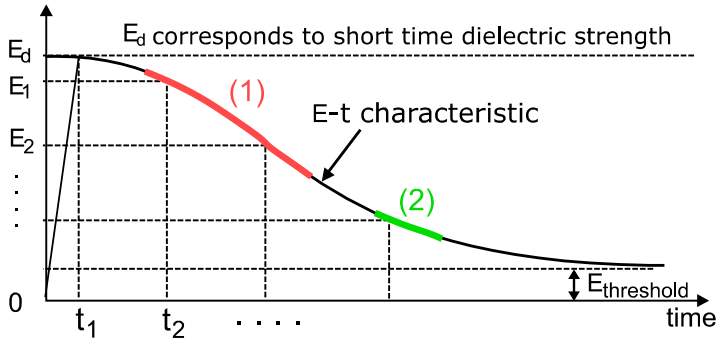

Figure 5.1.1. *Voltage endurance curve. Adapted from [47].*

5.2 The endurance testing set-up

In practice, the oxidation of BOPP films in intact capacitors is considered minimal (see Section 4.4.1), and so the oxidation of the samples was kept to a minimum by conducting the tests under a constant DC voltage in a temperature-controlled vacuum oven in inert nitrogen gas. The testing procedure, which is described in detail in the subsequent sections, consisted of the following seven stages: (1) Preparing a test sample and assembling it on a test bench. (2) Placing the test bench into the vacuum oven. (3) Establishing a vacuum, followed by nitrogen flushing. (4) Heating the sample to the test temperature using an adequate preheating period. (5) Conducting the endurance test. (6) Performing discharge analysis. (7) Performing statistical analysis of the breakdown data.

5.2.1 The capacitor films under test and the sample set-up

The experiments were carried out as part of the EU-funded Horizon 2020 project, GRIDABLE, which has developed and produced a number of silica-BOPP films. In this study, three materials were compared. The first was a commercially available BOPP film, herein referred to as “EC”. The other two materials were industrial-grade prototype materials produced under the GRIDABLE project. Both the experimental materials, and the commercial reference film, had the same base polymer. The difference between the two prototype materials was that one material had a nano-silica filler while the other did not. These materials are referred to as prototype 1 nanofilm “P1N” and prototype 1 reference film “P1”. The films were tested by preparing a simple test capacitor, and using the test materials as the dielectric film. A schematic presentation of the test capacitor is shown in Figure 5.2.1 (a).

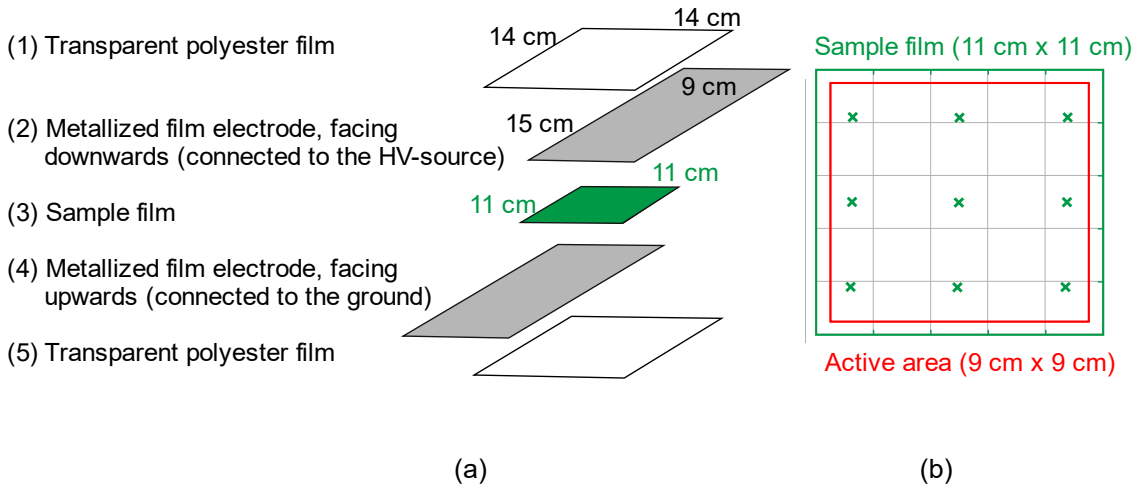

Figure 5.2.1. *Exploded view of the film arrangement in the test capacitors. Adapted from [51], [49].*

The prepared sample film (5.5 μm thick industrial-grade BOPP film) was placed in the middle of these layers. In order to later compute the electric stress across the film, the real thickness of the sample film was measured at 9 points as shown in Figure 5.2.1 (b). The thickness measurements after the endurance testing were performed with a MeasureItAll LE1000-1 electro-mechanical thickness measurement gauge (accuracy of 0.1 μm). Since the samples had such a low variation in thickness, the average value of these 9 measurement points was considered to be accurate enough to compute the electric stress. The other layers shown in Figure 5.2.1 (a) are the two 100 μm PET films (1, 5) which were used to facilitate mechanical handling of the specimen during testing and the two metallized films (2, 4) which were used as electrodes. The metallized film electrodes were placed so that their overlapping area (active area) was 81 cm^2. The test capacitors were assembled in a semi-clean space using disposable gloves and suitable clothing in order to minimize any dust accumulation.

Once a test capacitor was made, it was mounted onto a test bench in which there was a high voltage supply. Figure 5.2.2 shows a sketch of the test bench, which is composed of a Teflon base with clamping electrodes, and the test capacitor (i.e. a BOPP film sample between two metallized film electrodes). A photograph of the test bench that was used in the experiments is shown in Figure 5.2.3., which also shows how the metallized film was placed. Both metallized films were placed so that there was 1 cm clearance at each end of the sample film (illustrated by the dashed red lines). Once the test capacitor was mounted on the test bench it was placed into the vacuum oven and the preheating procedure was commenced.

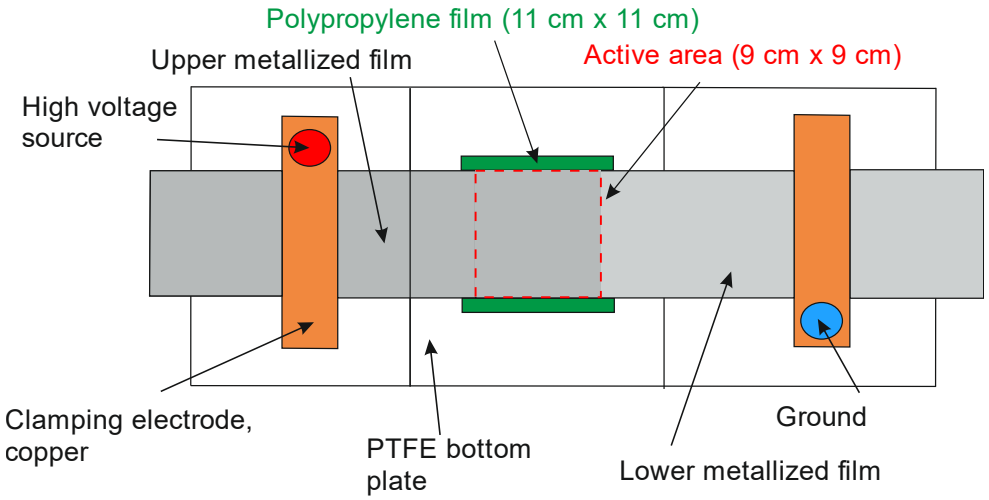

Figure 5.2.2. *Sample assembled into the test bench. Adapted from [51].*

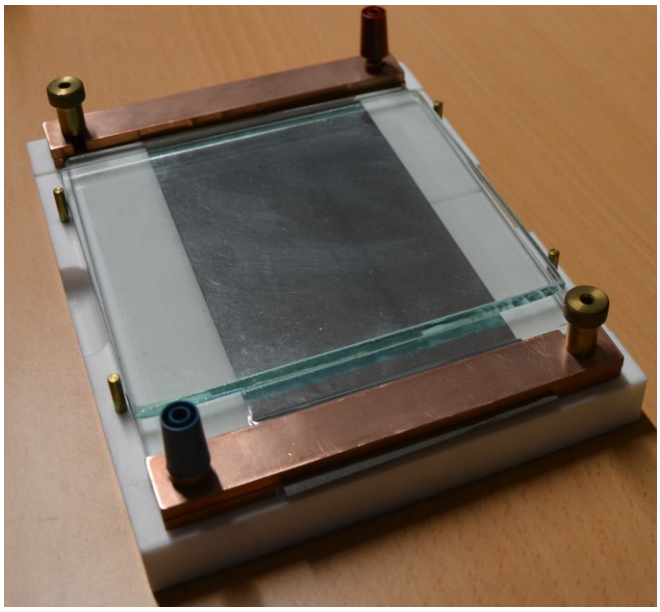

Figure 5.2.3. *The test bench used in the experiments.*

5.2.2 Sample preconditioning, test set-up and procedure

The first step of the preconditioning was to create a vacuum in the oven using a vacuum pump (Edwards XDS5). Once the vacuum (−15 psi) was established, nitrogen gas was released into the oven. The creation of the vacuum and the subsequent release of nitrogen gas was repeated 3 times for each sample. Thereafter preconditioning was applied. The purpose of the preconditioning was to heat the samples to the test temperature and stabilize them, which according to preliminary measurements took 3 or 4 hours depending upon the test temperature. At 60 °C it took 3 hours and at 70 & 85 °C it took 4 hours. For the last 30 minutes of the preconditioning, the sample was prestressed under a voltage of 1 kV, which roughly corresponds to an electric field of 190 V/μm. This produced an electrostatic force that compressed the metallized films towards the sample, thus removing/minimizing any gas bubbles between the sample film and the metallized electrodes.

Later, as the endurance tests were being conducted, it was noticed that the lifetime of some samples which had been preheated and tested at a higher temperature had longer lifetimes than their lower-temperature counterparts. Therefore, the preheating procedures – mainly the applied heating times and temperatures, but also the duration of electric stress – were varied. The effects of these variations in the preheating procedure on a sample's lifetime were thus compared systematically in endurance tests. The endurance tests that followed the preconditioning tests are referred to as "*secondary endurance testing*". This classification was made in order to differentiate these tests from the

original endurance tests that were used in the lifetime modelling of the films, hereafter referred to as "*primary endurance tests*". The primary endurance tests were always carried out using the described preconditioning procedure. All the experimental values for the preconditioning tests are given in Section 6.1.

When the preconditioning period was complete, the endurance testing was started. A specified test voltage was applied and the time-to-breakdown was measured. The first discharge, however, did not interrupt testing because the measurement was taken with a method called MultiBreak. This method had been developed in earlier research at Tampere University [51], [49] and it utilizes the self-healing capability of metallized films. When a breakdown occurs, the self-healing process isolates the fault, and the testing can be continued without interruption. Using the MultiBreak method, multiple breakdown events can be gathered from one sample film. In this thesis, 20 independent breakdowns were generally regarded as an end-of-life marker. After that, the test was stopped for that sample. All the breakdown tests were video-recorded, and a USB oscilloscope (Tie Pie Handyscope HS6) was used to capture each breakdown event. The information gathered provided the times of the breakdowns as well as the voltage and current graphs of the discharges, and these were later used in the measurement analysis.

A schematic representation of the measurement set-up is shown in Figure 5.2.4. The capacitance (C_s) represents a test sample inside the vacuum oven (Galli 21GV) whose specified temperature accuracy was $\pm$ 0.5 ˚C and temperature uniformity $\pm$ 3 ˚C. The discharge voltage (u_s) was measured with a Tektronix P6015A high voltage probe (HVP). The discharge current (i_a) was measured with a low-inductance current viewing resistor (R_a, 5 Ω) installed in series with the test sample. The discharging current from the high voltage (HV) DC source (Keithley 2290E-5) during the breakdown was limited by a series resistor (R_{series},100 kΩ) in the circuit. The energy dissipated during discharge was immediately recharged from the parallel capacitor (C, 0.5 µF) and from the capacitance of the healthy part of the sample (C_s) and subsequently from the HV DC source. The actual test apparatus is shown in Figure 5.2.5.

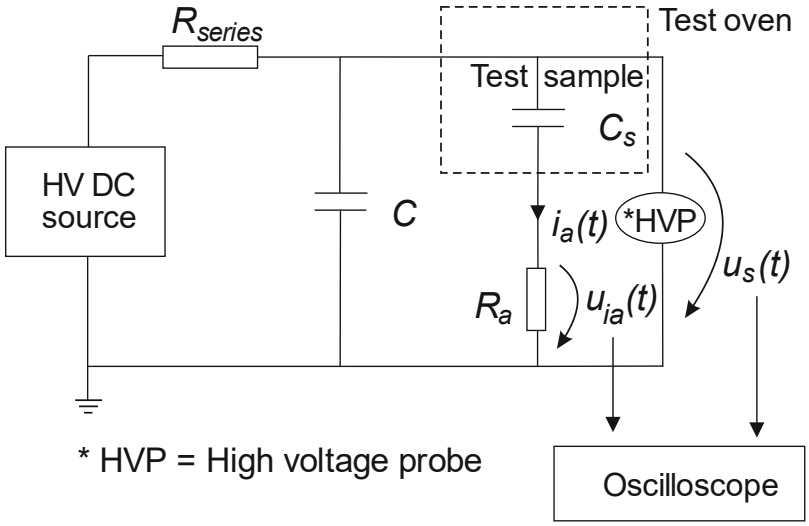

Figure 5.2.4. *Measurement circuit. Adapted from [52].*

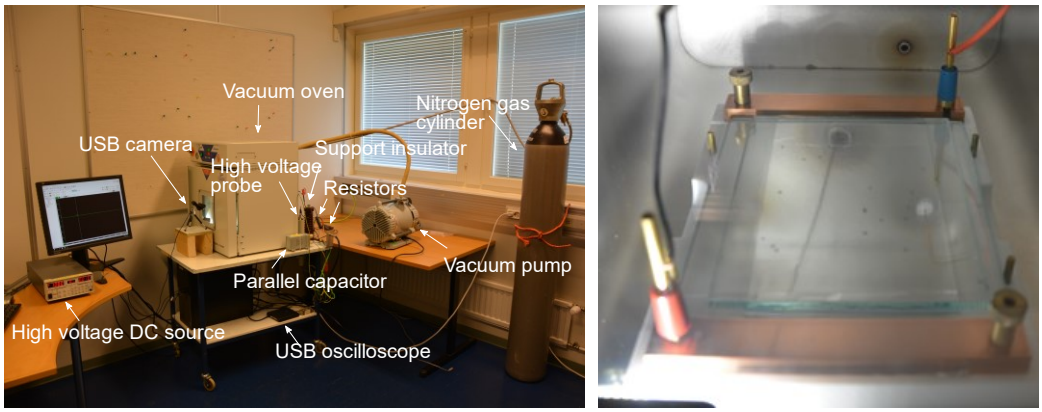

Figure 5.2.5. *The measurement set-up used in the experiments (on the left) and a photograph of a test bench inside the test oven (on the right).*

5.2.3 Discharge analysis

Since multiple self-healing events occurred during the endurance testing, discharges could appear near to each other both in time and space. Ordinarily, breakdowns were separated, but sporadically there was little time (<< 1 second) or space between discharges. In order to visualize the breakdown area of a self-healed discharge, a microscopic picture of one breakdown event is shown in Figure 5.2.6. The breakdown channel (i.e. the puncture hole) is visible in the middle of the cleared area wherein the metallization has been vaporized.

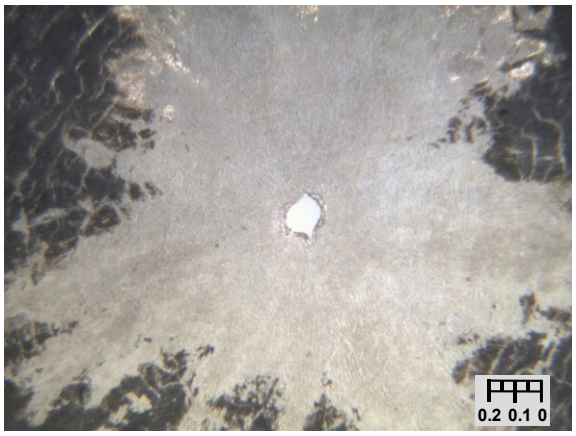

Figure 5.2.6. *A microscope image of a self-healed breakdown. The scale bar is in millimeters [51].*

Earlier studies [51] and [49] at Tampere University have shown that if self-healing breakdowns occur in the immediate vicinity of each other, i.e. one occurs at the edge of the metallization of the preceding self-healed discharge, the second event is often affected by the previous one due to field enhancement at the edge of the metallization (i.e. an electrode). The range of this influence, however, is not precisely known. Also, in some cases flashovers over the film surface to the previous breakdown hole were considered to be a possibility. The breakdowns in this thesis were generally regarded as independent of each other (a photograph of a test capacitor after an endurance test is shown in Figure 5.2.7), but some were discounted after using two forms of analysis.

Figure 5.2.7. *A photograph of a test capacitor after an endurance test demonstrating multiple self-healing breakdowns. The dashed red lines depict the active area.*

The first was the video recordings. These were reviewed using the following criteria: if an event was at the edges of the metallized electrode film or in the immediate vicinity of an earlier breakdown area it was discounted. The second analysis was of the energy of

the discharge. Discharge energy analysis was originally utilized in earlier work at Tampere University, [51] and [49], where it was employed for ramp testing with two criteria: (1) a voltage criterion, which assumes that the breakdown voltage must be higher than in the preceding breakdown, and (2) an energy criterion which states that the discharge energy has to follow a trend set by the first breakdown. As these endurance tests were done with a constant DC voltage, the first criterion was omitted, so the energy analysis was evaluated using only the second criterion.

According to the energy criteria, discharge energy adheres to the following equation

$$E_d = aCU^b, \tag{5.1}$$

where *C* is the capacitance of the capacitor, *a* and *b* are constants, and *U* is the applied voltage [49]. As the active area within the capacitor reduces, and thus the capacitance reduces, self-healing energies should have a gradually declining trend. A minimum energy threshold was determined based on the first two discharges that successfully passed the video recording criteria. If the discharge energy in any subsequent self-healing event was above the threshold, it was regarded as an independent breakdown. If the discharge energy was significantly below the threshold, the discharge was regarded as non-independent and not included in the breakdown data. However, nothing was discounted until it had been carefully analyzed visually in order to ensure that the event had indeed occurred at a supposed location (e.g. an electrode edge) and that no valid event was being disregarded. The discharge energy, E_d, was calculated by integrating instantaneous power *p(t)* over the entire pulse duration, *t,* while instantaneous power *p(t)* was calculated from the recorded voltage, *u(t),* and current, *i(t),* pulses:

$$p(t) = u(t) \cdot i(t). \tag{5.2}$$

An example graph for these variables is shown in Figure 5.2.8. The next section will present a statistical analysis of the breakdown data.

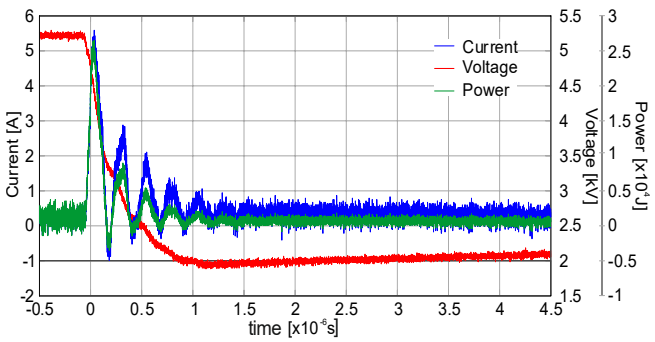

Figure 5.2.8. *Current, voltage and power versus time during a self-healing event. Breakdown occurs at 5.3 kV [49].*

5.2.4 Statistical analysis of breakdown data

The first step in the analysis of the breakdown data was to compare the time-to-failures of the self-healing discharges that had been stressed in equivalent electro-thermal conditions. In this study, 20 self-healings in an 81 cm^2 test area were regarded as an end-of-life criterion. This criterion was based on the fact that self-healings decrease the active area of a capacitor, and thus its capacitance. Furthermore, it was assumed that this number of failures would already represent substantial degradation or ageing of the sample, depending on the applied electric field (i.e. failures would not arise entirely from weak points). Even though this behaviour had only been confirmed in pilot tests under higher electric fields (580 V/µm), it was expected to occur under lower electric fields as well.

The more self-healings that are recorded, the better the data. However, as these were endurance tests, the duration of each test could not be pre-determined, and they could go on a long time. Long testing times were definitely expected to occur, particularly at the lower stresses which are a critical aspect of lifetime modelling, but there had to be a compromise between gathering as much data as possible and keeping the test times down to a reasonable length for a laboratory researcher. As a result, 20 self-healings per capacitor was considered to be a reasonable compromise. The same rationale applied to the sample size, which was kept down to two. Although a higher number of samples would have decreased sample variation, only 2 samples were used in each test to save time and to harmonize the sample size for all the tests. Hence, 40 data points (2 samples, 20 self-healings per sample) were generally gathered for each of the stress conditions. This data was analyzed using Reliasoft Weibull++ software in order to plot Weibull probability graphs (probability of failure vs. lifetime) and to calculate the Weibull parameters.

Before the Weibull probability graphs were plotted the question arose as to whether a single 2-parameter Weibull distribution would always fit well to the data due to the risk of interference from the weak points in the test material that result from the manufacturing processes. In a statistical sense, weak points form subpopulation(s), with lower dielectric strength in the case of ramp testing, or with earlier failure times in the case of constant DC stress. Such data can be valuable to improve production processes because advances in manufacturing should improve failure statistics, particularly in the first quantile. However, the weak points were not considered useful for these experiments, partly because the test samples had only been assembled in semi-clean room conditions, so it was possible that dust accumulation might interfere with the very first breakdown events, and thus they might not all necessarily represent real capacitor films. However, after excluding a defect subpopulation, the remaining distribution should correlate with the

material's inherent properties. Therefore, in theory, any improvements in the performance of the real material could be determined.

A single two-parameter Weibull distribution was used to perform data fitting with the following settings enabled in Weibull++ software: RRX (rank regression), SRM (standard ranking method), FM (Fisher Matrix), and MED (median ranks). To get more information on these variables, please refer to the website[1] for the software. Weak points were excluded from the parameter estimation but left in the Weibull probability graphs to demonstrate how many weak points the test films had. The goodness of the data fitting was evaluated visually and mathematically (correlation coefficient). For an adequate fit, the Weibull α parameter was calculated, which gives the time to reach 63.2% probability of the sample's end-of-life. These parameters were used later to model the films' lifetimes.

[1] http://help.synthesis8.com/weibull_alta8/weibull_standard_folio_control_panel_analysis_page.htm

6. RESULTS AND DISCUSSION

According to accelerated testing theory, the lifetime expectancy of the samples should decrease when the testing temperature is increased. Unexpectedly, some of the endurance tests (see 6.2) demonstrated the opposite result, i.e. the sample's lifetime noticeably increased when the endurance testing temperature was increased. It was thought that this somewhat counter-intuitive result could only be explained by the fact that preconditioning at a higher temperature (i.e. heating and stabilizing the film sample's temperature to the actual endurance test conditions) may have somehow increased the performance of the film. This could explain their longer lifetimes in the ensuing endurance tests. So, the objective of the research plan was extended to study this effect as well.

The endurance tests that are presented in Section 6.2 are referred to as "*primary endurance tests"*. These were carried first, before the lifetime modelling of the commercial reference material (EC) and the prototype 1 nanofilms (P1N), which is presented later in Section 6.3. The preconditioning procedure, i.e. the applied electro-thermal stress and its duration prior to the endurance tests, was experimented with in order to find out whether changes in the preconditioning may significantly influence the sample's lifetime in the primary endurance tests. For the reader's convenience these results are discussed first, in Section 6.1, even though some of the primary endurance tests had already been carried out before the effects of the preconditioning were investigated.

6.1 The effects of preconditioning

The preconditioning effect was studied by varying the preconditioning variables (the temperature, the electric field and their duration) and evaluating their effect on a sample's lifetime. The variations were compared by calculating the Weibull α parameters (i.e. time to reach 63.2% probability of failure) from the endurance tests that followed the preconditioning period. These endurance tests are referred to as "*secondary endurance tests"* in order to differentiate them from the primary endurance tests that were exclusively used in the lifetime modelling, and not for comparing the preconditioning effects.

For practical reasons, the secondary endurance tests were always performed at the same temperature (60 °C) while the electric field was varied. Various electric fields were used in order to compare the preconditioning effect in short-term and longer-term tests. The results of the short-term tests are discussed in Section 6.1.1 and the longer-term tests in Section 6.1.2 and they are summarized in Section 6.1.3.

6.1.1 The effects of preconditioning in the short-term tests

Most of the initial preconditioning tests were performed with prototype 1 nano (P1N) films, so the results of these tests are discussed first. Some of these experiments were duplicated for the commercial reference (EC) and for the prototype 1 reference (P1) films and these results are discussed later. In the short-term tests, after preconditioning each of the endurance tests was carried out at 60 °C and 480 V/μm and continued until 20 self-healings had appeared.

The preconditioning effect was always tested using two specific procedures which were carried out in exactly the same way in all cases. The first was the “normal” preconditioning procedure which is defined in Section 5.2.2. This was used in all the primary endurance tests that are presented in Section 6.2 and is considered as an “*initial test”* with which all the other preconditioning-effect tests are compared. The second test is an actual preconditioning test. This second test was initially found to increase the lifetime of prototype 1 nano samples, and thus, it was thereafter used extensively in all the short- and longer-term tests. This procedure is hereafter referred as the “*comparison test”*. The procedure is as follows: (1) preconditioning was performed at a temperature of 85 °C temperature with a 190 V/μm electric field for 3.5 hours. (2) The oven was set to 60 ˚C, and the sample was allowed to passively cool for 4 hours down to 60 °C in a 190 V/μm electric field. (3) When the preconditioning was complete, an endurance test was commenced at a temperature of 60 °C.

The preconditioning tests were generally done with one sample for each of the changes to the preconditioning parameters (temperature, electric field or their duration). However, some of these tests were repeated. In the graphs that follow, the “initial” and the “comparison” test are positioned in the lower-left corner of the figure and the other tests are in the lower-right corner. Additionally, the Weibull α parameter for all the preconditioning tests are tabulated in the upper-right and there is a Weibull graph in the upper-left corner of the figure.

In Figure 6.1.1, the preconditioning temperature and electric field are constant (60 °C and 190 V/μm) and only their duration is changed, except for the “comparison” test denoted by the yellow circle. It can be observed that when preconditioning goes on for longer than 3.5 hours (at 60 °C and 190 V/μm), the lifetime (Weibull α) of prototype 1 nanofilm increases by approximately 2-3 times as much as it was in the initial test. There is a strong probability that increasing the duration of the prestressing electric field removes more of the residual gas between the sample film and the metallized electrodes, which may have a positive effect on the sample’s lifetime. Despite the increase in the

prototype 1 nanofilm's lifetime, further iterations would be required to account for the variations between the samples. Nevertheless, it is unlikely that sample variation alone can account for the high differences in lifetimes between the comparison test and the other tests. Since the higher test temperature tended to result in a longer lifetime, the preconditioning experiments focused on higher temperatures.

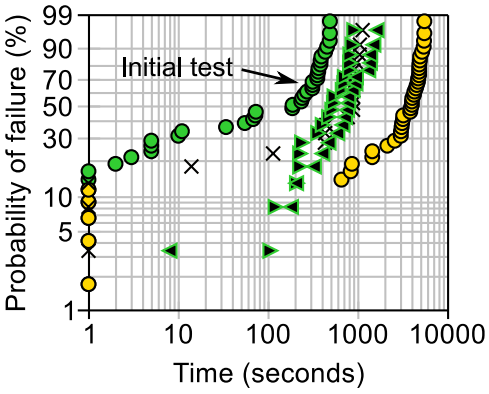

Test method	Weibull α (seconds)	*α, compared to initial test (%)*
●	276	–
▶	586	210
×	801	290
◀	907	330
●	4134	1500

Preconditioning

● 60 °C: 3.0 h; 190 V/µm: 0.5 h

● 85 °C: 3.5 h; 190 V/µm: 3.5 h +
60 °C: 4.0 h; 190 V/µm: 4.0 h

◀ 60 °C: 4.0 h; 190 V/µm: 4.0 h (1st test)

▶ 60 °C: 4.0 h; 190 V/µm: 4.0 h (2nd test)

× 60 °C: 7.5 h; 190 V/µm: 7.5 h

Figure 6.1.1. *Endurance test results for Prototype 1 nanofilm with different preconditioning procedures. The preconditioning i.e. applied electro-thermal stresses and their duration prior to the endurance tests are shown at the bottom. The endurance tests were carried out at a temperature of 60 °C temperature and in a 480 V/µm electric field until 20 self-healings appeared. The corresponding Weibull plots are shown on the upper left and the α parameters on the upper right*

In Figure 6.1.2, preconditioning tests for prototype 1 nanofilm are performed at 85 °C using either a small electric field or none at all. The results suggest that increasing the preconditioning temperature (from 60 to 85 °C), increases the lifetime expectancy of the samples. This effect remains observable even when the samples are initially heat-treated for 19 hours at 85 °C temperature (without an electric field) and then preconditioned for 4 hours at 60 °C and 190 V/µm. The lifetimes for these test samples are 6.5 and 7 times higher than in the initial test (two samples). It is worth noting that the second part of this test corresponds to two of the test results depicted in Figure 6.1.1 (the left and right green arrows). The lifetimes of those samples were approx. 2-3 times as high as they were in the initial test. Thus, the results indicate that a higher preheating temperature may increase the lifetime of prototype 1 nanofilm irrespective of whether or not a preconditioning electric field is applied. However, the results also show that a preconditioning electric field of even as low as 50 V/µm is still beneficial. In this case, the Weibull α parameter was 10 times as high as it was in the initial test (Figure 6.1.2). The results support the

assumption that there is a connection between the preconditioning electric field and the sample's lifetime.

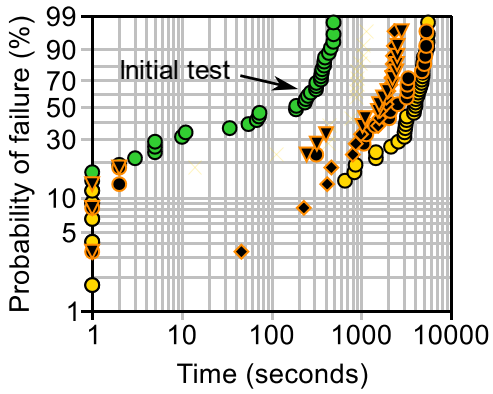

Test method	Weibull α (seconds)	*α, compared to initial test (%)*
●	276	–
▼	1788	650
◆	1923	700
●	2879	1040
○	4134	1500

Preconditioning

● 60 °C: 3.0 h; 190 V/µm: 0.5 h
○ 85 °C: 3.5 h; 190 V/µm: 3.5 h +
60 °C: 4.0 h; 190 V/µm: 4.0 h

▼ 85 °C: 19.0 h; 0 V/µm: 19.0 h +
60 °C: 4.0 h; 190 V/µm: 4.0 h (1st test)
◆ 85 °C: 19.0 h; 0 V/µm: 19.0 h +
60 °C: 4.0 h; 190 V/µm: 4.0 h (2nd test)
● 85 °C: 3.5 h; 50 V/µm; 3.5 h +
60 °C: 4.0 h; 50 V/µm; 4.0 h

Figure 6.1.2. *Endurance test results for Prototype 1 nanofilm with different preconditioning procedures. The preconditioning i.e. applied electro-thermal stresses and their duration prior to the endurance tests are shown at the bottom. The endurance tests were carried out at 60 °C and in a 480 V/µm electric field until 20 self-healings appeared. The corresponding Weibull plots are shown on the upper left and the α parameters on the upper right.*

Since the preconditioning tests at 85 °C consistently increased the lifetime of the prototype 1 nanofilms (compared to 60 °C), even higher preheating temperatures were tested. When the preheating temperature for prototype 1 nanofilm was increased (the other preconditioning parameters were the same as for the "comparison test"), there was no notable increase or decrease in the Weibull α parameter, even at 105 °C (Figure 6.1.3). Therefore, preheating prototype 1 nanofilm at temperatures above 85 °C does not significantly enhance the film's performance.

The preconditioning tests discussed so far for prototype 1 nanofilm indicate that an appropriate temperature and electric field can increase the film's lifetime (compared to the initial test). It is known from the literature that some polymer properties can be enhanced by heat treatment [3]. However, the reason(s) for the film's improved performance after the preconditioning electric field still remained unclear. As mentioned earlier, the prestressing electric field was originally considered to prolong the sample's lifetime by removing some of the residual gas molecules between the sample film and the metallized electrodes. However, it is also possible that the surface treatment of the polymer film

may also have influenced its performance during the endurance test, so this possibility had to be studied.

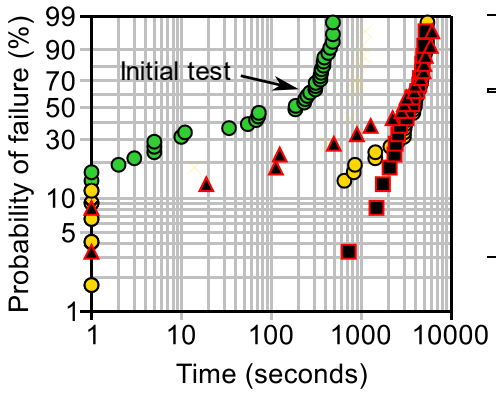

Test method	Weibull α (seconds)	α, compared to initial test (%)
●	276	–
▲	3636	1320
■	3887	1410
●	4134	1500

Preconditioning

- ● 60 °C: 3.0 h; 190 V/µm: 0.5 h
- ● 85 °C: 3.5 h; 190 V/µm: 3.5 h + 60 °C: 4.0 h; 190 V/µm: 4.0 h
- ▲ 95 °C: 3.5 h; 190 V/µm: 3.5 h + 60 °C: 4.0 h; 190 V/µm: 4.0 h
- ■ 105 °C: 3.5 h; 190 V/µm: 3.5 h + 60 °C: 4.0 h; 190 V/µm: 4.0 h

Figure 6.1.3. *Endurance test results for Prototype 1 nanofilm with different preconditioning procedures. The preconditioning i.e. applied electro-thermal stresses and their duration prior to endurance tests are shown on the bottom. Endurance tests were carried out at 60 °C temperature and 480 V/µm electric field until 20 self-healings appeared. Corresponding Weibull plots are shown on the upper left and α parameters on the upper right.*

Basically, the surface treatment of biaxially oriented polypropylene (BOPP) film involves an industrially applied corona treatment that increases the surface charge density on one side of the dielectric film to ensure sufficient adhesion of the electrode metal during the subsequent metallization [10][51]. This process may also induce a space charge in the film, which in theory may affect its endurance properties. It is possible that with a moderate preconditioning temperature and electric field, the stored space charge (particularly hetero-charges) could be depleted. This hypothesis was tested by evaluating the long-term dielectric strength on different sides of the film. If the surface treatment affects the long-term DC dielectric strength of the film, the times to breakdown should diverge to some extent when the polarity of the DC voltage is inverted. The results for the prototype 1 nanofilm are shown in Figure 6.1.4. Even though a slight change in the Weibull *α* parameter can be noticed, this is probably only due to the natural scatter of the breakdown phenomena. Therefore, the surface treatment most likely had no significant effect.

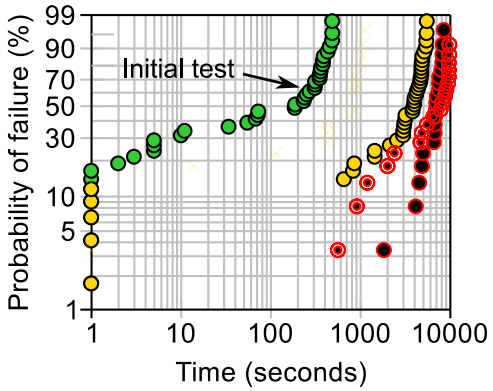

Test method	Weibull α (seconds)	α, compared to initial test (%)
●	276	–
●	4134	1500
●	7306	2650
●	8907	3230

Preconditioning

● 60 °C: 3.0 h; 190 V/µm: 0.5 h

● 85 °C: 3.5 h; 190 V/µm: 3.5 h + 60 °C: 4.0 h; 190 V/µm: 4.0 h

● 85 °C: 3.5 h; 190 V/µm: 3.5 h + 60 °C: 4.0 h; 190 V/µm: 4.0 h*

● 85 °C: 3.5 h; 190 V/µm: 3.5 h + 60 °C: 4.0 h; 190 V/µm: 4.0 h*

Figure 6.1.4. *Endurance test results for Prototype 1 nanofilm with different preconditioning procedures. The preconditioning i.e. applied electro-thermal stresses and their duration prior to endurance tests are shown at the bottom. The endurance tests were carried out at 60 °C and in a 480 V/µm electric field until 20 self-healings appeared. Corresponding Weibull plots are shown on the upper left and the α parameters on the upper right. *DC voltage polarity was changed as the temperature was lowered, i.e. after 3.5 hours.*

The preconditioning tests for prototype 1 nanofilm demonstrate that its performance may be increased by changing the preconditioning parameters. In order to determine the nanofillers' effect on the dielectric strength, some preconditioning test procedures were carried out for the BOPP films without nanofillers (Prototype 1 reference and commercial reference). Figure 6.1.5 illustrates the results for the Prototype 1 reference films. Four tests were performed, three of which were preconditioned in the same way. Despite the rather large variations in lifetimes, an increase can be observed for each test. The repeated tests had approximately 17, 29 and 64 times longer lifetimes than in the initial test. For the prototype 1 nanofilms the corresponding increase at 85 °C temperature was, depending on the preconditioning, in the range of 6.5-15 (not counting the polarity inversion test). So, the lifetime of the prototype 1 reference film increased even more than that of the prototype 1 nanofilm. The fourth test consisted of a 19-hour heating time at 85 °C temperature without a prestressing electric field. Surprisingly, this test sample exhibited the longest lifetime, which was 80 times as high as in the initial test. Based on these results, it may be concluded that the increased lifetime of the prototype 1 nanofilms was not due to their nano-structuration.

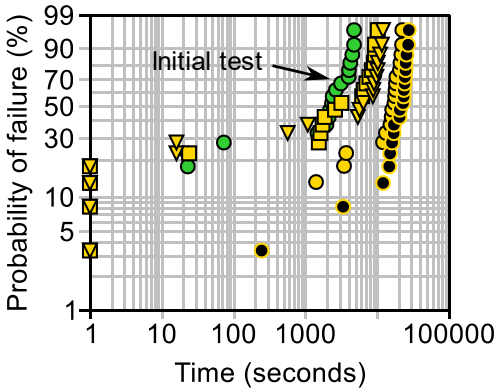

Test method	Weibull α (seconds)	α, compared to initial test (%)
●	276	–
□	4683	1700
▽	7945	2880
○	17762	6440
●	22162	8030

Preconditioning

- ● 60 °C: 3.0 h; 190 V/µm: 0.5 h
- □ 85 °C: 3.5 h; 190 V/µm: 3.5 h + 60 °C: 4.0 h; 190 V/µm: 4.0 h (2nd)
- ● 85 °C: 19.0 h; 0 V/µm: 19.0 h + 60 °C: 4.0 h; 190 V/µm: 4.0 h
- ○ 85 °C: 3.5 h; 190 V/µm: 3.5 h + 60 °C: 4.0 h; 190 V/µm: 4.0 h (1st)
- ▽ 85 °C: 3.5 h; 190 V/µm: 3.5 h + 60 °C: 4.0 h; 190 V/µm: 4.0 h (3rd)

Figure 6.1.5. *Endurance test results for Prototype 1 reference film with different preconditioning procedures. The preconditioning i.e. applied electro-thermal stresses and their duration prior to endurance tests are shown at the bottom. Endurance tests were carried out at 60 °C temperature and 480 V/µm electric field until 20 self-healings appeared. Corresponding Weibull plots are shown on the upper left and the α parameters on the upper right.*

The results for the commercial reference film (Figure 6.1.6) differ from the prototype 1 (nano and reference) materials. The lifetimes of the commercial reference films do not increase, even in the comparison test, i.e. when the heating is first performed at a temperature of 85 °C and then allowed to cool down for 4 hours to 60 °C. The lifetime of the commercial reference films, however, increased when the initial heating was extended to 19 hours without a prestressing electric field. The second step, i.e. the cooling part, was the same as for the previous test. In this case, the lifetime was approximately 2.5 times as high as in the initial test. This difference is rather small when compared to the prototype 1 nano and reference films.

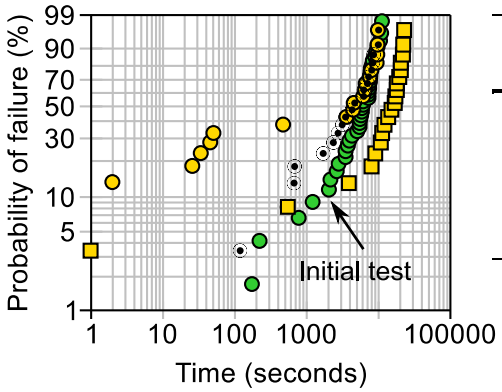

Test method	Weibull α (seconds)	α, compared to initial test (%)
●	6819	–
⊙	5380	80
○	6072	90
□	16883	250

Preconditioning

● 60 °C: 3.0 h; 190 V/µm: 0.5 h

⊙ 85 °C: 3.5 h; 190 V/µm: 3.5 h +
60 °C: 4.0 h; 190 V/µm: 4.0 h (2nd)

○ 85 °C: 3.5 h; 190 V/µm: 3.5 h +
60 °C: 4.0 h; 190 V/µm: 4.0 h (1st)

□ 85 °C: 19.0 h; 0 V/µm: 19.0 h +
60 °C: 4.0 h; 190 V/µm: 4.0 h

Figure 6.1.6. *Endurance test results for commercial 1 reference film with different preconditioning procedure. The preconditioning i.e. applied electro-thermal stresses and their duration prior to endurance tests are shown on the bottom. Endurance tests were carried out at 60 °C temperature and 480 V/µm electric field until 20 self-healings appeared. Corresponding Weibull plots are shown on the upper left and the α parameters on the upper right.*

6.1.2 The effects of preconditioning in the longer-term endurance tests

The preconditioning tests presented above clearly indicate that the preconditioning procedure may affect a film's performance in the ensuing short-term endurance tests (conducted at 60 °C and 480 V/µm). This effect was observed for both the prototype 1 films (nano and reference films) and also for the commercial reference film, although in the latter case the effect was notably lower. In practice, most endurance tests are conducted using much lower electric fields, and so preconditioning had to be studied with lower fields. This section presents the results for the endurance tests performed using lower electric fields (380 V/µm and 280 V/µm) at a single temperature (60°C). Only the initial and the comparison tests defined in Chapter 6.1.1 were carried out. Due to the long testing times, only 10 self-healings were recorded at a stress level of 280 V/µm. The results for the prototype 1 nano and the commercial reference films are discussed below.

Figure 6.1.1 shows that in the "comparison test" (i.e. when the sample is heated for 3.5 hours at 85 °C in an electric field of 190 V/µm and then allowed to cool down for 4 hours to a temperature of 60 °C in an electric field of 190 V/µm), the lifetime of the prototype 1 nanofilm increased in the ensuing endurance test (at 60 °C & 380 V/µm). According to the Weibull *α* parameter, its lifetime is 5.4 times longer than in the initial test (Figure 6.1.7). However, this increase is much less than it was in the endurance tests in an

electric field of 480 V/µm. There, the lifetime was 15 times longer than it was in the initial test. Even allowing for random variation between the tested samples, (i.e. individual tests cannot be compared directly) it is still apparent that at a stress level of 280 V/µm, this decreasing trend in the sample's lifetime continued. In fact, the samples' lifetimes were practically the same regardless of how preconditioning was performed (Figures 6.1.8). Thus, there is a strong indication that the preconditioning effect tends to attenuate in lower electric fields. It may be speculated that the changes in preconditioning are related to a similar type of "annealing" effect which occurs during the actual, longer-term endurance testing. This can be assumed because no effect was observed at the lowest stress (280 V/µm) even though it lasted much longer than the tests in the electric fields of 480 V/µm or 380 V/µm.

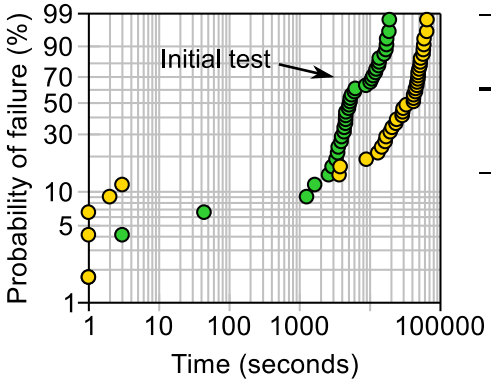

Test method	Weibull α (seconds)	α, compared to initial test (%)
●	8340	–
●	44873	540

Preconditioning
● 60 °C: 3.0 h; 190 V/µm: 0.5 h
● 85 °C: 3.5 h; 190 V/µm: 3.5 h +
60 °C: 4.0 h; 190 V/µm: 4.0 h

Figure 6.1.7. *Endurance test results for Prototype 1 nanofilm with different preconditioning procedure. The preconditioning i.e. applied electro-thermal stresses and their duration prior to endurance tests are shown at the bottom. Endurance tests were carried out at 60 °C temperature and 380 V/µm electric field until 20 self-healings appeared (2 samples were tested). The corresponding Weibull plots are shown on the upper left and the α parameters on the upper right.*

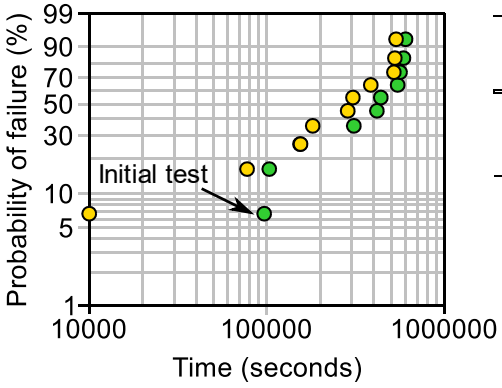

Test method	Weibull α (seconds)	α, compared to initial test (%)
●	435971	–
●	346318	80

Preconditioning
● 60 °C: 3.0 h; 190 V/µm: 0.5 h
● 85 °C: 3.5 h; 190 V/µm: 3.5 h +
60 °C: 4.0 h; 190 V/µm: 4.0 h

Figure 6.1.8. *Endurance test results for Prototype 1 nanofilm with different preconditioning procedure. The preconditioning i.e. applied electro-thermal stresses and their duration prior to endurance tests are shown at the bottom. Endurance tests were carried out at 60 °C temperature and 280 V/µm electric field until 10 self-healings appeared (1 sample was tested). Corresponding Weibull plots are shown on the upper left and α parameters on the upper right.*

When the above tests were replicated for the commercial reference film (EC), some peculiar results were observed. As the lifetime of the EC film did not change in the endurance tests at 480 V/µm, it was not expected that it would increase at a lower stress level (380 V/µm). Nonetheless, the lifetime increased by a factor of 3.3 (vs. the initial test, Figure 6.1.9), and additionally, there was a higher scatter of the breakdown data. At the lowest stress (280 V/µm), the preconditioning did not have any effect on the sample's lifetime (Figure 6.1.10). Thus, it may be concluded that results of endurance tests at 280 V/µm should be similar regardless of how the preconditioning is performed. At the stress level of 380 V/µm, the effect was observable, but since this result was determined using only one sample, some degree of variation could be expected. Moreover, because only 10 self-healings were used as the end-of-life criterion, the weak points in the material might have a more substantial impact on the calculated Weibull *α* parameters.

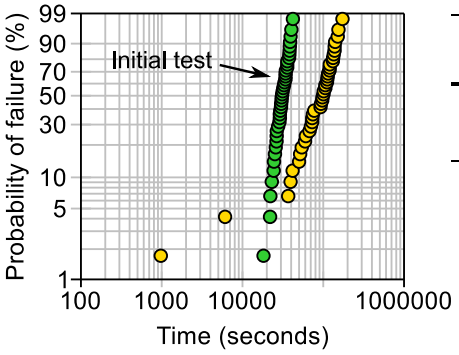

Test method	Weibull *α* (seconds)	*α, compared to initial test (%)*
●	33860	–
●	111256	330

Preconditioning
● 60 °C: 3.0 h; 190 V/µm: 0.5 h
● 85 °C: 3.5 h; 190 V/µm: 3.5 h **+**
60 °C: 4.0 h; 190 V/µm: 4.0 h

Figure 6.1.9. *Endurance test results for commercial reference film with different preconditioning procedures. The preconditioning i.e. applied electro-thermal stresses and their duration prior to endurance tests are shown at the bottom. Endurance tests were carried out at 60 °C temperature and 380 V/µm electric field until 20 self-healings appeared (2 samples were tested). Corresponding Weibull plots are shown on the upper left and α parameters on the upper right.*

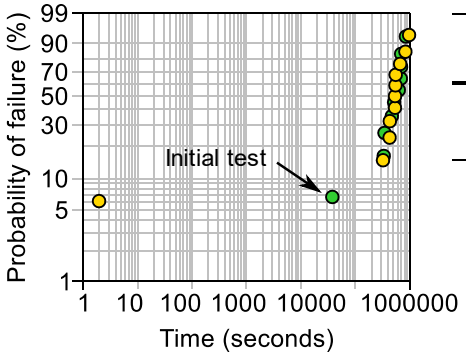

Test method	Weibull *α* (seconds)	*α, compared to initial test (%)*
●	622157	–
●	623981	100

Preconditioning
● 60 °C: 3.0 h; 190 V/µm: 0.5 h
● 85 °C: 3.5 h; 190 V/µm: 3.5 h **+**
60 °C: 4.0 h; 190 V/µm: 4.0 h

Figure 6.1.10. *Endurance test results for commercial reference film with different preconditioning procedures. The preconditioning i.e. applied electro-thermal stresses and their duration prior to endurance tests are shown at the bottom. Endurance tests were carried out at 60 °C temperature and 280 V/µm electric field until 10 self-healings appeared (1 sample was tested). Corresponding Weibull plots are shown on the upper left and α parameters on the upper right.*

6.1.3 Summary of the effects of sample preconditioning

According to the above measurements, the lifetime expectancy of the samples tended to increase in the ensuing endurance tests (which were conducted at 480 V/μm & 60 °C), (1) when the sample had been preconditioned at a higher temperature (85 °C vs. 60 °C) and (2) when the preconditioning electric field was longer (7.5 hours vs. 0.5 hours). This effect was noticed for both the prototype 1 films (nano and reference), and thus the nano-structuration of the film alone cannot account for this effect. For the commercial reference film, the same effect was observed, albeit at clearly more attenuated levels. Although the number of parallel samples was relatively small (three or less), each test demonstrated similar results. However, the results also suggest that the effect of preconditioning tends to decrease when the endurance tests are performed at lower stresses. In an electric field of 380 V/μm, a noticeable decrease was observed while in the lowest electric field (280 V/μm), the sample's lifetime was virtually the same regardless of how the preheating was performed.

Previous findings in the literature support the idea that thermal treatment may increase the dielectric strength of a polymer insulating material. In [49], thermal ageing was carried out for biaxially oriented polypropylene (BOPP) films. The heat was applied stepwise in 10 °C increments from 50 °C to 110 °C in inert nitrogen gas. Each step lasted for 144 hours. After each ageing period, ramped DC breakdown testing was performed at room temperature. The short-term dielectric strength of the BOPP films was determined from the Weibull *α*, which slightly increased when the temperature was above 80 °C, while at 70 °C and below it decreased. An inconsistent result was found in [55] wherein an AC voltage ramp (60 Hz and 500 V s^{-1}) was applied to thermally-aged commercial isotactic polypropylene (iPP) films. The thermal ageing was conducted in inert, oxygen-free conditions, and at 100 °C temperature for 100, 200 or 400 hours. The sample lifetime (Weibull α) steadily decreased as the heating time increased, i.e. the non-aged samples had the highest lifetime, whereas the samples aged at 100 °C for 400 hours had the lowest lifetime.

The tests performed in [50], however, indicate agreement with the previously presented results [49, 55]. In [50], the experiments done on the BOPP films were performed in much the same manner as in [49]. It was observed that the characteristic DC breakdown strength of these films was increased (three types of BOPP films were tested) when ageing had been performed at high temperatures (100 °C and 110°C), while at lower temperatures, weak points emerged [49]. The nature and mechanisms of this increase were not discussed.

The above three studies were only concerned with short-term dielectric strength. In [5], however, both short-term and long-term breakdown performance are discussed. Biaxially oriented polypropylene films were extracted from a failed HVDC filter capacitor bank. The failure rate of the capacitors started to increase sharply in the fifth year of its operation. When the short-term dielectric strengths of 10-year old films and their unaged counterparts were compared, the breakdown strength (the Weibull α value) was noticeably higher in the aged films (716.3 V/μm vs. 584.9 V/μm) than it was in the unaged ones. This improvement was partly attributed to the increase of crystallinity in the BOPP films during ageing, but more importantly, due to an increase in the number of traps. The authors considered that the traps resulted from molecular reorganization, which increased the number of nanocavities that could trap the injected homo-charges in the vicinity of the electrodes. Owing to the accumulation of these homo-charges, the electric field at the dielectric-metal interface is decreased but there is a corresponding increase in the dielectric bulk. As a result, the authors concluded that a sharp increase in the failure rate in long-term test statistics could be accounted for by the presence of the trapped homo-charges. Unfortunately, the long-term performance of the aged and unaged films was not directly measured in the same way as it was for this thesis (Section 6.1.2). Moreover, the films were exposed to very long periods of stress and thus most of the effects may be attributed to ageing. [5]

Overall, the annealing effect and its influence on the long-term dielectric strength of a capacitor has not been studied extensively in the literature. The mechanical strength of annealed samples has been investigated. For instance, in [55] tensile strength (tensile stress vs. time) and elongation (tensile strain vs. time) increased in samples which had been aged for up to 200 hours but decreased in the samples aged for 400 hours. These results are in good agreement with the theory about changes in the crystallinity and the dimensions of the crystal plane, both of which increased in the samples aged for up to 200 hours and decreased thereafter [55]. The short-term dielectric strength, however, did not increase in either of these tests [55]. It should be noted that even though the exact mechanisms of a dielectric breakdown are not known, the prevailing theory considers that the short- and long-term phenomena do have distinct mechanisms, and hence, a material's long-term properties cannot be predicted from short-term tests. Thus, there is a possibility that annealing films may increase their long-term performance. In fact, Montanari et al. have suggested that there is a correlation between the action of static mechanical stress affecting the whole volume of the insulation, and DC electromechanical stress providing enough local strain to bring about plastic deformation in a polymer [40][43]. As an insulation material ages, cavities or crazes can be expected to form,

and some of these will be large enough to cause highly energetic discharges, i.e. degradation.

Although some of the findings of the endurance tests in the electric fields of 380 and 480 V/µm may be due to random sample variation, the results point to the likelihood that a specific precondition procedure may increase the performance of an insulating material, as appears to have happened with the annealing of the commercial film and both the prototype 1 (nano and reference) films. Annealing of the biaxially oriented polymer film may result in increased crystallinity, which in turn, may increase the polymer's resilience to local strain formation. The endurance tests at a stress level of 280 V/µm, however, did not demonstrate the same effect. It is plausible that in this case, a similar type of annealing of the films may have occurred during the actual endurance testing (which was much longer), and that is why the performance of the films did not change. However, this hypothesis needs to be interpreted with caution because of the low number of samples. For the electric field of 280 V/µm, the lifetime of the material was determined from only one sample and 10 self-healings. Therefore, further tests are needed to confirm this hypothesis.

6.2 Endurance tests for the commercial reference and the prototype nanofilm

This section presents the results for the primary endurance tests, which were measured and analyzed as described in Chapter 5. The primary endurance tests were carried out for the commercial reference (EC) and prototype 1 nanofilms (P1N), the main parameters of which are given in Table 6.2.1. The endurance tests were performed at three thermal stresses (60, 70 and 85 °C), and depending on the material, up to five DC electric stresses (280-580 V/µm). The electro-thermal stresses used in the tests are specified in Table 6.2.2.

Table 6.2.1. *Properties of tested biaxially oriented propylene (BOPP) films.*

Code	Type	Silica [wt-%]	Thickness [µm]
EC	Commercial base film	0.0	5.5
P1N	Prototype nanofilm	1.0	5.5

Basically, the endurance tests expressed the time-to-failure for each of the 20 self-healing discharges. In order to utilize this data for the lifetime modelling, further data analysis was required. First, the Weibull distribution was fitted on the measured datasets (40 datapoints, 20 datapoints per sample) and this plot was used show the probability of failure versus lifetime. The Weibull probability graphs in Figures 6.1.1-6.1.5 are depicted as functions of electric field and temperature. These figures are discussed and then the

calculated Weibull *α* (i.e. time to reach 63.2% probability of failure) and *β* (failure rate behaviour) are given in Tables 6.2.3-6.2.4.

Common to each of Figures 6.1.1-6.1.5 is that they indicate early failures or so-called weak points. Some of the early breakdowns were expected to occur as the samples were only prepared in semi-clean conditions, which might have decreased their dielectric strength due to the presence of low amounts of foreign particles, such as dust. However, all insulating materials, even industrial-grade films, have weak points due to their manufacturing processes and consequently, these issues are not only related to the sample preparation. The long-term dielectric strength of materials can be compared by excluding these weak points, which allows the fitting to be done to the rest of the experimental data. Based on the results, this approach can be regarded as successful. A good fit was first confirmed by visual inspection of each of the Weibull plots and was further attested to by their correlation coefficients. These were greater than 0.90 in all cases and are specified in Table 6.2.2. More details of the Weibull plots are given below.

Table 6.2.2. *Correlation coefficient for the Weibull probability plots in Figures 6.1.1-6.1.5. The upper values correspond to the commercial reference (EC) films and the lower values to the prototype 1 nano (P1N) films.*

Temperature (°C)	Electric field (V/μm) 580	480	380	340	280	Film
60	0.982	0.966	0.993	0.973	0.969	EC
	–	0.947	0.974	–	0.970	P1N
70	0.986	0.935	0.984	0.988	–	EC
		0.969	0.975	–	–	P1N
85	0.992	0.984	0.985	0.960		EC
	–	0.989	0.979	–	–	P1N

The Weibull graphs for the commercial reference film (EC) in an electric field of 580 V/μm are shown in Figure 6.2.1. It can be observed that the longest lifetime occurs at 85 °C, not at the test temperature of 60 °C. While this result may be deemed exceptional, the difference in the α parameter is not particularly high (approximately 1.3 times as high), and, in addition, there is a decrease in the life expectancy at 70 °C. These variations in lifetime can be regarded as being caused by sample differences and statistical anomalies. The prototype 1 nano (P1N) films were not tested with this level of electric field (580 V/μm) as they failed in a few seconds once the test field was applied.

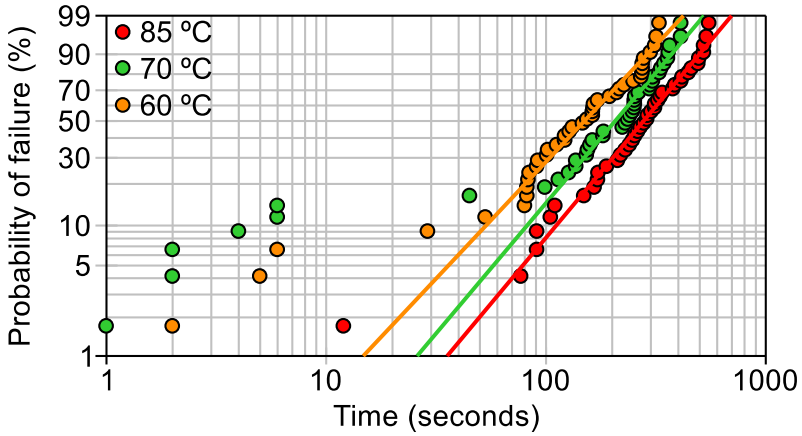

Figure 6.2.1. *580 V/µm Weibull probability plot for commercial reference films. 40 data points (2 samples, 20 self-healing events per sample).*

Figure 6.2.2 depicts the results for the commercial reference film (EC) and the prototype 1 nanofilm (P1N) at 480 V/µm. The EC films performed as expected: the lifetimes were longer at 60 °C than they were at 85 °C. However, the results for the P1N films are surprising. In addition to a cluster of weak points (Figure 6.2.2), the longest lifetime occurs at 85 °C and by a rather large margin (approximately 3.6 times as high an α). It is not really plausible that this difference results from a sample difference alone. Instead, this finding seems to imply that there is a mechanism which increases the sample's lifetime and is susceptible to sample preconditioning (i.e. preconditioning temperature and electric field prior to the endurance tests).

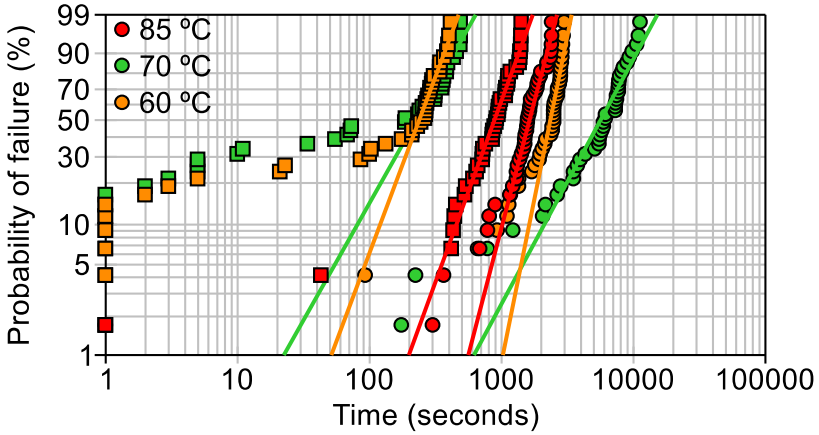

Figure 6.2.2. *480 V/µm Weibull probability plot. 40 data points (2 samples, 20 self-healing events per sample). Circles correspond to commercial reference films and squares to prototype 1 nanofilms.*

This was the point at which it was realized that the influence of sample preconditioning on the sample's lifetime should be experimented on separately from the endurance testing. Thus, the endurance tests were stopped temporarily so that the experiments on the effects of preconditioning could be performed. The results of these tests have been dis-

cussed in detail in Chapter 6.1. In summary, they showed that a higher preheating temperature tended to increase the lifetime of the prototype 1 films (nano and reference) in the higher electric field (480 V/µm), whereas in the lower electric field (280 V/µm) the preheating did not seem to have any effect on the films' lifetimes. in the 380 V/µm electric field, the effect of preheating was attenuated but still observable. For the commercial reference film, the effect was less distinct at each stress level. Even though the lifetime for the prototype 1 nanofilm increased in the short-term preconditioning tests (at electric fields of 380 and 480 V/µm), this was not regarded as a major error source, since it was known that much lower electric stresses are employed in practical accelerated testing. Additionally, for practical reasons the commercial reference film had already been tested in lower electric fields (up to 340 V/µm) before the preconditioning effect was examined. Thus, not all the samples would have been treated equally if different preconditioning procedures had then been used for the subsequent tests. In order to avoid lengthy re-measurements, the endurance testing procedure proceeded unchanged.

Figure 6.2.3 depicts the results for the commercial reference film (EC) and the prototype 1 nanofilm (P1N) at 480 V/µm. For the commercial reference film, the probability lines are relatively similar to those of Figure 6.1.2. For the P1N film, there are fewer weak points (at 60 °C and 70 °C) than in Figure 6.2.2, which is presumably due to sample variation. The probability lines are closer to each other, but the overall differences are small.

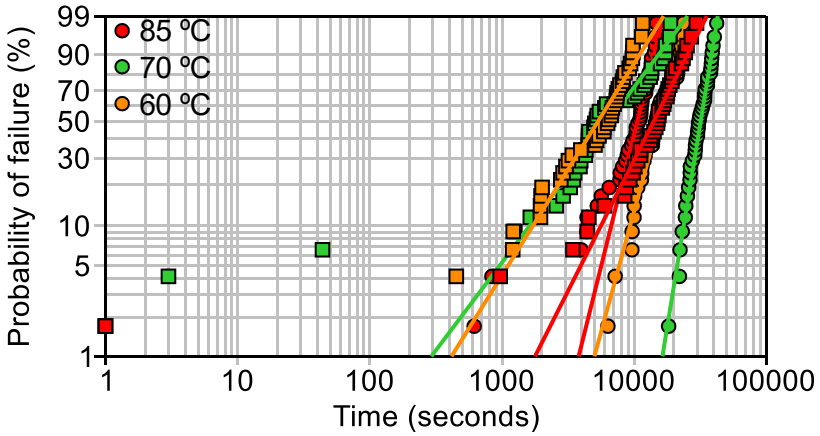

Figure 6.2.3. *380 V/µm Weibull probability plot (EC & P1N films). 40 data points (2 samples, 20 self-healing events per sample). The circles correspond to the commercial reference films and the squares to the prototype 1 nanofilms.*

Figure 6.2.4 shows the results for the EC film at 340 V/µm. The breakdowns first appear at 85 °C, but in the latter part (>60% probability of failure) a higher lifetime (than at 70 °C) is achieved due to the higher scatter of the data. Later inspection of the 85 °C data revealed that the first sample had more than twice as many early failures as the second

sample (9 vs. 4). This explains the rather miscellaneous early part. However, in the latter part, both samples had roughly the same number of failures. Thus, the data suggests that in latter part of the graph, the samples tested at 85 °C do indeed have a higher lifetime than at 70 °C. Further testing is required to determine the reasons for this behaviour. Based on the findings of Section 6.1, it seems that some type of annealing of the polymer film might cause this.

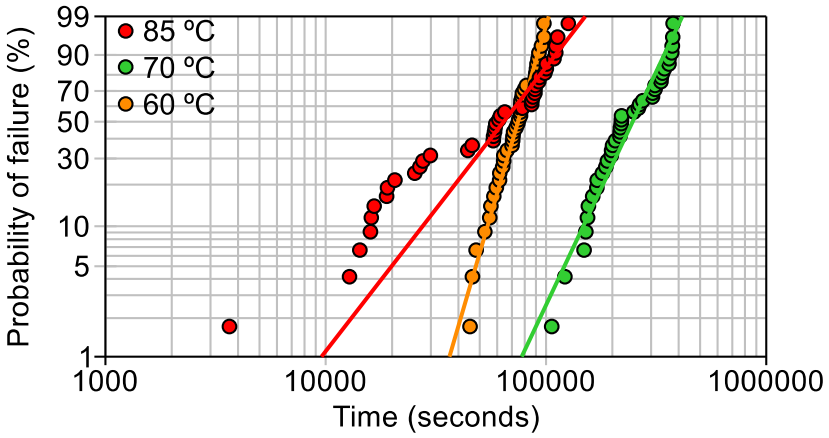

Figure 6.2.4. *340 V/µm Weibull probability plot for commercial reference films. 40 data points (2 samples, 20 self-healing events per sample).*

Figure 6.2.5 shows the results for the EC and P1N films at a stress level of 280 V/µm. Due to the length of the testing times, the test at 280 V/m was only conducted at 60 °C using only one sample (20 self-healings), and therefore no comparison between the samples could be made. Despite the four weak points in the P1N film, the rest of the distribution follows a steep line, clearly indicating a distinct degradation procedure. The EC film time-to-failures are more scattered, resulting in a more gentle slope.

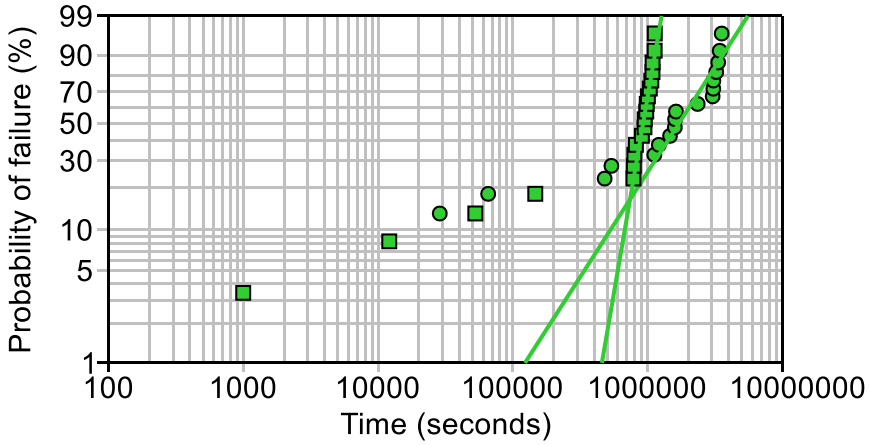

Figure 6.2.5. *280 V/µm Weibull probability plot at 60 °C temperature. 20 data points (1 sample, 20 self-healing events). Circles correspond to commercial reference films and squares to prototype 1 nanofilms.*

The Weibull α and β parameters for the above Weibull plots are specified in Tables 6.2.3-6.2.4. In the tables, the upper values correspond to the commercial reference film (EC)

and the lower values to the prototype 1 nanofilm (P1N). If the experiment at 380 V/µm and 85 °C is excluded from the comparison, it can be observed that the EC film outperforms the P1N film in all tests. That is, the Weibull *α* parameters were longer, and thus the P1N film failed earlier than the EC film. This difference tends to decrease at lower electric stresses. The Weibull *β* parameter indicates that the failure rate increases with time (*β* >1) and thus this signifies that the failures do not arise entirely from weak points, but instead represent genuine sample degradation.

Table 6.2.3. *Weibull α parameters for electro-thermally accelerated tests (Figures 6.2.1-6.25). The α parameter expresses the duration to reach 63.2% probability of failure and is given in seconds. For the reader's convenience the shortest and longest durations of the α parameter (not the test length) are also approximated on a more intuitive scale. The tested films are shown in the column on the right.*

Temperature (°C)	Electric field (V/µm) 580	480	380	340	280	Film
60	247	6819	33860	273388	2150006	EC
	–	276	8340	–	984571	P1N
70	183	2516	16954	79386	–	EC
	–	271	6653	–	–	P1N
85	332	1785	11555	75758	–	EC
	–	1005	16844	–	–	P1N
Duration	3–5 mins	3 mins–2 hours	2–9 hours	1–3 days	1–3.5 weeks	

Table 6.2.4. *Weibull β parameters for electro-thermally accelerated tests (Figures 6.2.1-6.25). The β parameter represents the failure rate behaviour. If β is less than 1, the failure rate decreases with time. If β is equal to 1, the failure rate is constant. If β is greater than 1, then the failure rate increases with time. The tested films are shown in the column on the right.*

Temperature (°C)	Electric field (V/µm) 580	480	380	340	280	Film
60	2.04	1.91	6.34	3.65	2.75	EC
	–	1.83	1.37	–	6.00	P1N
70	1.83	5.10	3.77	5.91	–	EC
	–	2.76	1.66	–	–	P1N
85	2.06	3.96	4.14	2.22	–	EC
	–	2.83	2.04	–	–	P1N

The lifetime calculations from Table 6.2.3 suggest that the difference in lifetime between the EC and P1N materials is highest at 60 °C and 480 V/µm stress (almost 25 times as high) whereas at the lowest stress (60 °C and 280 V/µm) the difference is 2.2 times as high. Based on this observation, there is a reasonable probability that the lifetime difference between the films may be much lower when projections for lower stresses are

made. This result is also in line with an earlier hypothesis of the performance of nano-composite films, i.e. that there is a threshold after which the improved dielectric performance is lost.

6.3 Modelling of the films' lifetime performance

This section presents the lifetime modelling for the BOPP films. The lifetime modelling is based on the results of the endurance tests presented in Section 6.2. Due to its practical importance in real-life applications, lifetime is modelled separately in terms of electric stress in Section 6.3.1. The thermal stress and its concurrent effects with electric stress are modelled in Section 6.3.2. The implications for lifetime modelling are given in Section 6.3.3.

6.3.1 The dependency of a material's lifetime on the strength of the electric field

The dependency of a material's lifetime on the strength of the electric field was modelled using the inverse power law (IPL). The characteristic lifetime parameters were taken from the endurance experiments conducted at different electric stress levels (Weibull α, from Table 6.2.3) and mathematically fitted using Equations 4-4 & 4-5. The fitting of the experimental data to the IPL model was performed in MATLAB using the curve fitting toolbox. For Equation 4-4, the fitting was done using *nonlinear least-squares* regression (hereafter, "nonlinear regression"). For Equation 4-5, the lifetime data was initially linearized by logarithmic transformation and then the fitting was done using *ordinary linear least-squares* regression (hereafter, "linear regression"). Finally, the resulting equation was back-transformed on the original arithmetic scale, thereby yielding estimates for the two parameters in Equation 4-4. For the reader's convenience, both results are plotted in a graph of log (lifetime) vs. log (electric stress) wherein the power law fit is seen as a straight line. The fitted equations are given in the legends for the figures. Note that x was used to express electric stress instead of E, in order to avoid confusion with scientific notation. The results for the commercial reference film are presented first, and then those for the prototype 1 nanofilm.

In Figure 6.3.1, the two nonlinear regression fittings for the commercial reference (EC) films are represented by green and black lines at a test temperature of 60 °C. The difference between the lines corresponds to the number of data points used in the fitting process: in the green line four (580-340 V/µm) data points are used and in the black line five (580-280 V/µm). The r-square parameter is higher than 0.99 for both cases. As can be observed, the black line shows a visually much better fit to the data due to the smaller

residuals of the regression line, particularly at the highest stresses (480 /µm and 580 V/µm).

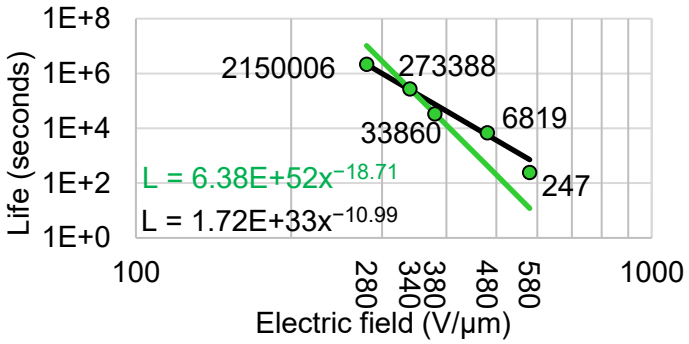

Figure 6.3.1. *Fitting of inverse power law using nonlinear regression method to measurements at 60 °C temperature* and *electric fields of 580, 480, 380, 340 and 280 V/µm. The green line corresponds to the (580-340 V/µm) datapoints and the black line to the (580-280 V/µm) datapoints. Lifetime datapoints are in seconds (commercial reference film, EC).*

When linear regression (Figure 6.3.2) is performed for the same data points and the same film (commercial reference film, EC), it can be noticed that there are only minor differences between the fitted lines and both lines seem to fit the data well in a log-log presentation. The residuals for the green line are improved at higher stresses (480 V/µm and 580 V/µm), and therefore the fitting appears to be visually improved. For the black line, the difference is much lower. However, log-log presentation is somewhat deceptive because the residuals at higher and lower stress levels are not as noticeable. At the highest stress, even somewhat small changes in the residuals (which correspond to high relative error) may be readily observed. In contrast, at the lowest stress the absolute change in the approximation error must be extremely high before it may be discerned. In fact, even though the lines in Figure 6.3.2 may seem to fit better through the data points, in both cases the sum of square errors (SSE) is increased compared to the previous fits (Figure 6.3.1). Thus, the results suggest that nonlinear regression may establish a better fit to the data.

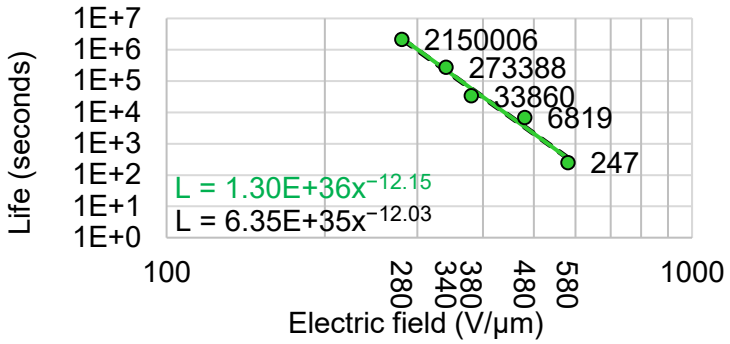

Figure 6.3.2. *Fitting of inverse power law using linear regression method to measurements at 60 °C temperature and* electric fields of *580, 480, 380, 340 and 280 V/µm. The green line corresponds to the (580-340 V/µm) datapoints and the black line to the (580-280 V/µm) ones. Lifetime datapoints are in seconds (commercial reference film, EC).*

In addition to the estimated lifetime equations, it is necessary to take statistical estimation errors into consideration as well. Therefore, prediction bounds (90 %) were graphed to depict the reliability of the statistically forecast errors for the above fittings. These are shown for nonlinear regression in Figure 6.3.3 (a) and for linear regression in Figure 6.3.3 (b). A log-log graph is used in both representations. For nonlinear regression, the prediction bounds vary more as a function of stress. The lower and upper bound errors are wide in the higher electric fields (480 and 580 V/µm), insignificant at 280 V/µm, and minimal at the design field (200 V/µm). Moreover, it can be noticed that the lower bound deviates from the fitted line at a faster rate and escalates at an electric field of approximately 385 V/µm. In fact, the lower bound was not graphed further because it would be negative beyond this boundary-value. For linear regression, the lower and upper prediction bounds are spread similarly, and both bounds widen towards the lower stresses. Overall, the prediction bounds are higher for linear regression (at lower stresses). Despite the lower mean value, a higher estimate would be predicted by the nonlinear regression, when the prediction bounds are acknowledged in the lifetime modelling.

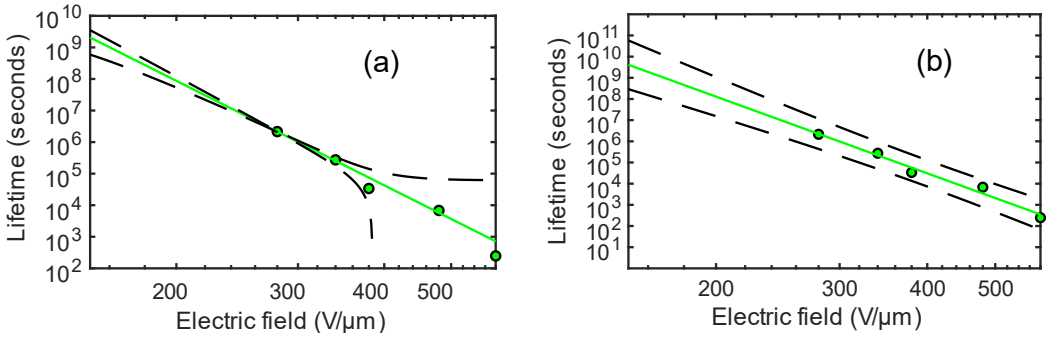

Figure 6.3.3. *Prediction bounds (90 %) for the nonlinear (a) and linear (b) regression methods presented in Figures 6.3.1-6.3.2. All data points were used (580-280 V/µm) when the prediction bounds were calculated (commercial reference film, EC).*

For the commercial reference film, both the nonlinear and linear regression were fitted at 70 °C and 85 °C. These lines are shown in Figure 6.3.4, wherein the dashed black line corresponds to nonlinear regression and the solid red line to linear regression. Overall, the fitted lines express a similar difference as they did at the test temperature of 60 °C, although a somewhat smaller difference is noticeable between the 70 °C fittings.

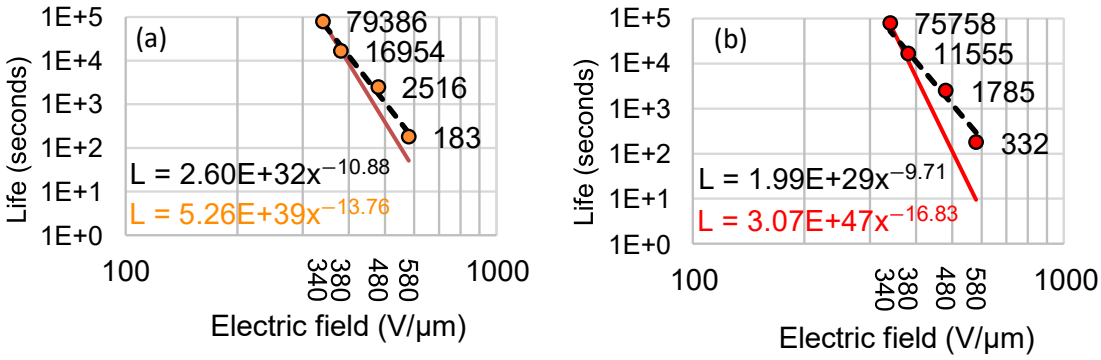

Figure 6.3.4. *Fitting of inverse power law using nonlinear and linear regression method to measurements at temperatures of 70 °C (a) and 85 °C (b) and electric fields of 480, 380, and 340 V/μm. A dashed black line corresponds to linear regression and a solid red line to nonlinear regression. Lifetime datapoints are in seconds (commercial reference film, EC).*

The lifetime predictions for the commercial reference film (EC) are tabulated in Table 6.3.1. Equations with unrounded coefficients (from Figures 6.31-6.3.2 and 6.3.4) were used in the calculations. As can be noticed, the lifetime estimates are affected by the chosen fitting method and the stress range for which the fitting is applied. For the data in the range of 580-340 V/μm, nonlinear regression predicts the highest lifetimes at all test temperatures. In contrast, for the data in the range of 580-280 V/μm, the higher lifetime is predicted by linear regression (at 60 °C). If the prediction is made using nonlinear regression at 200 V/μm and 60 °C for the data in the range of 580-340 V/μm, up to a 178-year lifetime (a design life of a power capacitor is approximately 30 years) might be predicted. However, this kind of debate is only of theoretical interest as the endurance test made at the lowest stress level is naturally the most important, and must thus be included in the IPL fitting. The endurance test at 280 V/μm lasted 1000 hours (~42 days), and thus it fulfils the general requirements of accelerated testing, i.e. at least three stress levels should be employed, from which one of these tests should result in a failure after 1000 hours or later [63]. Hence, neglecting the lowest stress (280 V/μm) result significantly limits the confidence of the prediction.

Table 6.3.1. *Estimated lifetime under different electro-thermal stresses. Estimations were done using equations with unrounded coefficients from Figures 6.31-6.3.2 and 6.3.4 using both nonlinear (NLR) and linear regression (LR). Fittings were done in the range of 580-340 V/µm and 580-280 V/µm (commercial reference films, EC).*

Temperature [°C]	Electric field [V/µm]	Life, NLR [years]		Life, LR [years]	
		580-340	580-280	580-340	580-280
60	200	178	2.75	4.52	4.09
70	200	3.72	-	0.75	-
85	200	18.2	-	0.29	-

Even though only one sample was tested at the lowest stress level due to time constraints, this result may, however, be indirectly compared to another 1000-hour electro-thermal *ageing test* (at 200 V_{dc}/µm and 65 °C) carried out in-house. That experiment was conducted in an inert, oxygen-free ambient atmosphere by supplying a continuous nitrogen flow through an airtight, temperature-adjustable ageing chamber. A test rack comprising a few test capacitors was placed into the ageing chamber. The test capacitors had a sample film and two separate sheets of metallized BOPP as electrodes between supporting glass plates. The active area of each test capacitor was approximately 1050 cm^2 (total test area was ~ 4000 cm^2), and their assembly was done inside an ISO class 6 cleanroom facility at Tampere University. Even though the active area in that test was different, results may be inferred for the active area of 81 cm^2 which was used in this thesis. According to these calculations, approximately 0.26 discharges corresponding to a failure probability of 1.3 % should ensue for this area. This is a very low amount and might just represent the weak points in the film. Based on the short-term dielectric breakdown strength distributions measured for the film before and after the 1000 h ageing, the short-time dielectric strength of the commercial reference film decreased for the electro-thermally stressed film (e.g. 7 % at Weibull α). Thus, the ageing of the films was observed in the experiment.

The nonlinear and linear regressions are presented only at 60 °C for the prototype 1 nanofilm because less than three data points were tested at other temperatures due to time constraints. Both the fitting methods are shown in Figure 6.3.5, wherein the dashed black line corresponds to linear regression and the solid green line to nonlinear regression. Contrary to expectation, both fitting processes seemed to fit well to the datapoints. It is not entirely understood why an established commercial reference film does not seem to visually comply with nonlinear regression, whereas the prototype 1 nanofilm does. One possible explanation is that the lower number of data points may give a better fit simply because there are fewer data points to which the line has to be fitted. In other words, there is a lower probability that some data will deviate from the fitted line. Since the fitting for the prototype 1 nanofilm was made using only three data points (vs. five for

the commercial reference film), it is likely that the lower number of data points resulted in a better fit. In fact, although the commercial reference film has a higher variation in the data, it also demonstrates a rather good fit to three of the data points (280, 340 and 480 V/µm in Figure 6.3.1).

Both fitting processes gave comparable IPL equations for the prototype 1 nanofilm, and as a result, the lifetime projection at 200 V/µm stress only had a one-year difference in the lifetime (5.0 vs. 6.0 years). The longer lifetime was predicted by the nonlinear regression. The prediction bounds (90 %) for the prototype 1 nanofilm are shown in Figure 6.3.6. For nonlinear regression, (Figure 6.3.6 a), there is an insignificant forecast error in either bound below 400 V/µm stress. For the linear regression (Figure 6.3.6 b), both bounds widen towards the lower stresses, which results in moderate forecast error. It can be observed that in both cases the results are similar to those of the commercial reference film (Figure 6.3.3 a and Figure 6.3.3 b). The only exception is that the upper and lower bounds are closer to the fitted line due to the lower scatter of the measured data.

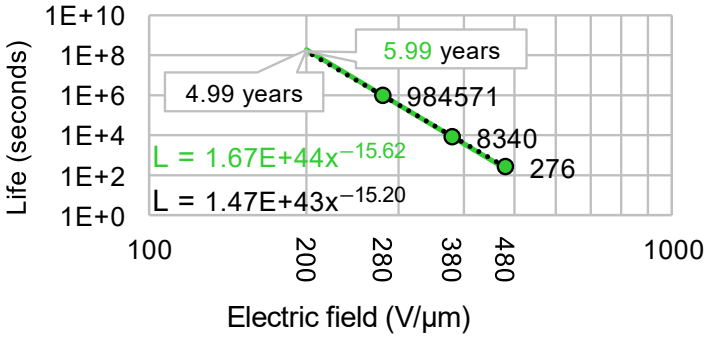

Figure 6.3.5. *Fitting of inverse power law using nonlinear and linear regression method to measurements at temperatures of 60 °C and electric fields of 480, 380, and 280 V/µm. A dashed black line corresponds to nonlinear regression and a solid colored line to linear regression. Estimated lifetime at electric field of 200 V/µm is also depicted. Lifetime datapoints are in seconds (prototype 1 nanofilm, P1N).*

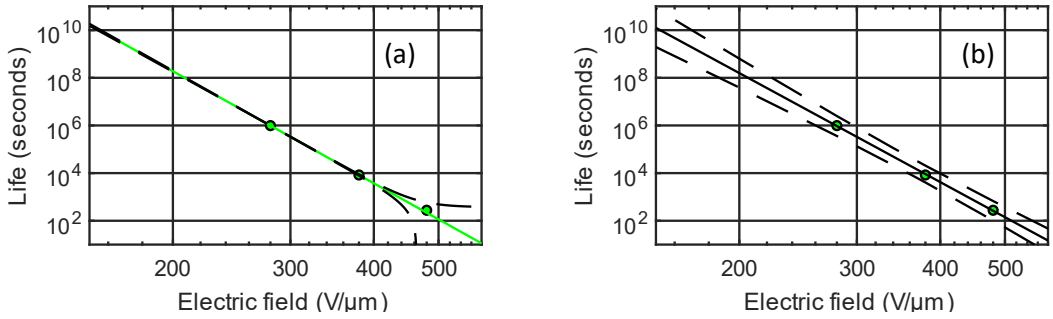

Figure 6.3.6. *Prediction bounds (90 %) for the nonlinear and linear regression method corresponding to Figure 6.3.5 (prototype 1 nanofilm, P1N).*

The lifetime predictions presented in Table 6.3.1 and Figure 6.3.5 indicate that both films may have a comparable performance in an electric field of 200 V/µm (60 °C). Due to the controversial lifetime estimates in the range of 580-340 V/µm, only electric stress in the range of 580-280 V/µm is taken into consideration. When the lifetime is estimated using linear regression there is an approximately 9-months difference in favor of the prototype 1 nanofilm (5.0 vs. 4.1 years). For nonlinear regression, this difference is greater and is 3.2 years in favor of the prototype 1 nanofilm (6.0 vs 2.8 years). However, if the inverse power law were to be fitted to the same set of data points (i.e. electric fields of 280, 380, and 480 V/µm), the calculations reveal that the lifetime for both films would be practically the same (6.2 years). The 1000-hour electro-thermal *ageing test* (at 200 V_{dc}/µm and 65 °C), which was conducted for the commercial reference film was also done for the prototype 1 nanofilm. Using equivalent calculations, approximately 1.08 discharges corresponding to a failure probability of 5.4 % should result for the tested area of 81 cm^2, a value which may also be considered as representing mainly the population of weak points in the film. Furthermore, when comparing just the experimental lifetimes of the films at the lowest stress level (280V/µm) (see Table 6.2.3), it can be noticed that the lifetime of the EC film was ~2 times longer than that of the nanofilm. Both results imply that commercial reference films may have somewhat better performance design stress (at 200 V/µm).

6.3.2 The concurrent effects of temperature and electric field

In this section, the temperature dependency of the lifetime is first modelled using the Arrhenius model. Later, the concurrent effects of temperature and electric field are considered. The lifetime parameters (Weibull α) were delineated from the endurance experiments (Table 6.2.3) and mathematically fitted by Equations 4.3 (Arrhenius model) and 4.14 (multi-stress model). The fitting was performed in MATLAB using the curve fitting toolbox and the *nonlinear* least-squares regression algorithm.

Arrhenius model

The fit of the data to the Arrhenius model is depicted in Figure 6.3.7, wherein the lifetime versus the reciprocal of absolute temperature (*1/T*) is shown in semilogarithmic coordinates, which results in a straight line at electric fields of 580, 480, 380, 340 V/µm. The Arrhenius plots and their equations are given for each electric field. Both analyses are only performed for the commercial reference film due to a lack of data for the prototype 1 nanofilm.

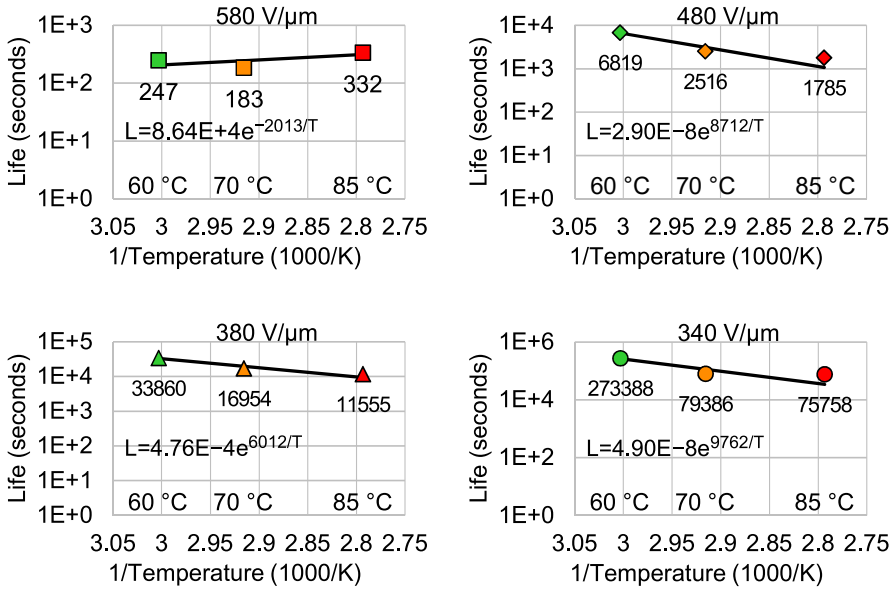

***Figure 6.3.7**. Arrhenius plots to measurements at 60, 70, and 85 °C and electric fields of 580, 480, 380 and 340 V/µm (commercial reference film, EC).*

The above Arrhenius plots indicate that the lifetime of the commercial reference film tends to decrease as the testing temperature is increased. However, according to the data points, the lifetime seems to decrease faster in the temperature range of 60 °C to 70 °C than it did in the range of 70 °C to 85 °C. Thus, there is a slight deviation from the straight-line behaviour at a higher temperature. This effect is most significant in an electric field of 580 V/µm, wherein the lifetime (at 85 °C) even increased, rather than decreased. As it is known from practical experience that the life expectancy of an insulating material should not increase with a higher temperature, it can be concluded that the lifetime in an electric field of 580 V/µm cannot be realistically modelled using the Arrhenius model. The increase in lifetime might be related to the annealing effect discussed in Section 6.1.

In all the other electric fields (340 V/µm, 380 V/µm and 480 V/µm), the lifetime of the commercial reference film can be modelled comparatively well with the Arrhenius equation. The quality of fit, the activation energies and the halving interval in Celsius (HIC) for these fields are shown in Table 6.3.3. The activation energies exhibit some deviation but are reasonably close to the thermal activation energy of the BOPP films, which is approximately 0.75 eV and should be independent of the electric field [25]. The HIC values were calculated from a temperature interval of 60 °C to 70 °C. The calculations indicate that lifetime is approximately halved for a 9°C rise in temperature, except for the test in the 380 V/um electric field, where a temperature increase of 12 °C is required to halve the lifetime. This corresponds quite well to the empirical rule of thumb, which states that the chemical reaction rate is doubled after every 10 °C increase in

temperature. As the ageing rate fundamentally arises from chemical reactions, doubling the reaction rates of these reactions may be expected to approximately halve the lifetime of an insulating material.

Table 6.3.3. *Parameters of Arrhenius model fitting corresponding to Figures 6.1.6-6.1.7 (commercial reference film, EC).*

Electric field (V/µm)	Quality of fit (R^2)	Activation energy (eV)	HIC* (°C)
480	0.940	0.75	9.37
380	0.955	0.52	12.2
340	0.886	0.84	8.70

** HIC (Halving Interval in Celsius): required change in temperature to halve insulator lifetime. HIC was calculated from temperature interval of 60 °C to 70 °C.*

Multi-stress model

When the electric and thermal stresses are varied, multiple stresses are involved. Hence, lifetime modelling becomes more difficult than it is for single-stress models. This complexity arises from the synergy effect of thermal and electrical stresses, which may hasten the ageing caused by the other stress. Here, the modelling was done using Equation 4-14 which presumes that the endurance coefficient (*n)* depends on the applied temperature (*T)*, but the thermal activation energy (*B)* does not depend on the applied electric stress (*E).* Nevertheless, the calculation of the fitting is affected by the starting point of the model's coefficients, and thus these may have some range of variation even in the optimized result. The fitting of the data was performed using electric fields of 340, 380 and 480 V/µm and temperatures of 60, 70 and 85 °C. The data for the electric field of 580 V/µm was neglected due to the increased lifetime at 85 °C (see Figure 6.3.7). However, this decision had a negligible effect on the fitting results. The fitted curve and its equation are depicted in Figure 6.3.8. Note that *X* was used to express electric stress instead of *E* in order to avoid confusion with scientific notation.

$$L(T,X) = 1.00E+40 \cdot e^{\frac{8440}{T}} \cdot X^{-(18.80-\frac{265}{T})}$$

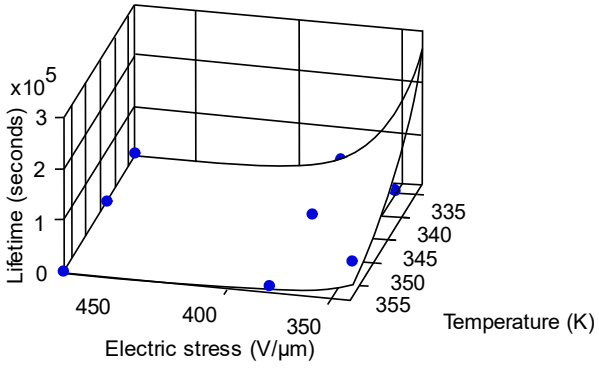

Figure 6.3.8*. Multi-stress fitting at 60, 70, and 85 °C and electric fields of 480, 380 and 340 V/µm (commercial reference film, EC).*

The lifetime predictions for the commercial reference film were calculated using the above equation with unrounded coefficients. The results at a stress level of 200 V/µm are shown in Table 6.3.4. In order to facilitate a lifetime comparison with the inverse power law (IPL), its estimates (lifetime and endurance coefficient from Subchapter 6.3.1) are also presented in the same table.

Table 6.3.4. *Lifetime of the commercial reference film* (EC*) estimated from endurance tests using multi-stress equation, see Figure 6.3.8. For the reader's convenience the inverse power law (IPL) results (lifetime and endurance coefficient) from Chapter 6.3.1 are tabulated here as well. The fitting of the inverse power law was done using nonlinear regression.*

Temperature [°C]	Electric field [V/µm]	Life, [years]		Endurance coefficient	
		Multi	IPL	Multi	IPL
60	200	119	178	-18.0	-18.7
70	200	50.2	3.72	-18.0	-13.8
85	200	15.1	18.2	-18.1	-16.8

Overall, the outcome of the multi-stress model is more logical than the IPL modelling, since the predicted lifetime (at 200 V/µm) decreases towards a higher temperature. Nevertheless, based on the results of Section 6.3.1, it is likely that these lifetimes are overestimated. This is probably related to the data measured in the range of 580-340 V/µm, for which the inverse power law also demonstrated inconsistent lifetime predictions. Consequently, the same data may cause unexpected results for the multi-stress models as well.

If the multi-stress equation from Figure 6.3.8 is compared to the single-stress equations, it can be noticed that the exponent term for thermal ageing corresponds to those of the single-stress models. In fact, because thermal ageing may be regarded as being independent of the electric stress, the starting point of the fitting's coefficients were chosen so that the corresponding exponent term would be equivalent. The endurance coefficient remains practically unaltered in the multi-stress model. This result is in contrast with the literature [47]. A study done in 1989 found that the endurance coefficient for BOPP film had a value of 14.11 at 23 °C and a value of 11.07 at 90 °C [47]. For modern capacitor-grade BOPP films, the endurance coefficient might be in the range of 20 to 30 at room temperature. While this outcome might be avoided by choosing different initial parameters for the optimization, this would lead to different thermal activation energy that would not be independent of the electric field.

6.3.3 Implications for lifetime modelling

In Sections 6.3.1-6.3.2, endurance graphs (lifetime vs. electric field) were plotted and lifetime modelling performed using single- and multi-stress models. The single-stress fitting to data was initiated by modelling the electric field dependency of the lifetime using the inverse power law (IPL). The temperature dependency of the lifetime was then modelled using the Arrhenius model. Finally, the concurrent effects of temperature and electric field were considered.

Fitting the inverse power law to the empirical data demonstrated somewhat inconsistent results. This depended on the fitting technique, (either (1) linear regression on the linearized data or (2) nonlinear regression on the original data) and the electric stress range for which the fitting was applied. Since the inconsistent result for the commercial reference film only recurred in one of the four cases, and most importantly, not in the paramount case that incorporated the lowest-stress data point (280 V/μm), it was attributed to variations in the data in the range of 580-340 V/μm. In fact, when the multi-stress model was fitted to the data for the 580-340 V/μm ranges, it seemed to overestimate the lifetimes as well. For the prototype 1 nanofilm, the fitting was done only using the inverse power law at a test temperature of 60 °C. Both fitting methods gave a similar, virtually perfect, fit in the range of 480-280 V/μm. The differences between the commercial reference film and the prototype 1 nanofilm may relate to (1) the number of data points used in the fitting process and (2) a high variation in the measured data. As well as these causes, however, the results of the inverse power law demonstrate that the two fitting methods do have some influence on the parameters of the fitted line.

Interestingly, the highest lifetime for the commercial reference (EC) film and the highest lifetime for the prototype 1 nano (P1N) film are predicted by different methods. For the EC film, the linear regression on the log-transformed (i.e. linearized) data predicts a higher lifetime, whereas for the P1N film, the highest lifetime is given by nonlinear regression (on original, untransformed data). Since the chosen fitting method may have a notable influence on lifetime modelling, it is surprising that the data fitting process is not explicitly defined in the literature. Presumably, logarithmic transformations were originally used to linearize data and thereby to facilitate data analysis in the early years of such research. For instance, a linear relationship between variables may be readily assessed by plotting the results in a logarithmic paper. Additionally, the parameters (the slope and intercept of the line) for linear least-squares regression can be calculated because an analytical solution exists for this problem. Nonlinear regression does not have an analytical (closed form) solution for estimating the parameters, and thus it must be solved using numerical (iterative) methods. The advent of the processing power of PCs

and statistical software has rendered linearization unnecessary, and the solution can nowadays be found using nonlinear regression as well. These fitting methods, however, are not entirely interchangeable.

In allometric research, the two fitting techniques for *power-law* models have been debated extensively; inverse power law, which is used in lifetime modelling for electrical insulating materials, is a particular instance of power law. It has been argued that neither of the methods is inherently superior for fitting power laws to data. Instead, the choice should be dependent on the distribution of the error term [59]. In other words, whether the error is normally distributed and additive on an arithmetic scale, or whether it is lognormally distributed and multiplicative on an arithmetic scale [59]. Both assumptions cannot be valid for a single data set, and any violation of statistical assumptions of error can lead to biased point estimates as well as inaccurate confidence intervals. If data transformations are used, the relationship between the predictor and the response variables is changed. Consequently, a regression analysis on a log transformation entails modelling a distribution that differs from that of the corresponding arithmetic values [45]. Since this effect is more significant at the high ends of the scales, the highest values will have less influence on the parameters in the fitted equation [46]. It has been suggested, for allometric data, that (1) linear regression on log-transformed data may provide good predictions for small values but poor predictions for high ones and (2) that this “effect” occurs in data sets that span large ranges in size [46]. Furthermore, fitting on the logarithmic scale will cause the predicted value of the lifetimes to be biased on the arithmetic scale since the error structure of the fitting methods is dissimilar [28]. Although this bias might be corrected by a certain correction factor, it is possible that such a correction may cause overestimation [28].

In this thesis, the inverse power law demonstrated a better fit (i.e. smaller residuals) for both films at lower stresses when the fitting was done using nonlinear regression. Moreover, nonlinear regression produced the best overall fit, i.e. the regression line that has the least squared approximation error among all the regression lines that can be drawn. By contrast, the linear regression on log-transformed data (not bias-corrected) fitted a line whose residuals were rather moderate at each point of the regression line. Thus, a somewhat better fit was established at higher stress levels due to the smaller residuals at higher stresses. As a result, the fitted line seemed to go through all data points on a logarithmic scale. In particular, this was the case for the commercial reference film for which there was a higher difference between the fitting methods.

As the linear regression on log-transformed data does indeed tend to favor higher stress data, as discussed above, it is plausible that when only lower stress levels are used, the

dissimilarities between the two fitting methods may be insignificant. Hence, both techniques may give comparable results. The prototype 1 nanofilm demonstrated similar fittings even though higher stress data (i.e. not only low-stress data) was used in the fitting process. However, in practice, it is also desirable to minimize forecast error (i.e. consider prediction bounds), particularly at the lowest stress level. The plotted prediction bounds (90%) indicated that there is a great deal of uncertainty of the fitted line if only high-stress data is utilized in the data fitting. Thus, besides different physio-chemical breakdown mechanisms at lower stress levels, accurate prediction bounds will also require measurements at the lower stress levels due to this uncertainty in the fitting process. Since the prediction bounds generally showed lower forecast errors for nonlinear regression, it can give a mathematically somewhat more accurate lifetime prediction at the service stress level.

The overall findings of the endurance tests indicate that the measured lifetimes versus the electric field may be expressed using a linear trend because no curvilinearity is manifest in the experimented range. This appears to be the case for both film types (the commercial reference film and prototype 1 nanofilm). Since the plotted endurance graphs do not indicate significant curvature, the results seem to suggest that there is no notable change in the ageing mechanisms over the stress range studied. This could partly explain the relatively short lifetime projections at lower stress levels (e.g. at 200 V/µm). However, this deduction has some flaws. Due to the use of logarithmic scales, a rather high difference in the lifetime would be required for it to be noticeable at the lowest stress levels. Thus, fitting results alone might not necessarily signify whether there is an actual change in the electrical ageing mechanisms.

The structure of the test capacitors in this thesis was relatively simple, and they do not entirely correspond to those of manufactured, optimized capacitor structures. Thus, it is understandable that somewhat shorter lifetimes may be measured for the test capacitors than for their commercial counterparts. Rough estimates may be given to assess how much performance must improve, so that the design lifetime would be attainable. Even though improvements would occur at each stress level, for simplicity, we restrict ourselves to a case wherein only lifetime expectancy at the lowest stress (280 V/µm) is increased. Thus, if the desired lifetime increases, then the inverse power law that is fitted to that data, in turn, will predict higher lifetimes at lower stresses.

Based on these computations, a design lifetime of 30 years requires a film's lifetime at the lowest stress (280 V/µm) to be increased by a factor of 2.49 for the commercial reference film. The duration of the measurement was approximately 25 days (from Table 6.2.3), which means that the corresponding Weibull α parameter would be approximately

62 days. For the prototype 1 nanofilm, a design lifetime of 30 years would require the test length to be increased by a factor of 2.16. These values seem reasonable, since it is known that the increase of pressure, which is realized to a greater extent during the manufacturing of commercial capacitors elements, is known to enhance the lifetime of polymer film [7]. Notably, this is due to mechanical compression caused by the factory winding of the capacitor elements and the subsequent heat treatment. In order to verify this, commercially wound capacitors elements should be subjected to the same stress levels as were used here, in this thesis. Transferring the performance increments to the test capacitors that were used in this thesis would require further experimental investigations so that pressure could be applied in such a manner that the increase in lifetime is realizable for the planar configuration as well.

Finally, it should also be remembered that the lifetime modelling in this thesis is directly dependent on the number of self-healing discharges, i.e. the decided end-of-life criterion. In real capacitors, capacitance loss is typically chosen as the end-of-life criterion, which is the net sum of the electrode area lost due to self-healings. In capacitor elements, the clearing area of each breakdown is also optimized. Twenty (20) breakdowns in the test capacitor structure with a clearing area diameter of 2 or 3 mm would mean a capacitance drop of only 0.8 % or 1.7 %, respectively. For high-reliability capacitors, a capacitance drop of approx. 3 % is typically accepted [63]. Based on this, the decided end-of-life criterion for the endurance tests of this thesis is very strict, which could also lead to the underestimation of the films' lifetimes. In addition, using the Weibull alpha as the characteristic end-of-life value is also a somewhat strict criterion as it refers to the 63 % probability of the breakdown distribution. It may be concluded that the utilized end-of-life criterion is strict and is thus partly the cause of the shorter lifetime estimations. However, the self-clearing phenomenon is complicated and depends on both capacitor design and the electro-thermal stress [11][48][49]. Therefore, there is no universal failure criterion that is applicable to all stress conditions. In order to assess the design lifetime of capacitors more accurately, the total clearing area of wound-capacitor elements should be studied, so that more specific end-of-life criteria may be used in the accelerated testing.

7. SUMMARY AND CONCLUSIONS

The purpose of this thesis was to study the long-term DC dielectric strength of polymer thin films used in metallized film capacitors. The thesis was done as a part of the EU-funded Horizon 2020 project, GRIDABLE, wherein various silica-BOPP films are developed and produced. In the literature part (Chapters 2-4) of this thesis, the underlying theory for the experimental part (Chapters 5-6) was presented.

In the experimental part, the lifetimes of commercial biaxially oriented polypropylene (BOPP) thin films and pilot-scale nanostructured (silica nanocomposites, 1.0 wt-%) BOPP thin films were evaluated under long-term DC electro-thermal (E-T) endurance tests. These endurance tests were carried out for self-constructed metallized film capacitors which employed an industrial-grade polymer film as insulation and two separate sheets of metallized films as electrodes. Endurance testing was conducted in a temperature-controlled vacuum oven filled with nitrogen gas and utilizing the self-healing capability of the metallized films. Twenty (20) independent breakdowns (in each test capacitor) were employed as end-of-life criteria, and the times to each breakdown were recorded. The endurance tests were performed twice at each stress level except for the lowest stress one (280 V/μm). Hence, 40 datapoints (2 samples, 20 self-healings per sample) were utilized for each E-T stress. The analysis of the data provided Weibull probability graphs (probability of failure vs. lifetime) and Weibull α (the duration to reach 63.2% probability of failure), which were used in further analyses.

The empirical part had two objectives. *The first* one was to conduct “primary” endurance tests for two types of BOPP film (commercial reference film and prototype 1 nanofilm). The aim was, first, to examine whether empirical lifetime modelling techniques may be used with novel materials. Then, based on the endurance test results, lifetime modelling at stress levels comparable to real service conditions (~200 V/μm) was performed. Two single-stress models and one multi-stress model were used. The single-stress models represented the electric field (inverse power law, IPL) and the temperature dependency of the lifetime (Arrhenius model), whereas the multiple-stress model represented their concurrent effects [2]. The results of the primary endurance tests and lifetime modelling are collected in Table 7.1. *The second* objective was to assess if changes in the *preconditioning*, i.e. the procedure of heating and preparing the sample for the conditions of the ensuing endurance test, could significantly influence the sample’s lifetime in the ensuing

[2] For prototype 1 nanofilm, lifetime modelling was done using inverse power law only.

endurance tests. The preconditioning effect was studied by varying the preconditioning variables (temperature, electric field and their duration) and evaluating their effect on the sample's lifetime in the endurance tests. These endurance tests were separate ("secondary endurance tests") and were not the ones used in the lifetime modelling.

Table 7.1. *The table shows the measured lifetime data (Weibull α parameters) from the primary accelerated tests done in the range of 580-280 V/µm on the left side of the table. The tested films (commercial reference film, EC, and prototype 1 nanofilm, P1N) are indicated on the right side of the table. The modelled lifetimes at the stress level of 200 V/µm are in the middle of the table (grey shaded area). Lifetime modelling was performed by three different models and the models were fitted to the widest range of electric stress, except for the multi-stress model for which the data at the highest stress (580 V/µm) was omitted. The fitting of the inverse power law to the empirical data was made using linear regression ("LR") on the log-transformed data and nonlinear regression ("NLR") on the original data. The fitting of the multi-stress model ("MS") to the empirical data was done using nonlinear regression.*

Measured life							**Modelled life**			
		Electric field (V/µm)					(V/µm)			Film
		580	480	380	340	280	200			
Temperature (°C)	60	4.12	114	9.41	3.16	24.9	2.75	4.09	119	EC
		–	4.60	2.32	–	11.4	5.99	4.99	–	P1N
	70	3.05	42.0	4.71	0.92	–	3.72	0.75	50.2	EC
		–	4.52	1.85	–	–	–	–	–	P1N
	85	5.53	29.8	3.21	0.88	–	18.2	0.29	15.1	EC
		–	16.8	4.68	–	–	–	–	–	P1N
Time		[min]	[min]	[h]	[d]	[d]	[a]	[a]	[a]	
						Model	**NLR**	**LR**	**MS**	

According to the preconditioning test measurements, the lifetime expectancy of the samples tends to increase in the ensuing endurance tests (at 480 V/µm & 60 °C), when the sample preconditioning is performed at a higher temperature (85 °C vs. 60 °C) and when the duration of the prestressing electric field is increased (7.5 hours vs. 0.5 hours). This effect was observed for both prototype 1 films (nano and reference films). However, this effect of the preconditioning (i.e. increased lifetime) tends to decrease when the endurance tests are conducted in lower electric fields. The endurance tests in an electric field of 380 V/µm (60 °C) showed lower effects, and the lifetime in an electric field of 280 V/µm (60 °C) was virtually the same, regardless of how the preheating was performed. While this decrease may be partly associated with the sample variation, the results point to the likelihood that a specific preconditioning procedure may increase the performance, e.g. due to annealing of the polymer film. Annealing of the biaxially oriented polymer film may result in increased crystallinity, which in turn, could increase the polymer's resilience to

local plastic deformation. Since the preconditioning did not influence the samples' lifetimes in the electric field of 280 V/μm, it is plausible that the changes in preconditioning are related to a similar type of "annealing" effect which also occurs during the actual, longer-term endurance testing at more moderate stresses. This is because no effect was observed at the lowest stress (280 V/μm), where the testing lasted much longer than it did for the tests in the electric fields of 480 V/μm or 380 V/μm. However, due to the low number of samples, further replications (particularly at lower stresses) are needed to verify this hypothesis.

The overall findings of the primary endurance tests and the lifetime modelling indicate, first, that the inverse power law (using either of the fitting methods) may be used to model the lifetime of both films. The reason for this is that no curvilinearity is manifest in the experimented range in a log-log presentation. As a result, the measured lifetimes versus electric field may be expressed using a linear trend in logarithmic scales for both films (commercial reference film and prototype 1 nanofilm). Second, there is a reasonable probability that both films have comparable lifetimes at lower stress levels. Although the modelled lifetimes are slightly in favor of the prototype 1 nanofilm, these small differences should not be overemphasized because lifetime modelling is typically volatile in terms of changes in the data. Furthermore, the result is, to some extent, in contrast with the measured data (primary endurance data) which indicates approximately twice as good endurance performance for the commercial reference film (vs. prototype 1 nanofilm) at a stress level of 280 V/μm. Third, the results imply that a design lifetime of 30 years cannot be predicted with a very high confidence level for either of the film types at service stress level (200 V/μm). However, despite the lack of agreement over the design lifetime, this testing method may be used to compare the lifetime behaviour of different films.

The shorter lifetime modelled for the test capacitors may be partly related to the fact that they do not entirely correspond to those of industrially manufactured, optimized capacitor structures. A notable difference is that the polymer film is subjected to high pressure and a rigid structure when wound into its final form during the manufacturing process [11]. It is known that an increase in pressure on a polymer film may enhance its lifetime [7]. Another factor that may contribute to the shorter lifetime of the test capacitors is the number of discharges that were applied as an end-of-life criterion for the lifetime modelling. The criterion used in this study is probably more stringent than the criteria that are typically used for commercial capacitors. Using Weibull α (63,2 %) as the characteristic lifetime parameter in the modelling makes the overall criteria even more stringent, compared to using, e.g. 100% breakdown probability as the characteristic lifetime parameter. Finally, the relatively short lifetimes predicted by the models, do not seem to be related

to the range of electro-thermal stresses used in the accelerated lifetime experiments. This is because the lowest measuring point is already quite close to the desired stress level to be modelled, and therefore it is probable that only a dramatic change in ageing mechanisms would notably change the observed trend over a lifetime. However, more measuring points in the lower stress range and a larger tested film area at each test point would definitely improve the reliability of the modelling results.

It is recommended that further research is undertaken to evaluate how much the lifetime improves if the commercially-wound capacitor elements are subjected to the same stress levels as in this thesis. Additionally, the total cleared area of these wound capacitor elements may be studied so that more specific end-of-life criteria may be used in the accelerated testing of the polymer films. Transferring the performance increments to the test capacitors that were used in this thesis also requires further experimental investigations so that, e.g. pressure could be applied in such a manner that the increase in lifetime is realizable for the planar configuration.

REFERENCES

[1] H. Bian, L. Yang, Z. Ma, B. Deng, H. Zhang, and Z. Wu, “Improved physical model of electrical lifetime estimation for crosslinked polyethylene AC cable,” IEEE Transactions on Dielectrics and Electrical Insulation, vol. 27, no. 1, pp. 132–139, 2020

[2] A. R. Blythe, Electrical properties of polymers. Cambridge U. P., 1979.

[3] W. D. Callister, Materials science and engineering, 9th ed., SI version. Wiley, 2015.

[4] M. C. Celina, “Review of polymer oxidation and its relationship with materials performance and lifetime prediction,” Polymer Degradation and Stability, vol. 98, no. 12, pp. 2419–2429, 2013

[5] L. Cheng, W. Liu, X. Liu, C. Liu, S. Li, and Z. Xing, “Online degradation of biaxial-orientated polypropylene film from HVDC filter capacitors,” IEEE Transactions on Dielectrics and Electrical Insulation, vol. 26, no. 1, pp. 26–33, 2019

[6] H. Chi Mi and D. Burger, “Accelerated lifetime-test for metallized film capacitors - HJC Whitepaper.” 2003.

[7] J.-P. Crine, “A molecular model to evaluate the impact of aging on space charges in polymer dielectrics,” IEEE Transactions on Dielectrics and Electrical Insulation, vol. 4, no. 5, pp. 487–495, 1997

[8] J.-P. Crine, “On the interpretation of some electrical aging and relaxation phenomena in solid dielectrics,” IEEE Transactions on Dielectrics and Electrical Insulation, vol. 12, no. 6, pp. 1089–1107, 2005

[9] P. Cygan and J. R. Laghari, “Models for insulation aging under electrical and thermal multistress,” IEEE Transactions on Electrical Insulation, vol. 25, no. 5, pp. 923–934, 1990

[10] M. T. DeMeuse, Biaxial stretching of film principles and applications. Cambridge: Woodhead Pub, 2011.

[11] R. P. Deshpande, Capacitors. McGraw-Hill Education: New York, Chicago, San Francisco, Athens, London, Madrid, Mexico City, Milan, New Delhi, Singapore, Sydney, Toronto, 2015.

[12] J. G. Drobny, Polymers for Electricity and Electronics: Materials, Properties, and Applications. Hoboken, UNITED STATES: John Wiley & Sons, Incorporated, 2012.

[13] E. A. Elsayed, “Accelerated Life Testing,” in Handbook of Reliability Engineering, H. Pham, Ed. London: Springer London, 2003, pp. 415–428.

[14] D. Fabiani, G. C. Montanari, and L. A. Dissado, “Measuring a possible HVDC insulation killer: fast charge pulses,” IEEE Transactions on Dielectrics and Electrical Insulation, vol. 22, no. 1, pp. 45–51, 2015

[15] J. C. Fothergill, “Ageing, Space Charge and Nanodielectrics: Ten Things We Don’t Know About Dielectrics,” 2007

[16] R. Gallay, “Metallized Film Capacitor Lifetime Evaluation and Failure Mode Analysis,” arXiv:1607.01540 [physics], 2015

[17] H. Ghorbani et al., “Long-term conductivity decrease of polyethylene and polypropylene insulation materials,” IEEE Transactions on Dielectrics and Electrical Insulation, vol. 24, no. 3, pp. 1485–1493, 2017

[18] A. Gupta, O. P. Yadav, D. DeVoto, and J. Major, “A Review of Degradation Behavior and Modeling of Capacitors,” 2018

[19] J. Ho and T. R. Jow, “High field conduction in biaxially oriented polypropylene at elevated temperature,” IEEE Transactions on Dielectrics and Electrical Insulation, vol. 19, no. 3, pp. 990–995, 2012

[20] J. P. Jones, J. P. Llewellyn, and T. J. Lewis, “The contribution of field-induced morphological change to the electrical aging and breakdown of polyethylene,” IEEE Transactions on Dielectrics and Electrical Insulation, vol. 12, no. 5, pp. 951–966, 2005

[21] A. Kalair, N. Abas, and N. Khan, “Comparative study of HVAC and HVDC transmission systems,” Renewable and Sustainable Energy Reviews, vol. 59, pp. 1653–1675, 2016

[22] K.-C. Kao, Dielectric Phenomena in Solids. Academic Press, 2004.

[23] S. O. Kasap, Principles of electronic materials and devices, 3rd ed. McGraw-Hill, 2006.

[24] A. Küchler, High Voltage Engineering. Berlin, Heidelberg: Springer Berlin Heidelberg, 2018.

[25] J. K. Kuffel, W. S. Z. Zaengl, Kuffel, and E, High Voltage Engineering Fundamentals. Newnes, 2000.

[26] N. Lahoud, L. Boudou, and J. Martinez-Vega, “A new approach to describe the electrical ageing by considering the distributed nature of processes in polymeric materials,” Journal of Non-Crystalline Solids, vol. 356, no. 11, pp. 652–656, 2010

[27] C. Laurent and G. Teyssedre, “Hot electron and partial-discharge induced ageing of polymers,” Nuclear Instruments and Methods in Physics Research Section B: Beam Interactions with Materials and Atoms, vol. 208, pp. 442–447, 2003

[28] Lei Cao and Haikui Li, “Analysis of Error Structure for Additive Biomass Equations on the Use of Multivariate Likelihood Function,” Forests, vol. 10, no. 4, p. 298, 2019

[29] W. Lei et al., “DC breakdown voltage tests may not be a good indicator of long-term ageing behaviour: A study of silica — XLPE nanocomposites,” 2017

[30] H. Li et al., “Polarization characteristics of metallized polypropylene film capacitors at different temperatures,” IEEE Transactions on Dielectrics and Electrical Insulation, vol. 22, no. 2, pp. 682–688, 2015

[31] H. Li et al., “Electric Field and Temperature Dependence of Electrical Conductivity in Biaxially Oriented Polypropylene Films,” IEEE Transactions on Plasma Science, vol. 42, no. 11, pp. 3585–3591, 2014

[32] J. Liu, D. Zhang, X. Wei, and H. R. Karimi, “Transformation Algorithm of Dielectric Response in Time-Frequency Domain,” Mathematical Problems in Engineering; New York, 2014

[33] M. Makdessi, A. Sari, and P. Venet, “Metallized polymer film capacitors ageing law based on capacitance degradation,” Microelectronics Reliability, vol. 54, no. 9, pp. 1823–1827, 2014

[34] M. Makdessi et al., “Lifetime estimation of high-temperature high-voltage polymer film capacitor based on capacitance loss,” Microelectronics Reliability, vol. 55, no. 9, pp. 2012–2016, 2015

[35] A. Maxwell, W. Broughton, G. Dean, and G. Sims, Review of Accelerated Ageing Methods and Lifetime Prediction Techniques for Polymeric Materials, 2005.

[36] G. Mazzanti, "What have we still to learn about the Inverse Power Model?," 2016 IEEE Conference on Electrical Insulation and Dielectric Phenomena (CEIDP), Toronto, 2016

[37] G. Mazzanti and G. C. Montanari, “Electrical aging and life models: the role of space charge,” IEEE Transactions on Dielectrics and Electrical Insulation, vol. 12, no. 5, pp. 876–890, 2005

[38] G. C. Montanari, “Bringing an insulation to failure: the role of space charge,” IEEE Transactions on Dielectrics and Electrical Insulation, vol. 18, no. 2, pp. 339–364, 2011

[39] G. C. Montanari, “Notes on theoretical and practical aspects of polymeric insulation aging,” IEEE Electrical Insulation Magazine, vol. 29, no. 4, pp. 34–44, 2013

[40] G. C. Montanari, “A contribution to unravel the mysteries of electrical aging under DC electrical stress: where we are and where we would need to go,” in 2018 IEEE 2nd International Conference on Dielectrics (ICD), 2018, pp. 1–15

[41] G. C. Montanari, D. Fabiani, P. Morshuis, and L. Dissado, “Why residual life estimation and maintenance strategies for electrical insulation systems have to rely upon condition monitoring,” IEEE Transactions on Dielectrics and Electrical Insulation, vol. 23, no. 3, pp. 1375–1385, 2016

[42] G. C. Montanari and G. Mazzanti, “Ageing of polymeric insulating materials and insulation system design,” Polymer International, vol. 51, no. 11, pp. 1151–1158, 2002

[43] G. C. Montanari, P. Seri, and L. A. Dissado, “Aging mechanisms of polymeric materials under DC electrical stress: A new approach and similarities to mechanical aging,” IEEE Transactions on Dielectrics and Electrical Insulation, vol. 26, no. 2, pp. 634–641, 2019

[44] T. A. Osswald, Material science of polymers for engineers, 3rd ed. Hanser Publishers, 2012.

[45] G. Packard, G. Birchard, and T. Boardman, “Fitting statistical models in bivariate allometry,” Biological Reviews, vol. 86, no. 3, pp. 549–563, 2011

[46] G. C. Packard and G. F. Birchard, “Traditional allometric analysis fails to provide a valid predictive model for mammalian metabolic rates,” Journal of Experimental Biology, vol. 211, no. 22, pp. 3581–3587, 2008

[47] T. S. Ramu, Diagnostic testing and life estimation of power equipment. New Academic Science, 2012.

[48] C. W. Reed and S. W. Cichanowskil, “The fundamentals of aging in HV polymer-film capacitors,” IEEE Transactions on Dielectrics and Electrical Insulation, vol. 1, no. 5, pp. 904–922, 1994.

[49] M. Ritamäki, “Effects of Thermal Aging on Polymer Thin Film Insulations for Capacitor Applications,” Lämpöikäännytyksen vaikutukset kondensaattorikäyttöön suunniteltuihin ohutkalvoeristyksiin, Tampere University of Technology, 2014

[50] M. Ritamäki, Steering Capacitor Film Development with Methods for Correct and Adequate Dielectric Performance Assessment. Tampere University, 2019.

[51] I. Rytöluoto, “Application of polypropylene nanocomposites in metallized film capacitors under DC voltage,” Polypropeeni-nanokomposiittien soveltaminen metalloiduissa ohutkalvokondensaattoreissa tasajännitteellä, Tampere University of Technology, 2011.

[52] I. Rytöluoto, “Large-Area Multi-Breakdown Characterization of Polymer Films: A New Approach for Establishing Structure–Processing–Breakdown Relationships in Capacitor Dielectrics,” Tampere University of Technology, 2016.

[53] L. Sanche, “Electronic aging and related electron interactions in thin-film dielectrics,” IEEE Transactions on Electrical Insulation, vol. 28, no. 5, pp. 789–819, 1993.

[54] H. Soliman, H. Wang, and F. Blaabjerg, “A Review of the Condition Monitoring of Capacitors in Power Electronic Converters,” IEEE Transactions on Industry Applications, vol. 52, no. 6, pp. 4976–4989, 2016

[55] M. Teixeira, I. Hoyo, F. Wandrowelsti, V. Swinka-Filho, and M. Munaro, “Evaluation of thermal degradation in isotactic polypropylene films used in power capacitors,” Journal of Thermal Analysis and Calorimetry, vol. 130, no. 2, pp. 997–1002, 2017

[56] G. Teyssedre and C. Laurent, “Charge transport modeling in insulating polymers: from molecular to macroscopic scale,” IEEE Transactions on Dielectrics and Electrical Insulation, vol. 12, no. 5, pp. 857–875, 2005

[57] W. Wang, D. Min, and S. Li, “Understanding the conduction and breakdown properties of polyethylene nanodielectrics: effect of deep traps,” IEEE Transactions on Dielectrics and Electrical Insulation, vol. 23, no. 1, pp. 564–572, 2016

[58] Xiao Xiao, Ethan P. White, Mevin B. Hooten, and Susan L. Durham, “On the use of log-transformation vs. nonlinear regression for analyzing biological power laws.” Figshare, 2016

[59] V. A. Zakrevskii, V. A. Pakhotin, and N. T. Sudar, “Ageing and breakdown of thin insulating polymer films,” Journal of Applied Physics, vol. 115, no. 23, 2014

[60] V. A. Zakrevskii, N. T. Sudar, A. Zaopo, and Yu. A. Dubitsky, “Mechanism of electrical degradation and breakdown of insulating polymers,” Journal of Applied Physics, vol. 93, no. 4, pp. 2135–2139, 2003

[61] V. A. Zakrevskii and N. T. Sudar’, “Ionization mechanism of the electrical degradation (breakdown) of polymer dielectric films,” Phys. Solid State, vol. 55, no. 7, pp. 1395–1400, 2013

[62] IEC 61071:2017 Capacitors for power electronics

[63] IEC 61251:2015 Electrical insulating materials and systems - AC voltage endurance evaluation Edition 1.0. IEC.

APPENDIX A: COMPUTATION PARAMETERS

Table A.1. *Computation parameters for different lifetime models with accuracy of twelve decimals (commercial reference film).*

Model	Parameter	Electric field [V/µm]	Temperature [°C]
Inverse power law $L(E) = K_E E^{-n}$			
Nonlinear regression	K_E=6.376838480852E+52 n=18.711536302089	340-580	60
	K_E=5.260276506402E+39 n=13.755377880319		70
	K_E=3.065217666157E+47 n=16.830908586791		85
	K_E= 1.72345167478E+33 n=10.993893581490	280-580	60
Linear regression	K_E=1.295257903433E+36 n=12.150186649711	340-580	60
	K_E=2.600183271840E+32 n=10.881828415899		70
	K_E=1.993902940936E+29 n=9.7086494854786		85
	K_E=6.348909969923E+35 n=12.034691355862	280-580	60
Arrhenius $L(T) = K_T e^{B/T}$	K_T=8.642411669122E+04 B=-2.013313584856E+03	580	60-85
	K_T=2.895550464447E-08 B= 8.711679788671E+03	480	
	K_T=4.760381923421E-04 B= 6.011952956987E+03	380	
	K_T=4.898706049950E-08 B= 9.762222175304E+03	340	
Multi-stress $L(T,E) = Ke^{B/T} \cdot E^{-(n_1 - n_2/T)}$	K= 1.000000000000E+40 B= 8.439240852727E+03 n_1=1.880159727465E+01 n_2=2.648838388917E+02	340-480	60-85

Table A.2. *Computation parameters for inverse power law with accuracy of twelve decimals (prototype 1 nanofilm).*

Model	Parameter	Electric field [V/µm]	Temperature [°C]
Inverse power law $L(E) = K_E E^{-n}$			
Nonlinear regression	K_E=1.674620816374E+44 n=15.622476750759	280-480	60
Linear regression	K_E=1.472062565225E+43 n=15.197934283632		